CHALMERS
UNIVERSITY OF TECHNOLOGY

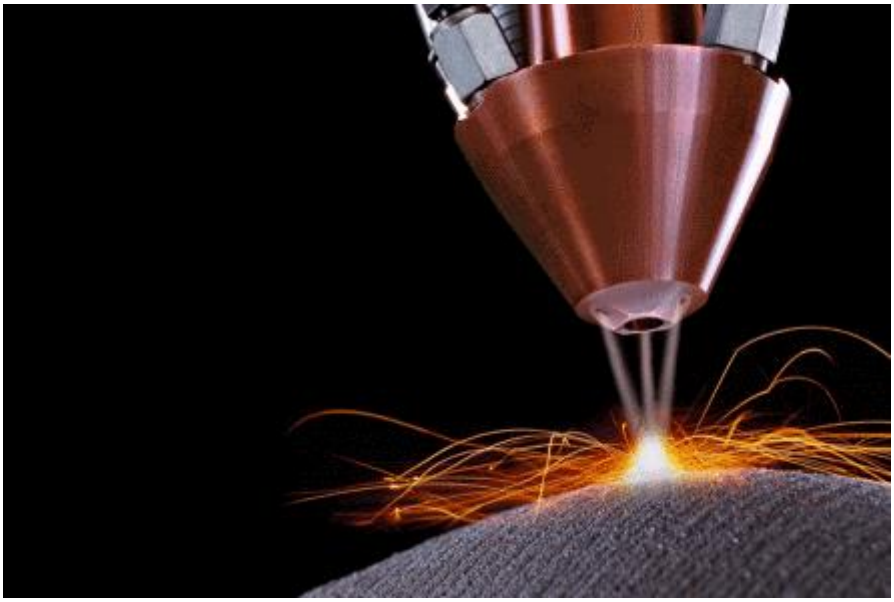

STUDY ON LASER SURFACE ENHANCEMENT OF MARINE PROPELLERS

Master's thesis in the International Master´s Programme Naval Architecture and Ocean Engineering

SHUBHAM PATEL

PRADEEP PATIL BELLARY

Department of Mechanics and Maritime Sciences
CHALMERS UNIVERSITY OF TECHNOLOGY
Gothenburg, Sweden 2019
Master's Thesis 2019/62

MASTER'S THESIS IN THE INTERNATIONAL MASTER'S PROGRAMME IN NAVAL ARCHITECTURE AND OCEAN ENGINEERING

STUDY ON LASER SURFACE ENHANCEMENT OF MARINE PROPELLERS

SHUBHAM PATEL

PRADEEP PATIL BELLARY

Department of Mechanics and Maritime Sciences

Division of Marine Technology

CHALMERS UNIVERSITY OF TECHNOLOGY

Gothenburg, Sweden 2019

STUDY ON LASER SURFACE ENHANCEMENT OF MARINE PROPELLERS

SHUBHAM PATEL
PRADEEP PATIL BELLARY

Master's Thesis 2019/62
Department of Mechanics and Maritime Sciences
Division of Marine Technology
Chalmers University of Technology
SE - 412 96 Gothenburg
Sweden
Telephone: + 46 (0)31-772 1000

Cover: Laser technology (Voestalpine HPM International, 2019)

Printed by Chalmers Reproservice

Gothenburg, Sweden 2019

STUDY ON LASER SURFACE ENHANCEMENT OF MARINE PROPELLERS

Master's Thesis in the International Master's Programme in Naval Architecture and Ocean Engineering

Department of Mechanics and Maritime Sciences
Division of Marine Technology
Chalmers University of Technology

Abstract

Due to the effects of global warming reducing the extent of the sea ice, more and more merchant ships enter ice-infested waters. Ice damages on ships are frequently reported. Propeller is among the most vulnerable parts of a ship subject to ice damages. Propeller damages lead to efficiency loss, deterioration of cavitation and noise, and even malfunction of the propulsion system. Reparation of damaged propellers are costly. In this study, we aimed at enhancing a propeller's ice strength while keeping its open-water profile. This was achieved by implementing cladding material on the bronze propeller blades through laser treatment.

In this thesis work, numerical analyses of laser cladding process was carried out using finite element (FE) method to investigate if the laser cladding improves the resistance of the marine propeller materials against repeated ice impact loads. A Co-Cr alloy was cladded on two different substrate materials. The laser cladded surfaces were grounded where the effect of a grinding wheel was derived using a combination of rectangular distribution of heat source and grinding forces instead of the presence of actual grinding wheel. Repeated ice impact loads were applied on both the non-cladded substrate and the cladded substrates after grinding for a certain period of time. The efficiency of the cladding and grinding processes was estimated using the impact load simulations.

It was observed that after the application of every impact load on the non-cladded substrate, the longitudinal residual stresses and the equivalent plastic strain were increased. But, after grinding the cladded substrate, there was an improvement in the equivalent plastic strain. The inference obtained after multiple simulations were that the grinding process improves the equivalent plastic strain on the cladded substrate. It thus concludes that the laser cladding and grinding processes improve the performance of the propellers against repeated ice impact loads considerably.

Keywords: finite element analysis, ice-propeller interaction, laser cladding, residual stresses, surface grinding

Contents

Preface

This thesis is part of the requirements for the master's degree at Chalmers University of Technology, Gothenburg, and has been carried out at the Division of Marine Technology, Department of Mechanics and Maritime Sciences, Chalmers University of Technology between January and June of 2019.

We would like to thank our supervisor and examiner Zhiyuan Li, at the Department of Mechanics and Maritime Sciences, Chalmers University of Technology for his knowledge, feedback and encouragement throughout this work. The thesis would not get its shape without his wise and timely suggestions. We would like to thank Professor Jonas Ringsberg, Deputy Head of Department and Head of Division of Marine Technology, Chalmers University of Technology who provided us various insights and feedbacks, which gave us the necessary directions in this thesis.

We would like to thank Jim Brozoulis, at the Department of Mechanics and Maritime Sciences, Chalmers University of Technology for his kindly suggestions regarding the heat transfer analysis that is carried out in ABAQUS software. We also thank Michele Maglio at the Department of Mechanics and Maritime Sciences, Chalmers University of Technology for his guidance regarding the modelling of heat source and other topics.

We would also like to thank all the authors and researchers who have put lots of effort into various research work from whom we have benefited directly or indirectly.

Finally, we would like to thank our family and friends for their continuous support and love during the entire thesis work.

Gothenburg, June 2019

Shubham Patel

Pradeep Patil Bellary

Nomenclature

List of acronyms

2D	Two-dimensional
3D	Three-dimensional
BC	Boundary Condition
CE	Cavitation erosion
CO_2	Carbon dioxide
Co	Cobalt
Cr	Chromium
DFLUX	Distributed heat flux
DOF	Degrees of freedom
DSS	Duplex Stainless Steel
FE	Finite Element
FEA	Finite Element Analysis
FEM	Finite Element Method
HAZ	Heat affected zone
HBsC1	High strength brass casting
LC	Laser cladding
MAB	Manganese Aluminum Bronze
NAB	Nickel Aluminum Bronze
NiAl	Nickel Aluminide
pH	Hydrogen level concentration in acid/base
Ti	Titanium
UN SDG	United Nations Sustainable Development Goals

Roman Upper-Case letters

A	Cross sectional area
A_s	Surface area
C_k	Material parameter
E	Young's modulus
N	Number of backstresses
NT11	Nodal temperature
PEEQ	Equivalent plastic strain
P_z	Vertical force (grinding)
$Q_{surface}$	Surface heat flux
Q_{volume}	Volumetric heat flux
S	Deviatoric stress tensor
S11	Longitudinal residual stress
S12	Shear residual stress
T	Temperature
V	Voltage
V_s	Speed of grinding wheel
V_w	Speed of workplace
Z	Coordinate axis

Roman Lower-Case letters

a	Depth of cut
c	Specific heat
f	Heat flux matrix
f_f	Weight fraction of front ellipsoid
f_n	Normal force
f_r	Weight fraction of rear ellipsoid

f_t	Traction force
h	Film coefficient of convection
k	Thermal conductivity
l	Length of model
p_0	Normal pressure load
q_f	Heat flux distribution in front quadrant
q_r	Heat flux distribution in rear quadrant
t	Time
t_s	Thickness of substrate
t_c	Thickness of cladding

Greek letters

λ	Coefficient of thermal conductivity
α	Coefficient of thermal expansion
υ	Poisson's ratio
σ_y	Yield strength
σ^0	Yield surface size
θ	Material temperature
θ^0	Sink temperature
θ^z	Absolute zero temperature
ε	Emissivity
$\wr$	Material density
γ_k	Material parameter
$\bar{\varepsilon}^{pl}$	Equivalent plastic strain
$\bar{\varepsilon}^{pl}\|_0$	Initial equivalent plastic strain
$\dot{\varepsilon}^{pl}$	Plastic flow rate
$\dot{\bar{\varepsilon}}^{pl}$	Equivalent plastic strain rate
α	Backstress matrix
α_k	Backstress component

α^{dev}	Deviatoric part of backstress
σ	Second order stress tensor
ζ	Time lag in heat source position
η	Efficiency of heat source
μ	Traction coefficient
ω	Angular velocity

Variables

Laser beam parameters		*Unit*
P	Laser Power	W
v	Scanning Speed	mm/s
η	Efficiency	%
I	Current	A
V	Voltage	V

List of figures

1 Introduction

In this chapter, the need for this thesis and the motivation that drives to complete the set of tasks are discussed. The objectives and goals that put up the direction to proceed in this thesis are elaborated. The limitations as per the scope of the thesis help us assume some concepts that may not be possible to include due to the limited time frame.

1.1 Background and Motivation

Due to the excessive usage of fossils fuels, accumulation of CO_2 has devastatingly increased in the atmosphere. In addition to this, the deforestation has reduced the concentration of flora which is increasing the greenhouse effect. These unusual changes in climate have been showing a considerable effect on the transportation of ships and vessels all around the globe. Figure 1.1 shows the drastic increase in the annual temperature which has considerable effects on both land and aquatic life. Because of global warming, the glaciers and icebergs are melting which is leading to a drastic rise in sea level. This also has contributed to the increase in sea surface temperature which makes sea ice melt during summer (Karlsson, 2016). This has been enlarging the area of navigation and has opened new routes for ships to travel. But, during winter, the sea water turns into ice which creates an obstruction in the path of these ships (Sarwar, 2014).

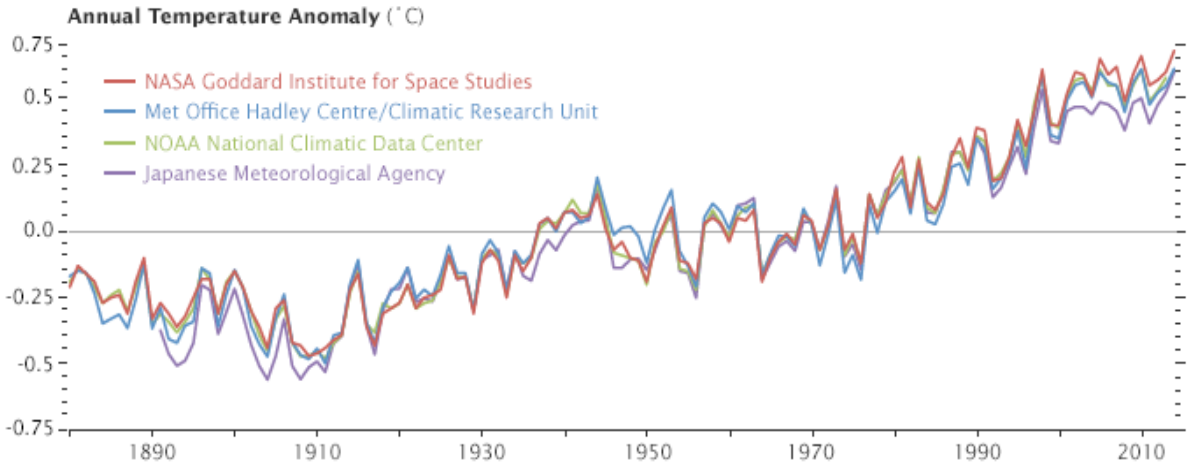

Figure 1.1:Yearly temperature anomalies from 1880 to 2014 as recorded by NASA, NOAA, the Japan Meteorological Agency, and the Met Office Hadley Centre (United Kingdom) (Earthobservatory.nasa.gov. ,2019)

The ice formed due to freezing of sea water is very strong that it affects the various parts of the ships and vessels directly or indirectly. Especially, the propellers have direct contact with the ice which may lead to a reduction in performance of the propellers over a period. As the ships travel with high speeds, the sudden contact of ice with propellers give rise to impact loads which generate various stresses on the propeller. Also, the environment in which the propeller operates leads to combined physical-chemical process such as cavitation erosion which results in the formation of pits on the surface of propellers (Kwok et al., 2016). Due to repeated impact with ice loads, the material of the propeller undergoes fatigue and sometimes untimely fracture. All these negative influences decrease the performance of the propellers and generate undesired noise. This ultimately increases the fuel consumption with a reduction in overall efficiency.

Though the effects of ice loads seems to be less in the beginning, over a long period of time, the consequence of these ice loads is more hazardous. The various maritime industries have already employed advanced methods to combat hazardous scenarios including ice loads. It is still necessary to employ a bit sophisticated yet powerful method to improve the resistance of the ship propellers functioning in such environmental conditions. One of the simplest methods is to manufacture the propellers with suitable material. Earlier, the cast iron was used because of its properties such as high strength and toughness. Later the usage of bronze has improved due to the desired properties such as resistance against corrosion in saline water and good machining properties like weldability and ductility (Arias-González et al., 2017). Recently, the stainless steels are being used due to high toughness to have resistance against impact loads generated by ice in the sea (Alam et al., 2017).

One option to combat these undesired effects is that the ice class of the propeller can be increased. This is not desirable because of an increase in the thickness of the propellers blades can increase fuel consumption to increase the efficiency of the propulsion system. So, it is required to use the suitable material and manufacturing method for making the propellers function better against all these obstacles. Also, the method used must make use of less material comparatively yet increase the efficiency of the propulsion system. Laser surface enhancements can be a virtue in tackling all of these problems. Amongst them, Laser cladding method which makes use of high-power laser beam to form the coating of the material on the actual substrate of the propeller that can have all the desired properties of the ideal propeller as mentioned above.

As a part of laser cladding on the propeller, it is important to choose the suitable coating material amongst a wide list of materials. In the actual manufacturing location, it is tedious and non-economical to test the performance of various substrate and cladding (coating) materials by producing physical prototypes. This can be eliminated by making use of virtual prototypes in the simulation environment (Gan et al., 2017). The various material models are created and the same type of boundary conditions, loadings, heat treatments as that of the real-time environment are applied to see how the respective model combination behaves.

1.2 Objective and Goals

The main objective of this thesis is to enhance the performance of marine propellers against ice impact loads. Here, the open water profile is considered without compromising the efficiency. Kwok et al., (2016) suggests that there are various laser-based surface modification processes that can protect the material surface against hazardous effects such as cavitation erosion and ice impact loads. Laser cladding is one of such laser surface treatments that can be employed (Arias-González et al., 2017). Practically, the suitable cladding material is coated on the bronze propellers using a high-power laser beam. This is expected to increase the resistance of the propellers against the failure by impact loads. This is followed by grinding of the cladding layer. The challenging part is to visualize the effect and efficiency of the laser cladding on the propeller in the simulation environment. So, the main scope is to simulate the laser cladding and grinding processes using a commercial FE package, ABAQUS.

The following tasks are carried out to achieve the main objective of the thesis:

- Creation of two material FE models with suitable boundary conditions and appropriate meshes to carry out the thermo-mechanical analyses of cladding and grinding processes.
- Identify the potential parameters that affect the efficiency of cladding and grinding simulations.
- Verify the improvement in performance of the propeller after cladding and grinding processes using ice-impact loads.

1.2.1 Contribution of thesis to achieve UN SDG

Figure 1.2: The United Nation's 17 Sustainable Development Goals (United Nations.,2015)

According to the United Nations Organizations (United Nations, 2019), all the nations must have activities or projects that can collectively contribute to Sustainable Development. These must benefit human beings, flora, fauna and in turn whole earth. To achieve this, the UN has constituted 17 goals, and these are shown in Figure 1.2. In accordance with the scope of this thesis, many of these goals can be addressed and some of them are goals No. 9, 12, 13 and 14 that can be explained below. All these goals which are motivated for sustainability and in turn maintenance of ecological balance are addressed directly or indirectly through this thesis.

The **Goal No.9: Industry, Innovation, and Infrastructure** can be achieved as the laser cladding is one of the advanced manufacturing methods. Especially, in the marine industry for the development of propellers, laser cladding is employed to clad the non-corrosive, high strength, fatigue and fracture resistant material on the substrate. The selection of coating materials is still under continuous research and thus helps in reaching the goal of innovation as per UN SDG. This thesis involves finding the innovative method for the simulation of laser cladding and grinding those benefits industries as well.

The **Goal No.12: Responsible Consumption and Production** holds good for this thesis as lots of marine components manufacturers are employing new technology for production with efficiency and effectiveness, laser cladding supports this goal considerably. The results

obtained after the simulation of laser cladding suggest the suitable materials used for cladding that may increase the necessity of these materials to some extent. This increases the mining of the materials from the core of the planet earth which may create imbalance. Hence, this goal directs the manufacturers to be cautious in the number of materials they consume to produce cladded propellers.

The **Goal No.13: Climate Action** can be addressed in this thesis as the propellers designed by laser cladding process are mainly used in the environment where high amount of ice is present, it helps to combat the challenge of ice loads. Also, the laser cladding process is efficient and uses pure energy, there are fewer chances of producing adverse effects as in the case of welding which produces harmful gases during the operation. This allows the maintenance of an optimal environment where laser cladding process is carried out.

The **Goal No.14: Life Below Water** is in accordance with the scope due to several reasons. Though the coating materials selected for laser cladding process must satisfy almost all the desired properties, it is also important to see that the materials are neither toxic nor involve in creation of harmful effects in an environment where the cladded propeller works. There is a wide variety of aquatic life which may directly or indirectly encounter the propeller in seas or oceans which may get affected by hazardous materials. Hence, it is also important to choose the materials for both substrate and cladding by keeping this in mind in the product development stages.

1.3 Limitations

As per the scope of the thesis, it is required to simulate the laser cladding process using ABAQUS which requires moving heat source. The characteristics of the heat source designed in the thesis are different from the heat source used in the laboratory or manufacturing location where actual laser cladding is carried out. This is because of difficulty in the creation of a heat source which has all the properties of moving laser beam. Hence, only the main parameters of a laser beam such as the heat flux and the scanning speed are used.

The various researchers have explained the simulation of laser cladding in other FE software such as Ansys (Shukla & Verma, 2014). Based on our previous experience of working in Ansys, it can be said that it is a bit easier to handle simulations in Ansys because the approach is comparatively simple. For instance, the loading types are few and are easy to follow. But it is a bit difficult to simulate in ABAQUS due to the complexity such as the need for the creation of time-dependent multi-steps and various types of loading. One of such problems is the setting up of material models where it is required to use the highly temperature dependent physical and material properties in ABAQUS. As the materials for substrate chosen are NAB and Steel, we have assumed these properties which have not been verified. As the scope of the thesis was to find the appropriate methodology to enhance the desired properties of a propeller, we went with the available material properties by referring to some study references that will be explained later.

The grinding process needs the grinding wheel to remove the material from the cladded surface. In all the simulations, the 2D models were used to reduce the simulation time even though there are limitations of visualizing the effect in another model plane. But the FE model used in the grinding simulation was 2D which does not give possibility to create the 3D model of grinding wheel. This does not give any information regarding the thickness of the grinding wheel.

According to the ABAQUS reference manual and the online discussion led by Sudhakar Indurthi (2014), ABAQUS/Explicit is generally used to simulate such process which comes under the wave propagation analysis. But, when we tried with ABAQUS/Explicit to simulate the grinding process, it required the design of the 3D model of grinding wheel. Hence, the ABAQUS/Standard is used in all the simulations. To derive the effect of grinding wheel, the alternative method is used (which needs various parameters of grinding wheel, that will be discussed in the next sections). For this, the grinding forces are created using a combination of normal pressure and traction load that gives almost the same effect of grinding wheel. Parameters for the generation of normal pressure and traction load are assumed based on the study references.

Another challenge is to get the exact magnitude of the ice impact loads as it is difficult to get that due to many factors. Hence, we have used Newton's laws of motion and few studies references to estimate these impact loads that are used to find the accuracy of laser cladding and grinding process. Also, the frequency of the ice impact loads hitting the propeller is difficult to understand and hence we have gone with 50 cycles of impact loads that seem to be enough to see the effect of impact loads on both the non-cladded and cladded cum grounded substrate.

1.4 Outline of Thesis Work

The following outline of the thesis work gives the number and name of each chapter, relevant page numbers and a summary of the contents.

Chapter	Title	Pages	Description
1	Introduction	1	The background and the motivation for fixing the scope of the thesis are delivered in this chapter. The main goals and objectives that put the plan for the work are defined. The limitations which give the necessity to assume some of the things that led to ignoring some of the conceptual considerations in the entire thesis work are motivated.
2	Literature Review	7	The State-of-the-art research is carried out to understand what laser cladding is and how is it beneficial for improving performance of propellers. The grinding process on the cladded substrate is understood. The FE simulation of both laser cladding and grinding is understood so that it can be applied in accordance with the scope of the thesis. Also, the materials for both Cladding and Substrate are studied and are fixed for the simulation. After this, the effect of ice impact loads on the marine propellers is analyzed.
3	Methodology	23	The thesis plan is described from the selection of suitable software, setting up of material models, FE models and meshing, BCs of Laser cladding and grinding process. The two approaches of simulations of laser cladding, one approach of

			grinding simulation and then impact load simulation is carried out systematically.
4	Analyses of results and discussions	43	The thermal analyses and mechanical analyses result of the simulation of cladding, grinding and impact loads in the form of nodal temperatures (NT11), residual stresses (S11 and S12) and equivalent plain strain (PEEQ) are verified using study references. Also, the behavior of the combination of substrate and cladding materials after cladding, grinding and impact load simulations are analyzed to derive the conclusions for the efficiency of simulations.
5	Conclusions	69	The summary of the methodology and results are analyzed to give overall insights on the thesis work. This allows the reader to understand all the main milestones that have been reached in the entire thesis lifecycle.
6	Recommendations and Future Work	71	In this section, the summary of the results is used to generate some of the possibilities for the companies or future master thesis students to derive the possibility to overcome the limitations of this thesis. This may give rise to improved methods or new technology that can improve the performance of the propellers in the most suitable manner.

2 Literature Review

An overview of the state-of-the-art of propeller properties as well as procedure of laser cladding are made. The simulation of laser enhancements using commercial FE software is referred. The various possibilities on how to make use of these approaches to make them work are analyzed and discussed. This is like finding different alternatives to solutions for the same problem by following what the researchers suggest. By referring to all of these, there are possibilities of obtaining the new systematic way of problem-solving for the existing problem with accuracy and efficiency.

2.1 Desired properties of a marine propeller

The desired properties of the propellers like toughness, high strength, stiffness, resistance to corrosion, cavitation, and erosion, ability to withstand high ice impact loads and others are studied. The propellers must possess some of the desired properties like hardness, resistance against corrosion, cavitation and erosion, fatigue strength, better bonding of microstructure, excellent machinability and weldability. However, it is extremely difficult to achieve all of these in a propeller made of a single material. Hence, the need for designing the two-material propeller comes into existence which can help to inculcate most of the required properties in it. Some of these are explained in brief to understand what materials enhance what kind of properties.

The material for the propeller should possess a high level of bulk properties like formability, machinability, strength, and toughness along with surface-dependent properties. Here, the surface hardness is necessary as the components have to resist indentation by bodies that come in contact with them; as the hardness increases, the wear resistance also increases. Surface engineering is required to design the composite system (coating plus substrate) whose performance is improvised such that the new performance is better than either the coating or the substrate alone (Brückner & Lepski, 2017).

One of the common causes of failure of marine components like propellers is Cavitation Erosion (CE) which is like nausea for maritime industry (Duraiselvam et al., 2006). As per the hypothesis, CE is the result of the conversion of the potential energy contained in the cavity into emitted acoustic power after the collapse. Erosion is a progressive loss of material from solid surfaces by the action of sliding or impact of solids, liquids, gases or a combination of these substances (Duraiselvam et al., 2006) . The high strength cavitation can give rise to the serious material loss which results in catastrophic failure of the components (Kwok et al., 2016). To increase the durability, reliability and economic performance of the hydraulic components working in the corrosive and cavitating environment, it is most important to reduce the material damage from the surface phenomena such as CE (Zhang et al., 2017).

The presence of corrosive particles in the cavitating liquid makes the material loss more intense because the corrosive particles reach the surface at a greater speed. The erosion rate is greater than either the solid-particle erosion or cavitation erosion alone in the highly corrosive environment filled with erosion particles (Kwok et al., 2016).

In the environment where there is an enormous amount of ice (like in the Arctic ocean and Baltic sea), the impact loads of the propellers are the resultant of either by chopping off the

edge of the blade by ice or exceeding the crushing endurance of the propeller blade when it is compressed against ice or sometimes both combined. The relative velocities existing between propeller and ice controls the direction of propeller ice loads. These ice loads give rise to both axial and transverse forces that in turn gives rise to bending and spindle moments on blades. Also, the torque is generated on the propeller which then shows the effect of load into the shafts system (Norhamo et al., 2009).

The study conducted by Koskinen & Jussila (1991) shows that the geometrical profile of the propellers has a significant influence on the propeller's ice load. The study done is open profile propellers shows that there are extreme loads acting on the tip of the propeller. These loads are impacted in nature and tend to bend the blades both forward and backward respectively. As the ship moves forward, the tip loads bend the blade backward as shown in Figure *2.1*. This happens when the ice hits the propeller in the radial direction at curves (Zou, 1996) .

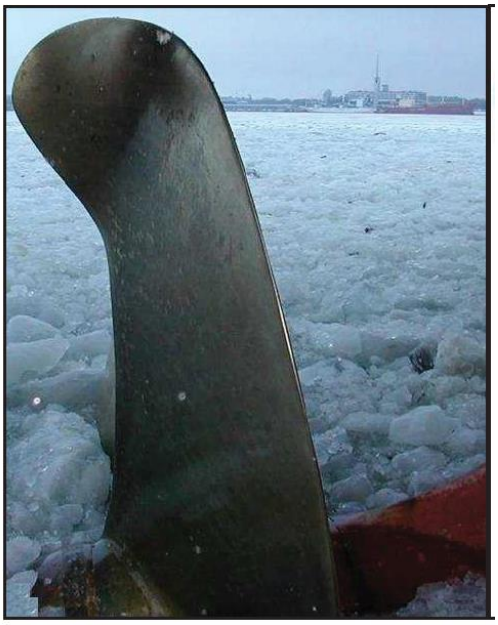

Figure 2.1: Bending of tip of open profile propeller due to ice-propeller interaction (Norhamo et al., 2009)

The main parts of propellers such as propeller blades, blade bolts/shear pins, hub and pitch mechanism are designed for both static and dynamic loads. Propeller blades are subjected to both backward and forward loads that can undergo bending. The stress undergone by the blades must not go beyond material reference stress. Also, the materials fatigue resistance should be better (Norhamo et al., 2009).

2.2 Materials for propellers

The materials of propellers are and the various manufacturing methods including the laser surface enhancements are studied. Marine propellers are manufactured with various materials for ages. In the early 1960s, cast iron was used as a propeller material. But, later the copper alloy materials were used because of its excellent properties like corrosion resistance.

According to research, Duplex stainless steel (DSS), Nickel aluminium bronze (NAB) and Manganese Aluminium Bronze (MAB) are commonly used materials for propellers. All have advantageous properties such as high strength, resistance to corrosion and they are easy to repair. For the machines that function in a highly corrosive environment, the electrochemical reaction occurring on the surface of alloy enhances the Cavitation Erosion. The intensity of aggression of electrochemical reaction depends on pH, the concentration of corrosives, fluid flow and pressure. It is known that the synergistic effect between erosion and corrosion may contribute to much more damage than the pure CE.

Copper-based alloys have excellent combination of strength and corrosion resistance properties (Cottam & Brandt, 2015). Phosphor bronze can be chosen for the propellers because of good fatigue strength, excellent wear properties in a corrosive environment, the ability to withstand high temperature and high loads (Arias-González et al., 2017). High strength brass casting (HBsC1) has high strength and toughness, good wear and corrosion resistance in marine condition, hence it is used for the ship components (Kim et al., 2004).

2.3 Need for Laser surface treatments

One of the methods of protecting the surface material of the propeller is by coating it with highly erosive resistant alloys or composites. The heat treatment is applied to eliminate porosity and cracks effectively between the clad and substrate layers (Duraiselvam et al., 2006). There are various ways to reduce failure of the propeller by CE and ice-based impact loads. One method is to alter the design of the propeller so that the hydrodynamic pressures do not affect much. The second one is to improve the environmental conditions such as temperature, the concentration of chemicals, reduce the corrosion properties of fluids and others. The third one is to use the superior quality material that can be coated on a substrate of the propeller which can resist the ill effects of corrosion, cavitation and high impact loads to the maximum extent.

Practically, it is easier to apply a coating to reduce these undesired effects than to change the design or environment. Hence, lots of emphases have been made to develop these kinds of materials to a large extent. The material chosen must have better hardness, work-hardenability, martensitic transformability in order to absorb cavitation energy and promote high resistance to corrosion (Duraiselvam et al., 2006). As the corrosion, erosion, and cavitation occur on the surface of the materials, it is enough to improve the quality of the surface to protect the overall bulk of the marine component. Even though the desired material used for coating is expensive, the remaining bulk of substrate material can be less expensive. Also, it gives a wide variety of chances to change the usage of various types of cladding (coating) materials that can help to achieve the desired properties of the propeller. The typical laser processing of NAB workpiece can be seen in Figure 2.2.

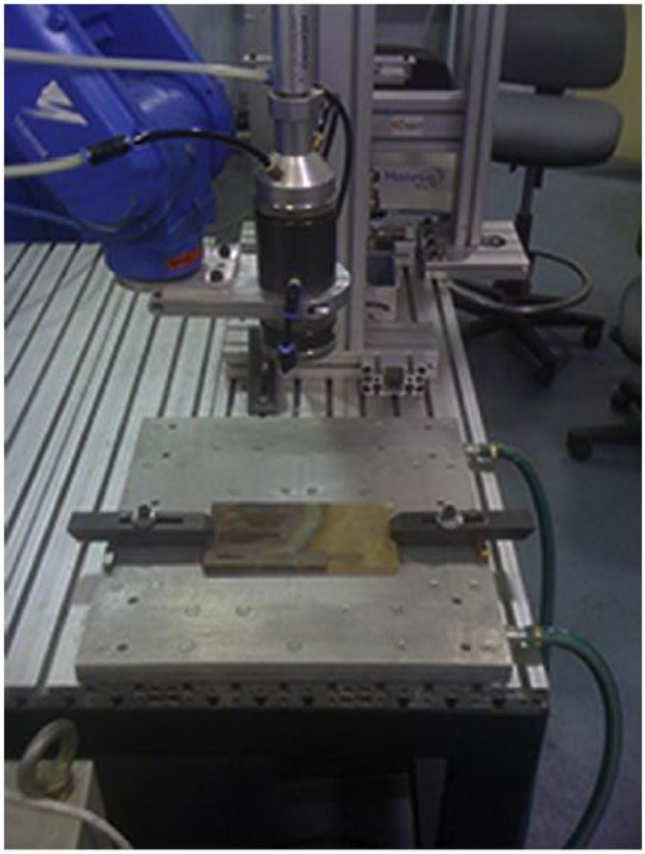

Figure 2.2: An example of Laser processing of NAB workpiece (Cottam & Brandt, 2015)

Previously, the various traditional manufacturing techniques such as electroplating and spraying were used to enhance the surface properties of the substrate material (Kwok et al., 2016). Due to the advancement of technology and the properties such as monochromaticity, unidirectionality, high coherence, and intensity, the high-intensity laser beam is being in the process called 'laser cladding'. It is a widely used method where it acts only on the surface, not on the bulk of materials (Sexton et al., 2001). Laser cladding is commonly used in these kinds of applications because it adds a layer of metallic or ceramic materials on the surface of the substrate materials which has very good metallurgical bonding between the substrate and the surface layer (Vilar, 2003).

2.4 Laser cladding

Laser cladding is a flexible, economical and efficient surface modification method for complex coatings on the irregular and intricate geometrical surfaces. It has the ability to mix a variety of coating materials in the form of powders or wires during injection into the cladding zone to produce cladding with the desired amount (Smurov, 2008). Laser cladding is better for deposition of one material on the other base material with better quality, free from distortion and resulting in good physical, chemical and mechanical properties (Sexton et al., 2001).

The laser cladding process involves the formation of the cladding layer by melting of coating material and a thin layer of the substrate with a laser beam that is scanned perpendicular to the substrate layer to create a melt pool. Laser cladding can be done either with preplaced powder on a substrate or by powder injection delivered to the melt pool by means of carrier gas. The

coating thickness is variable and depends on the application. A perfectly, defect-free coating is achieved when a thin surface layer of the previous task and of the substrate are melted as a new track is deposited (Arias-González et al., 2017). The laser cladding can contribute to improved wear and corrosion resistance, worn parts reclamation and improvement in thermal and electrical conductivity. The cladding is a surface coating process which need not cover the entire area of the parts or assemblies which saves the materials (Sexton et al., 2015).

Laser cladding can be carried out either by pre-placing the powder/wire of coating material on the substrate and then heating up using a high intensity laser beam to create the melt pool of both cladding and substrate using carrier gas. The solidification rates obtained in laser cladding is high that results in finer microstructure and defect free cladding layer on the substrate (Ringsberg et al., 2005). The bulk of the substrate material under the thin surface involved in the cladding process is unaffected by acting as a heat sink which helps in rapid cooling of the surface layer as the laser beam moves (Kwok et al., 2016).

In laser cladding, the various process parameters have control over the homogeneity, microstructure and chemical composition (Sexton et al., 2015). For the components which are coated, the residual stresses after the laser cladding (either compressive or tensile near the surface) are controlled by the combination of coating and substrate materials, coating thickness, pre-heat treatment, cooling rate, welding time and the number of passes. The final residual stress state in surface coated components are influenced by the post-treatment processes like annealing and grinding (Ringsberg et al., 2005). Figure 2.3 shows the laser cladding process where the nozzle injects the copper-based cladding particles and the laser beam melts the thin layer of substrate and the cladding particles to form the molten pool. There are layers such as a clad layer, bonding zone and HAZ and the substrate.

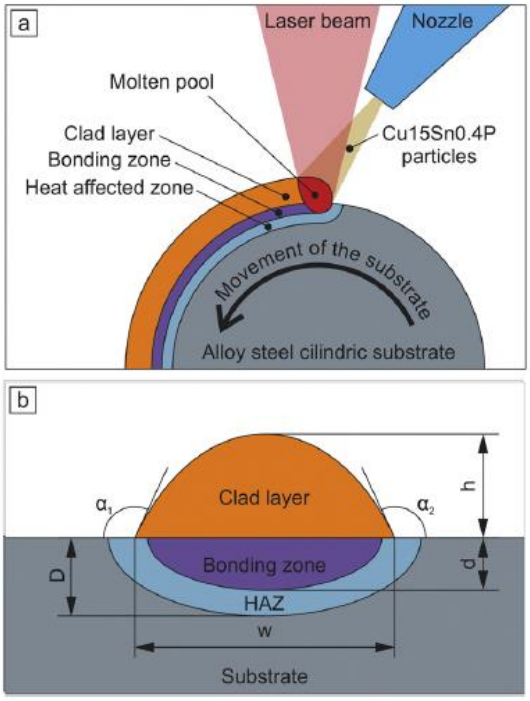

Figure 2.3: An example of laser cladding process where the nozzle injects the copper-based cladding particles and the laser beam melts the thin layer of substrate and the cladding particles to form the molten pool (Arias-González et al., 2017).

If the dilution of coating material by the substrate is avoided, we can expect better performance. The effect of laser radiation on a material depends mainly on power density and interaction time. The choice of laser and processing parameters affects the microstructure and the properties of the laser treated material (Brückner & Lepski, 2017).

2.4.1 Advantages of LC

The laser cladding is an efficient technique for improving the surface properties with homogeneity, refined, dense and uniform microstructure, which forms metastable phases. There is a strong metallurgical bonding between the cladding layer and substrate layer (Kwok et al., 2016).

The bulk is affected with no or little distortion because of the formation of small and shallow heat affected zone. Laser cladding zones are free of microcracks and pores (Shepeleva et al., 2000). Faster heating and cooling rate and superior metallurgical properties such as non-equilibrium phases and supersaturated solid solutions are achieved using laser cladding (Wesling et al., 2006).

The laser beam has various parameters that can be controlled easily by both manually and with automation which doesn't require much machining of the surface after the process (Kwok et al., 2016). Laser cladding zone has a smooth interface with the substrate which prevents stress concentration at the clad-substrate interface during operation (Shepeleva et al., 2000).

The high performance of the laser cladding surface against wear and corrosion gives a chance to choose a variety of materials from both soft to hard materials including dissimilar materials. Many times, lower heat input and smaller grain structure obtained because of rapid cooling enabled laser cladding which gives a superior solution to various industrial sectors (Kukreja et., 2014).

2.4.2 Limitations of LC

The beam size is very narrow and limited to finite size. It requires many laser beams to cover a wide surface. In order to increase the energy of the laser beam, a number of diode lasers are coupled with each other using optic fibers to widen the surface handling of the laser beam (Kwok et al., 2016).

The beam is unidirectional hence, it is efficient on the materials with a flat surface. If the materials have complex geometry, it takes a lot of time for processing. In the case of a metallic surface, the laser shows the lesser absorptivity (Kwok et al., 2016).

2.4.3 Materials for laser cladding

As explained in the previous sections, the materials used for cladding must possess extraordinary properties that can withstand the hazardous consequences in the marine environment which has an undesired effect on the substrate material. The cladding materials form the coating layer on the base material and protect it. Based on the application, various materials are being used as cladding materials. Laser surface enhancement processes are widely used to resist mainly cavitation corrosion behavior due to the formation of Widmanstatten morphology of the microstructure after processing. K_{III} phase present in the as-cast microstructure gives rise to selective phase corrosion and holds the responsibility for a deterioration in its stagnant seawater corrosion properties (Cottam & Brandt, 2015) .

For laser cladding, the materials used are Cobalt and Nickel-based alloys, Stainless Steel, Copper, Aluminium, Titanium, Bronze alloys and certain composite materials. These materials can be used as a dry powder or can be fed into the melt pool in the form of wire, strip, foil/sheet, tape or even in the form of a slurry (Arias-González et al., 2017). Nickel aluminides (NiAl and Ni3Al) have better properties such as low density, high melting point, high-temperature strength, hot corrosion resistance, and cavitation resistance. Also, have the poor temperature ductility and fracture toughness of these intermetallic. NiAl shows good CE erosion produced by high work hardening rate and yield strength (Duraiselvam et al., 2005).

The Erosion resistance can be improved by using new materials such as Titanium (Ti-based alloys) which have low density, high strength, good corrosion resistance along with excellent mechanical, physical and chemical properties. As these alloys are expensive, these are not commonly used in large scale marine applications.

By referring to various literatures, the coating materials such as Stellite and Hastelloy forms an excellent option for laser cladding in marine applications such as propellers and modelled in a combination of substrate materials like Nickel Aluminium Bronze (NAB), Manganese Aluminium Bronze (MAB) and Duplex Stainless Steel (DSS). In this thesis, Stellite is used as cladding material and NAB and Steel as substrates.

2.5 Simulation of laser cladding

The simulation of laser cladding is tedious because of non-linearity due to the change in the material properties and transient due to change in temperature with respect to time and position. It also requires the modeling of moving heat source which is time-dependent. There are various literatures which explain the simulation of welding process which is quite similar to laser cladding process for a long time. Recently, studies are being carried out for the simulation of laser cladding process. It is required to formulate some strategies that can assist in modelling of the moving heat source and simultaneously clad the coating on the substrate. After referring to various references such as Trivedi et al., (2011), Pilipenko, (1992), Eagar & Tsai, (1983), it is found that heat sources can be modeled with any of the existing models such as cylindrical, conical, semi-ellipsoidal, double ellipsoidal and others. Of all these, a double-ellipsoidal model is efficient in modelling the heat source and can be explained in detail.

2.5.1 The heating source model (3D approach of LC simulation)

In the process of laser cladding, the formulation of a transient heat source has to be modeled that moves from one point to another in a predefined period of time. Rosenthal (1941) was the first person who tried to model the moving heat source using mathematical models. Now, there are different models to explain the nature of the heat source as used by various authors such as Jeyakodi (2016), Esfahani (2016), Hongyuan et al., (2005). Amongst them widely accepted one is the double ellipsoidal model due to its greater accuracy and efficiency (Fu et al., 2015). This model has the advantage to show both the surface melting phenomenon as in welding and the deep melting as in the case of laser beam processes (Anca et al., 2011).

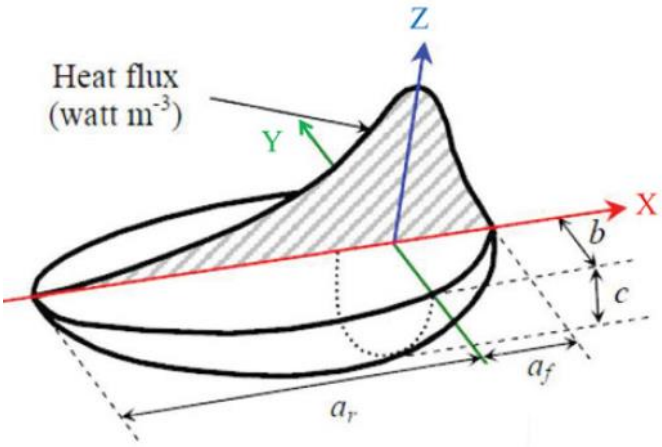

Figure 2.4: The Double ellipsoidal model of heat source used in writing DFLUX Subroutine (Fu et al., 2015)

Gery et al., (2005) infers that the shape of Gaussian distribution of heat flux is seen along the longitudinal axis. The heat source can be divided into front and rear quadrants where they act as separate quadrants of two different ellipsoidal sources. Here, the ellipsoidal model as shown in the Figure 2.4 is defined by the Goldak parameters (Goldak et al., 1984) represents the dimensions of the zone of melting (Muthukumaran et al., 2014).

Flint et al., (2017) and Winczek, (2016) state that to simulate the heating effects of the laser beam, the equivalent heat input is assumed as a constant internal heat generation per unit volume. For modelling, the coordinate axis (Z) is introduced which is firmly fixed on the moving heat source. This reference frame associated with the moving heat source is related to the coordinate system of the main geometry and is given by $\mathcal{E} = z - v\,(t-\varsigma)$ where v is the speed of laser beam and ς is time lag needed to define the position of heat source at a time (t)=0 (De Freitas et al., 2014).

In the equation, f_f and f_r denote the weight fractions of the front and rear ellipsoids and these fractions should be $f_f + f_r = 2$ and q is power the density of laser beam in W/m^3 within ellipsoid. Let a,b,c be the semi-axes of the ellipsoid parallel to x, y, $\mathcal{E}$ axes

The power density (heat flux) distribution within the front quadrant (q_f) is calculated by equation 2.1 (Fu et al., 2015) as shown.

$$q_f(x,y,z) = \frac{6\sqrt{3} f_f \eta Q}{a_f bc\pi\sqrt{\pi}} \exp\left(-\frac{3x^2}{a_f^2} - \frac{3y^2}{b^2} - \frac{3z^2}{c^2}\right) \tag{2.1}$$

The power density (heat flux) distribution within the rear quadrant (q_r) is calculated by equation 2.2 (Fu et al., 2015)as shown.

$$q_r(x,y,z) = \frac{6\sqrt{3} f_r \eta Q}{a_r bc\pi\sqrt{\pi}} \exp\left(-\frac{3x^2}{a_r^2} - \frac{3y^2}{b^2} - \frac{3z^2}{c^2}\right) \tag{2.2}$$

Q is the heat flux of the laser beam source and is given by equation 2.3

$$Q = \eta VI \tag{2.3}$$

Where V = voltage, I = current, ϩ = heat source efficiency

The parameters Goldak parameters a, b, c_f and c_r are independent of a heat source. The heat distribution in the space is calculated from the above 2 equations and represents volumetric heat generation.

The parameters of the laser beam have some influence on the quality of clad (coating) formed. Temperature and cooling rate are the main parameters that affect the properties of the clad layer and heat affected zone (Kim & Peng, 2000). The cooling rate is dependent on the cladding time, cladding speed, distance from melt pool and preheating temperature (Cottam & Brandt, 2015).

The cooling rate depends on the position, cladding time, cladding speed and preheating temperature. Some experiments showed that the temperature near the melt pool changes at a faster rate than away from the melt pool. As the cladding speed increases, the cooling rate also increases. But, the cooling rate decreases with increase in preheating temperature (Winczek, 2016). Also, it is shown that the shape of the clad layer is influenced by the physical properties of both cladding material and base material (Kim & Peng, 2000) .

2.5.2 Effect of parameters on properties of cladding and substrate

The cooling rate influences the microstructure and further determines the mechanical properties of the material. So, the prediction of cooling rate may be useful when predicting the mechanical properties of a microstructure. A non-uniform temperature field induces thermal stress. The study of temperature field of laser cladding may be helpful when predicting residual stresses of the structure (Kim & Peng, 2000).

The laser cladding residual stresses can have either positive or negative effects on fatigue life of the material propeller (or any structure) which depends on the magnitude and distribution of stresses and different loading conditions. Tensile residual stresses are harmful in the magnitude of the yield stress of the material, and these stresses are the common reasons for failure by fatigue (Bhatti & Barsoum, 2012).

The combination of constant volumetric and surface heat flux is made as to the heat flux to the cladding elements and is shown in the equation 2.4 (Bhatti & Barsoum, 2012).

$$Q_{total} = Q_{volume} + Q_{surface} = \eta VI \tag{2.4}$$

Where, η= efficiency, V and I are voltage and arc current,
Q_{volume} = Volumetric heat flux ($J/m^3/s$) and $Q_{surface}$ is the surface heat flux ($J/m^3/s$) applied to the external surface area A

The moving heat source method is employed by first deactivating the elements which represent the cladding material and then the heat is added as a volume and/or surface flux to each block of elements activated one after another. The efficiency of moving heat source method is evaluated by the comparison of obtained nodal temperatures before cladding and after cladding.

2.5.3 Thermo-Mechanical Analysis

This thesis involves two types of thermo-mechanical analyses namely, fully coupled thermo-mechanical analysis and sequentially coupled thermo-mechanical analysis. The theory involved in both thermal and mechanical analysis is explained here.

Thermal analysis

The thermal analysis for both laser cladding and grinding processes should possess appropriate boundary conditions and are governed by heat conduction, convection and radiation type of heat transfer mechanisms.

The conduction is the mode of heat transfer that happens within the solid substance or between two substances having direct contact. The conduction rate is governed by the Fourier law of heat transfer as given by the equation 2.5.

$$q = - k A \nabla T \tag{2.5}$$

where q = heat flow vector

k = thermal conductivity

A = cross-sectional area

$\nabla T = \partial T/\partial x$ = gradient of temperature

The convection is the mode of heat transfer that happens between the solid surface and the fluids (liquid or gas). The convection rate is governed by Newton's law of cooling as given by the equation 2.6.

$$Q = h A_s \Delta T \tag{2.6}$$

Where q = heat flow from the surface of solid

h = film coefficient (taken as 10 $W/m^{2o}c$ as in Ringsberg et al, 2005)

A_s = surface area

$\Delta T = T_s - T_\infty$ = temperature difference between surface and the coolant

Here coolant temperature is the sink temperature of 20°C

Radiation is the mode of heat transfer that happens in the absence of any medium. It is governed by Stefan-Boltzmann's law as given by the equation 2.7.

$$q = \varepsilon \sigma A (T_s^4 - T_{sur}^4) \tag{2.7}$$

where q = heat transferred by radiation

ε = surface emissivity (taken as 0.8 as in Ringsberg et al., 2005)

σ = Stefan Boltzmann constant (5.67×10^{-8} $W/m^2\cdot K^4$)

T_s = Absolute temperature of surface (K)

T_{sur} = Absolute temperature of surrounding (K)

Here ambient temperature is taken as 20°C

By using these thermal heat transfer conditions, the output of the thermal analysis (nodal temperatures) is fed as input to the mechanical analysis. Thus, this is called the sequentially coupled thermo mechanical analysis.

Mechanical analysis

Mechanical analysis in this thesis is largely dependent on the material model. Kinematic hardening is considered as hardening type of material plasticity instead of isotropic hardening. The main reason for considering this isotropic hardening is to simulate the cyclic loading effect on metals. In our case, the cladding surface after grinding is subjected to repeated ice impact pressure loads (Dassault Systemes, 2013).

Furthermore, annealing temperature is also defined under material plasticity to simulate the effects of melting and re-solidification process. At the point when the temperature of a material surpasses an annealing temperature, ABAQUS expects that the material point loses its hardening from the memory and then the effect of earlier work hardening is evacuated by setting the equivalent plastic strain to zero (Dassault Systemes, 2013).

Our expected mechanical analysis outputs are stresses and plastic strains which are denoted as S (deviatoric stress tensor) and ε^{pl} (equivalent plastic strain) and can be calculated from equations 2.8 to 2.14 (Dassault Systemes, 2013f).

$$\bar{\varepsilon}^{pl} = \bar{\varepsilon}^{pl}|_0 + \int_0^t \frac{\boldsymbol{\sigma} : \dot{\boldsymbol{\varepsilon}}^{pl} dt}{\sigma^0} \tag{2.8}$$

$$\dot{\boldsymbol{\varepsilon}}^{pl} = \frac{\partial f(\boldsymbol{\sigma} - \boldsymbol{\alpha})}{\partial \boldsymbol{\sigma}} \dot{\bar{\varepsilon}}^{pl} \tag{2.9}$$

$$\dot{\bar{\varepsilon}}^{pl} = \sqrt{\frac{2}{3} \dot{\boldsymbol{\varepsilon}}^{pl} : \dot{\boldsymbol{\varepsilon}}^{pl}} \tag{2.10}$$

$$\boldsymbol{\alpha} = \sum_{k=1}^{N} \boldsymbol{\alpha}_k \tag{2.11}$$

$$\dot{\boldsymbol{\alpha}}_k = C_k \dot{\bar{\varepsilon}}^{pl} \frac{1}{\sigma^0} (\boldsymbol{\sigma} - \boldsymbol{\alpha}) - \gamma_k \boldsymbol{\alpha}_k \dot{\bar{\varepsilon}}^{pl} + \frac{1}{C_k} \boldsymbol{\alpha}_k \dot{C}_k \tag{2.12}$$

$$f(\boldsymbol{\sigma} - \boldsymbol{\alpha}) = \sigma^0 \tag{2.13}$$

$$f(\boldsymbol{\sigma} - \boldsymbol{\alpha}) = \sqrt{\frac{3}{2} (\mathbf{S} - \boldsymbol{\alpha}^{dev}) : (\mathbf{S} - \boldsymbol{\alpha}^{dev})} \tag{2.14}$$

In thermo-mechanical analysis of cladding and grinding processes, the equivalent plastic strain ($\bar{\varepsilon}^{pl}|_0$) is taken as zero initially and contraction a:b = $a_{ij}b_{ij}$ *is denoted by* ":". The rate of plastic

flow and equivalent plastic strain rate are denoted by $\dot{\varepsilon}^{pl}$ and $\dot{\bar{\varepsilon}}^{pl}$ respectively. $\boldsymbol{\alpha}$ is the "kinematic shift" or back stress matrix, α_k is back stress component, the number of back stresses that happens during the kinematic shifts is N, C_k and γ_k are taken as material parameters, size of material surface exposed to the yield stress is denoted by $\boldsymbol{\sigma}^{\mathbf{0}}$, $\boldsymbol{\sigma}$ is the second order stress tensor, and $\boldsymbol{\alpha}^{dev}$ is the deviatoric part of the back stress (Li, 2018) & (Dassault Systemes, 2013)

The highly localized transient heat and high strength nonlinear temperature fields during both heating and cooling processes give rise to non-uniform thermal expansion and contraction, which further results in plastic deformation of the cladding and surrounding areas. This results in a permanent location of residual stress, strain, and distortion in the components. High tensile residual stress give rise to fracture and fatigue whereas the compressive residual stress results in undesired and unpredictable global and local buckling during or after cladding (Zhu & Chao, 2002).

2.5.4 Parameters Selection

The material density (ῥ), the specific heat (c) and the thermal conductivity (k) are three primary thermo-physical properties in the thermal analysis. The yield stress is referred to as the function of temperature in the thermo-mechanical simulation. Some studies show that thermal conductivity effects the transient temperature field distribution during laser related heating processes (Zhu & Chao, 2002).

By laser cladding, distortion and residual stresses of the components are reduced due to low heat input of the laser beam when compared to other joining processes such as welding. Some materials need a high-power laser beam like copper alloys processing of the laser beam is difficult due to high reflectivity and thermal conductivity (Kim et al., 2004).

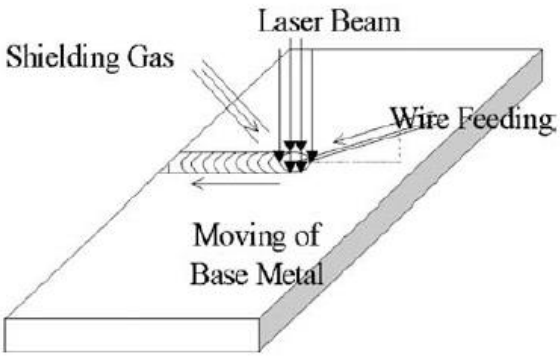

Figure 2.5: Process of laser cladding on the base metal workpiece (Kim et al., 2004).

Laser power and cladding speed i.e., the rate at which the heat source moves determine the shape of the clad as shown in Figure 2.5. As the cladding speed increases, the dilution decreases (Kwok et al., 2016). As the preheating temperature increases, the dilution increases. As the laser heat input decreases, the hardness of the clad layer increases (Kim et al., 2004). As discussed earlier, the various parameters influence the quality of cladding layer formed and by referring to the various studies such as (Gedda, 2004), parameters used in the simulation of laser cladding by moving heat source (using DFLUX subroutine) is shown in the **Error! Reference source not found.**.

Laser Cladding process parameters

The **Error! Reference source not found.** shows the parameters of the laser beam source where power is specified by the manufacturer. Here, the laser heating source is 90 % efficient in functionality.

Table 2.1: Process parameters of laser cladding using DFLUX Subroutine approach

Laser Power (rated)	2156 W
Scanning speed	3 mm/s
Power feed rate	0.618 g/s
Efficiency	90%
Current	135 A
Voltage	14 V

The various parameters of the ellipsoidal heat source model that is used to write DFLUX subroutine are given as follows:

The Goldak parameters of ellipsoidal heat source model as shown in figure 2.4 and equations 2.1 and 2.2 respectively are as follows:
a_f and a_r = 0.0005 m and 0.0017 m
b = 0.0018 m
c = 0.0030 m

The heat flux is calculated by $Q = \eta V I = 0.1*14*135$ (by taking η =10% because of loss due to material reflection).

The heat flux generated by moving laser beam is Q=190 W.

2.6 Simulation of grinding process

Grinding is a common surface finishing process where an unwanted or distorted material layer is removed from the workpiece using a grinding wheel. There are various parameters to be considered during the grinding process such as the speed of the grinding wheel, the diameter of grinding wheel, depth of indentation or cut (feed), shear force (traction), normal pressure of indentation, material removal rate, power of grinding wheel motor, friction between the grinding wheel and workpiece etc.

The typical grinding process on the surface of workpiece with the help of grinding wheel can be seen in the Figure 2.6. The wheel rotates with the speed of V_s against the surface of the workpiece moving with speed of V_w. Here 'a' is called the depth of cut which means during a single pass of the grinding wheel, 'a' amount of depth of material is removed from the workpiece. The accuracy of the grinding depends on various factors such as the abrasive property of grinding wheel, the speed of the wheel, the grinding forces and so on. The study conducted by Ringsberg et al., (2005) shows that the number of passes affects in a small amount on the final residual stresses after grinding. For instance, 1 mm of material layer can be removed in 2 cases, like two passes of 0.5 mm each or four passes of 0.25 mm each.

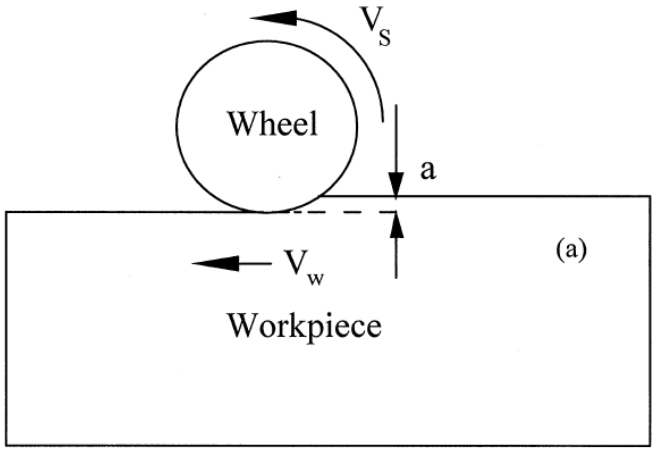

Figure 2.6: The movement of grinding wheel on the workpiece (Moulik et al., 2001)

The grinding is used to remove the uneven cladding surface layer so that the better surface finish is achieved. Also, the grinding process on the cladding layer improves the equivalent plastic strain (Li, 2018). But, in our case, we have decided to remove 0.25 mm of cladding layer as used by Ringsberg et al., (2005). So, the depth of cut is 0.25 mm and in order to achieve this, we need to consider all the parameters of the grinding process. Micro-grinding is common in industrial applications for better surface finish. But, if we go with micro-grinding, it needs a greater number of passes to achieve the required depth of cut which is time-consuming in our case (requires the creation of a greater number of steps in ABAQUS). Also, it is difficult to model the grinding wheel and assign all the necessary properties in the 2D simulation. Hence, we need to go with another alternative method that can replace the design of the actual grinding wheel but create a similar effect as that of grinding wheel. For this, the thermo-mechanical models of grinding as suggested by Doman et al., (2009).

If we analyze the grinding process, we can conclude that it is a thermo-mechanical process where the grinding forces generated by the grinding wheel removes the material. The thermal process because the heat is generated due to the friction between the grinding wheel and the surface and the mechanical processes because of the grinding forces which are a combination of the normal pressure exerted by the wheel on the workpiece and the traction load which is along the direction of motion of the wheel. So, it is required to create both frictional heat and the grinding forces in the simulation environment. The frictional heat generated as the wheel moves can be considered as the moving rectangular heat flux as shown in the Figure 2.7.

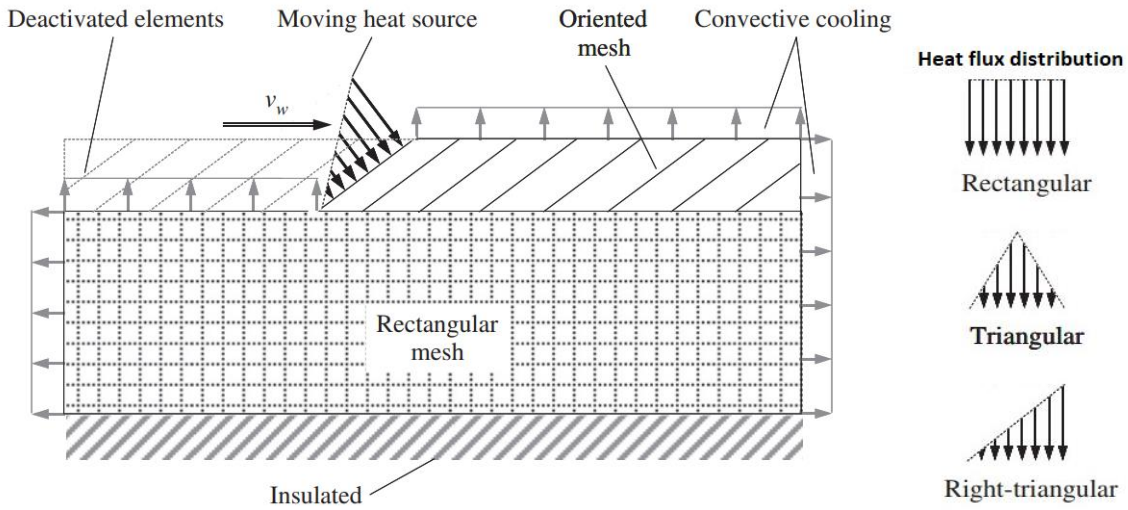

Figure 2.7: Moving heat source model during thermal simulation of grinding process (Doman et al., 2009)

The grinding forces are the combination of the moving normal pressure (rectangular distribution) and the moving shear (traction) pressure as shown in the Figure 2.8.

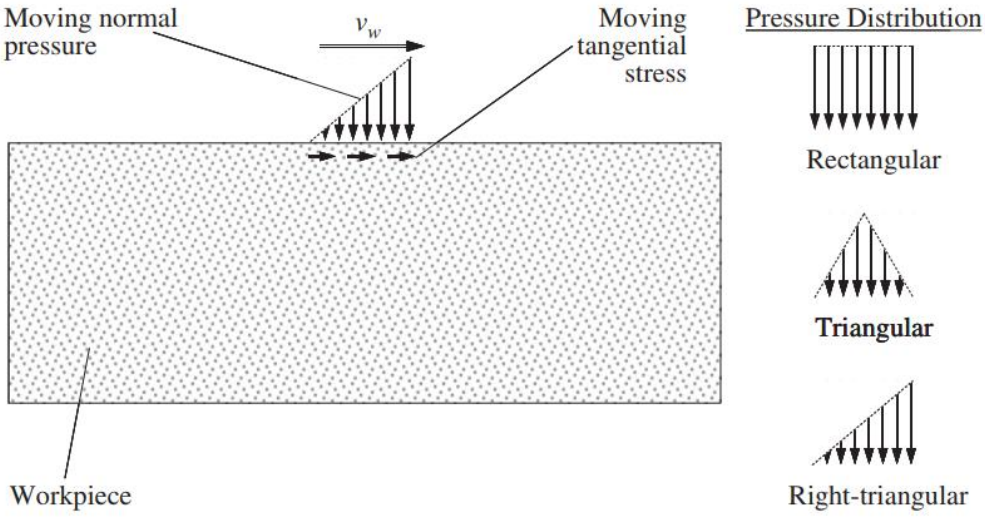

Figure 2.8: Moving pressure-load distribution model during mechanical simulation of grinding process (Doman et al., 2009)

The combined effect of the rectangular distribution of heat flux along with rectangular distribution of normal pressure and traction pressure indicates the grinding operation.

3 Methodology

The current chapter deals with the methodology adopted to simulate both the laser cladding process and grinding process which is followed by the ice-propeller interaction (impact load) analysis. At first, the selection criteria of the Finite Element (FE) simulation software is discussed. The material models for both substrate and cladding are constituted which is followed by a discussion of key process parameters that are necessary to simulate the moving heat source and coating of cladding material on the substrate. All the necessary steps in pre-processing and post-processing is elaborated for a better understanding of the overall simulation processes.

3.1 Selection of Software

This thesis work requires more than one software to simulate the laser cladding and grinding process. The basic software to run the simulation is ABAQUS. Also, the other software were required to link FORTRAN to ABAQUS. The material databases JMatPro software and Cambridge Engineering Selector (CES) material selection software were used to take some temperature dependent material properties.

3.1.1 FE software

As mentioned in the previous sections, the two approaches were employed in this thesis work. One was to model the moving heat source using a 3D FE model with DFLUX subroutine to simulate the laser cladding process. Another one was to use 2D FE model to show both laser cladding and grinding process. For achieving both, ABAQUS 6.13-3 of Dassault Systemes was used because of the wide variety of simulation strategies available. Further, the subroutine code can be used by interlinking ABAQUS with other software for simulation of moving heat flux. Also, the software has better visualization capability for displaying the interactions that occur during the processing of the results.

3.1.2 Software for linking ABAQUS with FORTRAN

As previously discussed, the subroutine code written in FORTRAN language has to be linked to ABAQUS 6.13-3 to model moving heat source. This was achieved by using specific versions of software namely Microsoft Visual Studio (Professional 2012) and Intel Parallel Studio (SP1-2013). After lots of effort, we found that these versions support well for running the subroutine codes in ABAQUS 6.13-3.

3.2 Procedure for simulations

The main scope of the thesis is to enhance the performance of marine propellers against ice impact loads by laser cladding technology. Here, the cladding of suitable material has to be deposited on the substrate with the help of a high energy laser beam. This process has to be analysed in the simulation environment to study the effect of impact load of ice before cladding and after cladding. As discussed in the theory, the laser cladding surface is filled with a non-uniform bulged like structure which needs to be grounded for better surface finish. Hence, the grinding process must also be simulated to see the effect of the surface grinding of the cladding layer. Once, the properly cladded and grounded propeller is ready, it is subjected to the impact

loads (identical to the impact loads during ice-propeller interaction) to see how the performance of the marine propeller is enhanced.

In this thesis, different approaches were used to simulate all the above-mentioned processes systematically in the simulation environment. At first, the laser cladding was simulated with two different approaches that will be discussed in the next sections. Later on, the grinding of the cladding layer was carried out by the application of grinding forces from the grinding wheel. Once the grinding was completed, the propeller was subjected to the impact load in the form of pressure loads with a magnitude as that of the ice loads in the sea waters. Then, the thermal and mechanical analysis was carried out to study the before and after effects of the cladding, grinding and impact loading processes.

3.2.1 Material Data for Substrate and Cladding

One of the important and challenging tasks in this thesis was to set up the material models for both substrate and cladding. This is because of the necessity of collection of temperature dependent physical and mechanical properties of both substrate and coating in the ABAQUS which was a difficult task because of uncertainty in the data. As the main idea of the current thesis is to focus more on the methodology of laser cladding and grinding simulations, some materials were assumed systematically, and some were collected from the sources even though these materials are not used in propellers (for instance, 900 A Steel). The various materials that were used for both substrate and cladding are discussed in the previous sections. In the current thesis, we have considered two materials as substrate and one material as a coating.

Also, as used by Ringsberg et al., (2005) in their studies, non-linear isotropic and kinematic hardening model is used to simulate the material characteristics and to achieve this annealing material behavior and phase transformation in the substrate material is taken into account**.** Many studies interpreted that non-existing data of material properties at high temperature have very nearly no effects on the distortion and residual stresses (Zhu & Chao, 2002).

Material for Substrate: 900 A Steel

In the railway industry, the UIC grade 900A steel is widely used due to better strength, economical and better wear resistance. This material was used as a substrate by Ringsberg et al., (2005) along with Stellite as a coating material in their study of laser cladding and grinding effects on rolling contact fatigue of rails. Though in actual conditions it is not used as a substrate material for the propeller, the data are used just to show how the cladding behaves when compared to the actual NAB that is used as the substrate material for the propeller. The density of 900 A steel is 7850 kg/m^{3}and the melting point is 1470^{o}C The chemical composition is collected from Maya-Johnson et al., (2015) and is shown in

Table 3.2: Material properties of 900 A Steel at various temperatures (Ringsberg et al., 2005). The mechanical and thermal properties that collected from Ringsberg et al., (2005) are shown in **Error! Reference source not found.**.

Table 3.1: Chemical composition (weight, %) of 900 A Steel (Maya-Johnson et al., 2015)

Material	C	Si	Mn	P	S	Cr
900A steel	0.736	0.27	1.056	0.032	0.023	0.026
	V	Cu	Ti	Ni	Mo	Fe
	0.003	0.002	0.016	0.021	0.006	Bal.

Table 3.2: Material properties of 900 A Steel at various temperatures (Ringsberg et al., 2005)

Material	λ (W/m°C)	α (10^{-6}/°C)	E (GPa)	υ	σ_y (MPa)	c (Ws/kg°C)	T (°C)
900A steel	48	1.33E-5	210	0.30	441	490	20
	32	1.58E-5	115	0.37	179	712	600
	10	1.74E-5	20	0.45	20	1000	1000
	10	1.74E-5	20	0.45	20	1000	1500

Material for Substrate: NAB

NAB is commonly used substrate material for propellers because of the properties such as high corrosion resistance and mechanical strength. But, NAB made propellers suffers from repeated impact loads caused by ice-propeller interaction which gives rise to need for the enhancement of the properties of propellers. Propellers made of NAB are basically limited by corrosion fatigue which is further damaged by Cavitation erosion (Hyatt et al., 1998). Though NAB is extensively used in the marine industry, it is difficult to get the temperature dependent properties of the actual alloy. Hence, the nearly same composition of C95400 was extracted from JMatPro software by assuming some of the uncompleted properties (using linear extrapolation) to create the required temperature dependent properties of NAB. Also, the plasticity properties such as yield stress and plastic strain are extracted from the data of 900A steel (Ringsberg et al., 2005) and are embedded with the properties of NAB. The conductivity properties are assumed based on linear interpolation with respect to the range as specified in CES material selection software. Though this is not a proper NAB material, it is used to see how the cladding of Stellite on NAB affects the performance of the propeller.

Also, Copper alloy processing of the laser beam is difficult due to high reflectivity and thermal conductivity. Hence, the suitable material composition of NAB has to be chosen that is good for laser cladding (Kim et al., 2004). The density of this NAB is 7600 Kg/m^3 and annealing temperature is 1055^{o}C which is a few degrees more than the melting point of 1050 ^{o}C. The chemical composition and various physical and thermal properties as extracted from JMatPro and Ringsberg et al., (2005) are shown in Table 3.4: Material properties of C95400 NAB at various temperatures (JMatPro and Ringsberg et al., 2005) and **Error! Reference source not found.**.

Table 3.3: Chemical composition(weight%) of C95400 NAB (JMatPro software)

Material	Al	Ni	Fe	Mn	Cu
NAB (C95400)	11	2.5	4	0.5	82

Table 3.4: Material properties of C95400 NAB at various temperatures (JMatPro and Ringsberg et al., 2005)

Material	λ (W/m°C)	α (10^{-6}/°C)	E (GPa)	υ	σ_y (MPa)	c (Ws/kg °C)	T (°C)
NAB (C95400)	62	1.75E-005	132.8	0.34	441	444.5	20
	98.83	2.08E-005	98.45	0.37	179	533.9	600
	106.4	3.73E-005	2.90	0.45	20	3659.26	1000
	112.91	4.70E-005	2.90	0.45	20	684.2	1500

Material for Cladding: Stellite (Co-Cr alloy)

Cobalt-Chromium alloy which is similar to Stellite 21 is used for cladding because of the desired properties such as better resistance against corrosion, oxidation, and wear. Also, it has good ductility, good resistance against repeated impact loads and reduces pitting. Thus, this is extensively used for turbine blades, propeller vanes, and rail wheels and is durable (Ringsberg et al., 2005). The density of Co-Cr alloy is 8332 Kg/m^3 and the melting point temperature is 1350^{o}C which is taken as annealing temperature as well. The chemical composition of Stellite 21 is as shown in

Table 3.6:Material properties of Stellite at various temperatures (Ringsberg et al., 2005). and is collected from Ganesh et al., (2010). Ringsberg et al., (2005) has used Stellite as a coating material in their study of laser cladding of the railway steels and thermo-mechanical properties are collected from the paper which is shown in **Error! Reference source not found.**.

Table 3.5:Chemical composition (weight%) of Stellite Co-Cr alloy (Ganesh et al., 2010).

Material	C	Cr	Ni	Mn	Si	Mo	Fe	Co
Co-Cr Alloy	0.26	26.3	2.8	0.65	1.88	5.53	1.4	Bal.

Table 3.6:Material properties of Stellite at various temperatures (Ringsberg et al., 2005).

Material	λ (W/m°C)	α (10^{-6}/°C)	E (GPa)	υ	σ_y (MPa)	c (Ws/kg°C)	T (°C)
Co-Cr alloy	48	1.10E-5	207	0.30	494	490	20
	32	1.36E-5	146	0.37	258	712	600
	10	1.52E-5	20	0.45	20	1000	1000
	10	1.52E-5	20	0.45	20	1000	1500

3.3 Laser cladding simulation approaches

This section includes the two different approaches of simulating laser cladding process. The first one is called 3D approach which uses 3D model of substrate and cladding, and the moving heat source is modelled using DFLUX subroutine. The second one is known as 2D approach which used 2D model and the temperature is applied at nodes.

3.3.1 Laser cladding simulation in 3D

It is a transient laser cladding process simulation using the DFLUX subroutine. It starts with the creation of the geometrical model and meshing. After this, the time-dependent steps such as boundary conditions, loads, pre-defined loads, interactions are created. Then the moving heat source is modeled using DFLUX Subroutines and is linked to ABAQUS. Then the coupled thermo-mechanical analysis is carried out. The results thus obtained are analyzed to understand

the performance of the propeller surface after laser cladding. Figure 3.1 shows the flow chart of the steps employed in this approach of laser cladding.

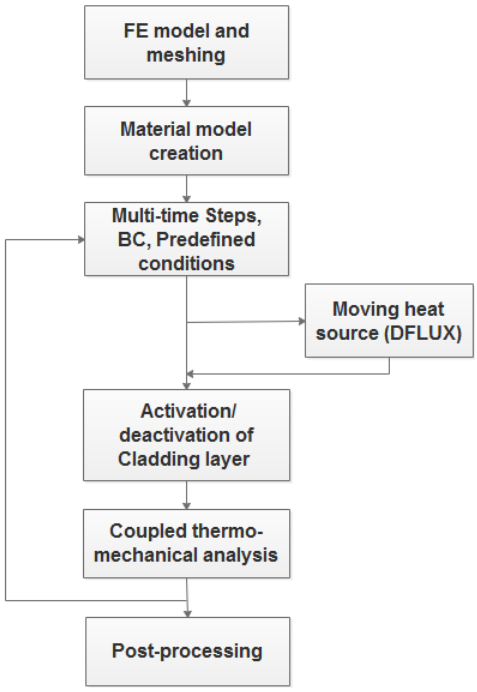

Figure 3.1: Flow chart describing the steps in laser cladding in 3D using DFLUX Subroutine approach

FE model geometry

The first step in the simulation procedure was to create the geometrical model which is a combination of both cladding and substrate by placing a plate of cladding on the plate of the substrate as shown in the Figure 3.2. Both the coating and substrate are 10 mm long and 16 mm wide. The thickness of cladding is 1 mm and that of the substrate is 10 mm. The heat affected zone (HAZ) was assumed to be 2.5 mm. The assembled model showing cladding layer, HAZ and substrate can be seen in Figure 3.2. The coordinate system is at the centre which acts as the reference point for the movement of the laser beam during simulation that means it helps to write the user subroutine by taking coordinates of the origin point as a reference.

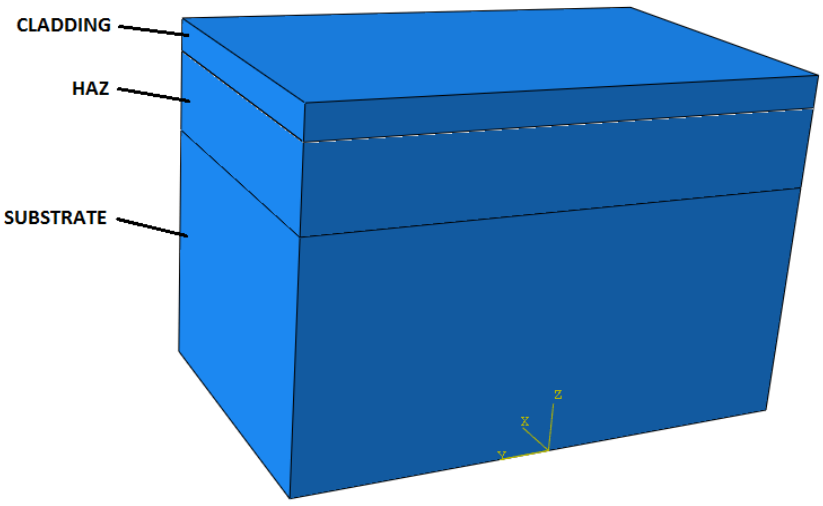

Figure 3.2: Geometry model for cladding simulation in 3D using DFLUX Subroutine approach

These are the choices that were made in ABAQUS software to simulate the Laser Cladding process in this approach.

ABAQUS/Standard

There are two structural analysis types (Element library) in ABAQUS namely Standard and Explicit. The problems which are smooth, nonlinear can be solved using ABAQUS/Standard. As the simulation of laser cladding is of non-linear type, the Standard (Implicit) analysis was used in our work.

Transient Analysis

There are both steady-state and transient types of analysis in heat transfer. In our work, the heat flux to be modelled is time-dependent. Also, the thermal loads generated as the laser beam moves varies with time. Hence, this is a transient type of heat analysis.

Nonlinear Analysis

As the stiffness of the structure changes during thermal loading, the non-linear structural analysis is considered. Also, the behaviour of both coating and substrate is non-linear hence, the non-linear analysis is necessary to obtain the convergence results.

Coupled temperature-displacement analysis

In accordance with the scope of the thesis, it is required to find both the thermal and residual stresses of the clad layer formed between the coating and substrate. The coupled thermo-mechanical approach commonly called as temperature-displacement analysis in ABAQUS was used.

Mesh and Element types

There are a variety of element types available in ABAQUS for different analysis types and strategies. The 3D models have a continuum (Solid) element type in the mesh family. This element consists of six faces and eight nodes at the corners of the crystal lattice. During analysis, the fundamental variables that are calculated are degrees of freedom (DOF). In stress/displacement analysis, the degrees of freedom are translations at each node. As we use coupled temperature-displacement type of analysis in our simulation, the nodes have both thermal and mechanical degrees of freedom. Therefore, the element selected for our simulation is C3D8T which is linear 8- node brick element (C3D8). The meshing used in this analysis is shown in Figure 3.3.

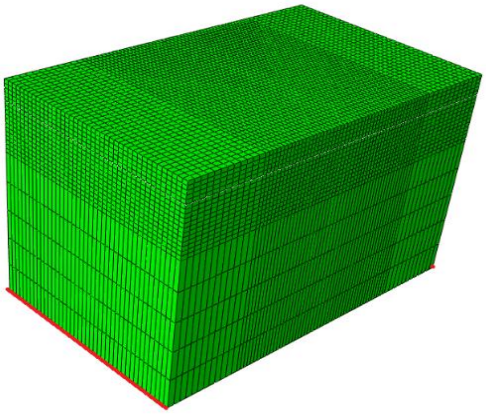

Figure 3.3: Meshing and mechanical BC for model used in cladding simulation in 3D using DFLUX Subroutine approach

Thermal and Mechanical boundary conditions (BC)

In mechanical BC, both the bottom edges are fixed in length wise to have zero DOF for displacement as highlighted by red line in Figure 3.3. This influences the thermal BC as well.

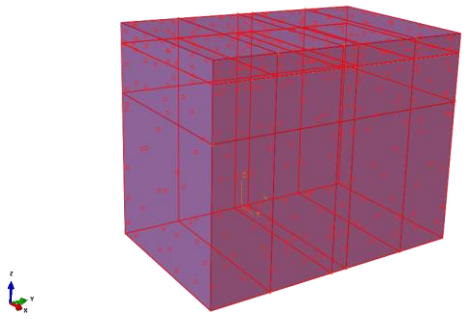

Figure 3.4: Thermal BC for model used in cladding simulation in 3D using DFLUX Subroutine approach

In the thermal BC, the entire model is subjected to convection and radiation type of BCs as shown in Figure 3.4. The surface film condition (convection) has the film coefficient of 10 W/(m^2K) at sink temperature of 20^{o}C and surface radiation has emissivity is 0.8 at an ambient temperature of 20^o C.

Procedure for laser cladding simulation

The procedure of simulation was divided into a series of steps which makes the model to be ready for the processing of simulation. The initial step began with the assigning necessary BCs and predefined loads constant throughout the region (ambient room temperature of 20^{o}c) to the model. Next step was to deactivate all the elements of the cladding layer (using model change interaction) to signify the absence of cladding during the preheating of the substrate to 100^{o}c. Once, the preheating was completed, the cladding layer was activated again (using the model change interaction) to signify the presence of cladding layer in all the fore coming steps.

The next step was to show the movement of a laser beam on the cladding layer. This creates a need to generate thermal loads which act as a heat input. To achieve this, the DFLUX subroutine code (Techniques, 2017) was written in FORTRAN language which generates the

time-dependent distributed body heat flux (for DFLUX code, see Appendix C). This body heat flux was applied on the workpiece as the user-defined loads as it moves. This was carried out with one cycle of heating step and cooling step in one path on the model. The workpiece underwent heating for 10s for each path (from one end to another end) followed by cooling of 5s. In this approach, we have considered 5 paths of moving heat source (double ellipsoidal model of heat source). The moving heat source in the first path, third path and fifth paths are shown in Figure 3.5, Figure 3.6, and Figure 3.7 respectively.

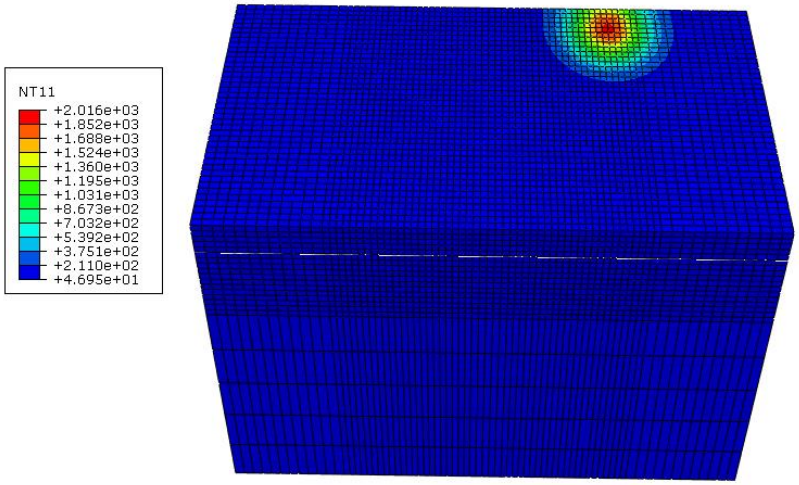

Figure 3.5: Heat source moving in 1st path during cladding simulation in 3D using DFLUX Subroutine approach

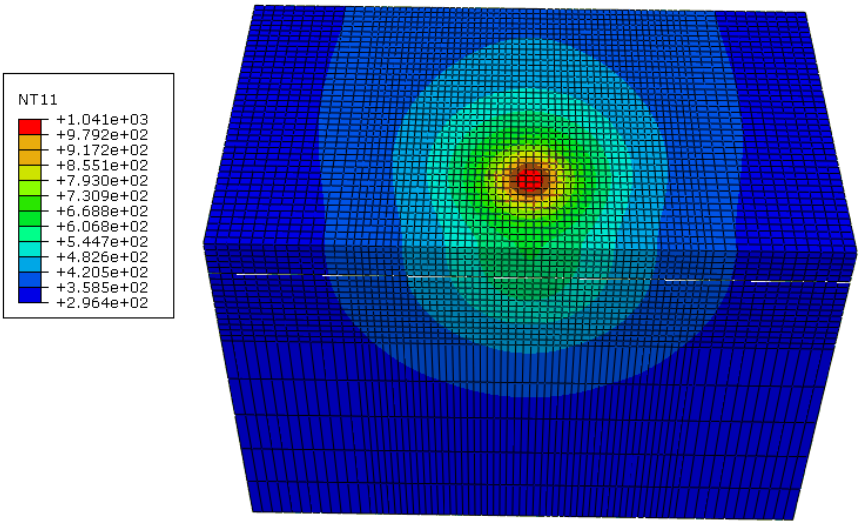

Figure 3.6: Heat source moving in 3rd path during cladding simulation in 3D using DFLUX Subroutine approach

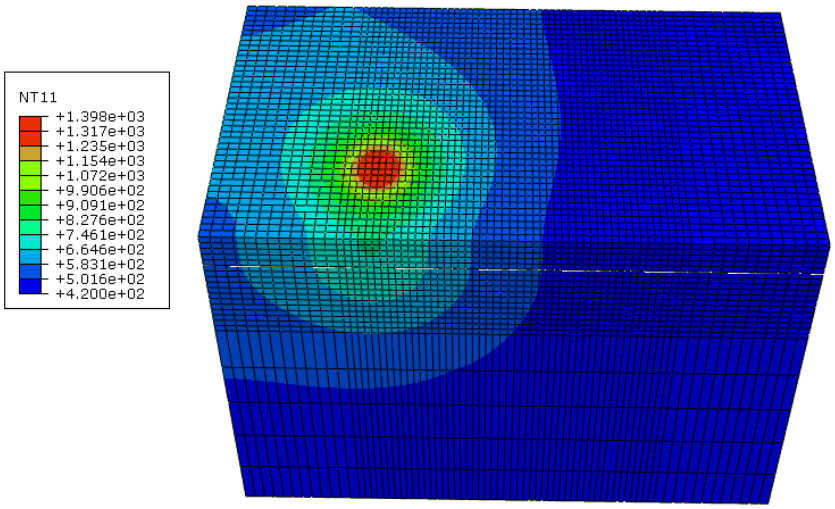

Figure 3.7: Heat source moving in 5th path during cladding simulation in 3D using DFLUX Subroutine approach

Once all the steps were created, the field outputs of analysis were requested to get the simulation results in the forms of temperatures, residual stresses, and equivalent plastic strain. After this, the job was created to run the simulation and get the desired outputs.

After the simulation, the output database file (.odb) was generated which has all the necessary outputs as requested earlier. The thermal simulation outputs are nodal temperatures (NT11). One problem with this type of approach was difficulty in controlling the nodal temperatures and recording the magnitudes at a specific point in the model. From the nodal temperature result, laser beam temperature was not constant throughout the path of laser beam and gradient of temperature at the interface was high. All these factors created the necessity to go for any other alternative method of laser cladding simulation that can try to eliminate these problems.

3.3.2. Laser Cladding simulation in 2D

The flow chart showing the sequence of steps in sequentially coupled thermo-mechanical simulations of cladding and grinding process (will be explained later) is seen in Figure 3.8. These are the choices that were made in ABAQUS software to simulate the laser cladding and grinding process in this approach. Similar to the previous approach, ABAQUS/Standard was used because of the same kind of problem-solving. Due to the requirement of moving heat source, the transient heat analysis was considered. Because of a change in material properties at each point due to change in temperature, it is a non-linear analysis.

This is a sequentially coupled thermo-mechanical analysis as it was required to find both the nodal temperatures and residual stresses of the clad layer formed between the coating and substrate. The mesh used in both thermal and mechanical analysis remains the same. At first, the thermal analysis was carried out to find the nodal temperatures which are obtained as an output database file. This file was used as input for the mechanical analysis which acts as the thermal loads. Though the stresses and strain generated during the mechanical simulations were influenced by the results of thermal analysis, the temperatures are not at all influenced by any

stresses. This method was used by Ringsberg et al., (2005) during their simulation of the cladding process in the study of rolling contact fatigue of rails.

As the modelling of geometries are easier in 2D (have elements only in two planes), the computational time is comparatively less in 2D than 3D. This approach gives temperature control unlike 3D approach, 2D models were considered in this approach of simulation for cladding, grinding and ice-propeller interaction.

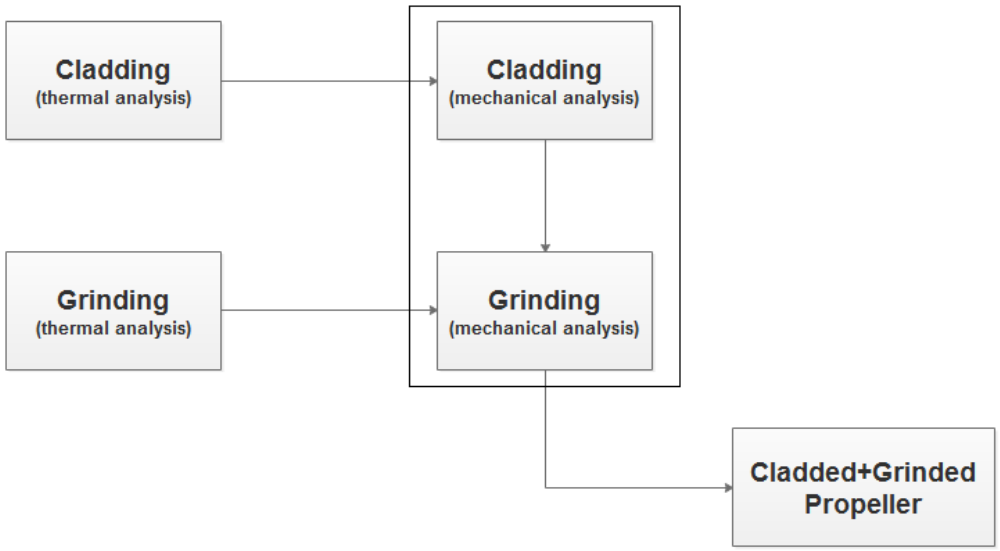

Figure 3.8: Flowchart of the sequentially coupled thermo-mechanical simulations of Cladding and Grinding Process using 2D models

FE model geometry

In this thesis, the end part of the propeller (tip) was taken for the study and the geometry of the model is shown in the Figure 3.9. The 2D geometry has a length of 200 mm where the substrate thickness (t_s) is 20 mm and cladding layer thickness (t_c) is 2 mm as verified with convergence study by Li (2018) in his master thesis work.

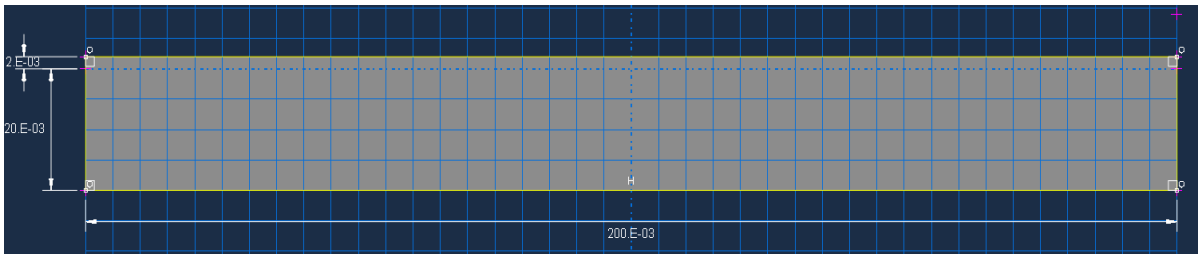

Figure 3.9: 2D FE model geometry used in both cladding and grinding simulation

The

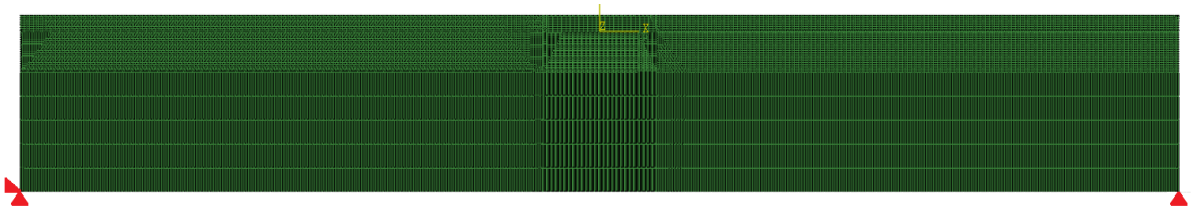

Figure 3.10 shows the meshing of FE model which includes the cladding layer, heat affected

zone, and the substrate layer. Here, the middle region has the finer mesh density compared to the other regions of the model to apply ice induced impact loads and to collect the results which are to be analyzed. This was to get the comparatively accurate results of nodal temperatures, residual stresses, and equivalent plastic strain. The entire cladding layer was divided into 40 identical blocks of 5mm each. There are 8 vertical elements in a cladding layer of 0.25 mm each. This was used to achieve the thermal energy input for a time period of which indicates the 5mm/s scanning speed of laser beam. (Man et al., 2000). The rate of moving cladding beam(laser) determines the shape of the clad (Kim et al., 2004).

Mesh and Element Types

The

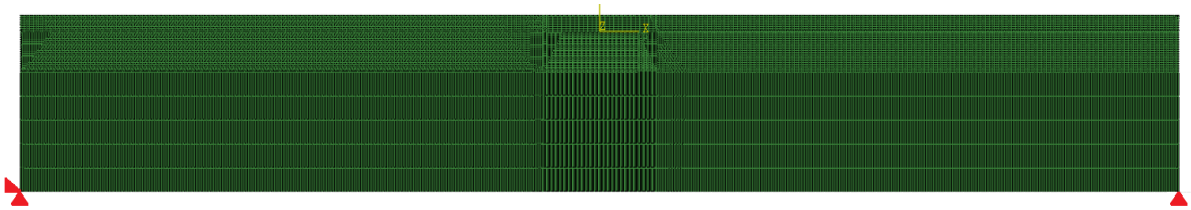

Figure 3.10 shows the meshing of the FE model which has 27720 elements in total. There are 6720 elements in the cladding layer, 16800 elements in Heat affected zone (HAZ) and 4200 elements in the substrate. In the thermal analysis, DC2D4 element type was used for the whole model. In ABAQUS, it is a 4-node linear quadrilateral heat transfer element type that is used to determine the nodal temperatures. In mechanical simulations, CPE4R element type was used for the whole model. It is a 4-node plane strain bilinear element (with reduced integration and hourglass control) used to determine the residual stresses and equivalent plastic strain. Also, the geometric order of elements is quadratic for efficient simulation.

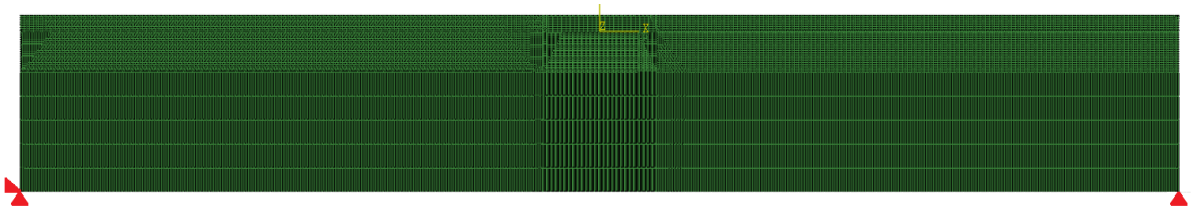

Figure 3.10: Meshing and mechanical BC for 2D model used in cladding simulation

Thermal and Mechanical Boundary Conditions

As the model is subjected to various thermal loads including the heat convection and radiation, it was necessary to have some thermal boundary conditions. These thermal BCs were fixed in accordance with the mechanical BCs. In convection BC, film coefficient was 10 W/(m^2K) at sink temperature of 20^o C. In radiation BC, emissivity was 0.8 at an ambient temperature of 20^o C. The thermal BC was changed as the cladding layer was deposited block after block, for instance, the boundary conditions of both Surface film condition and surface radiation when the cladding of 1st block and 20th block is completed are shown in Figure 3.11 and Figure 3.12 respectively.

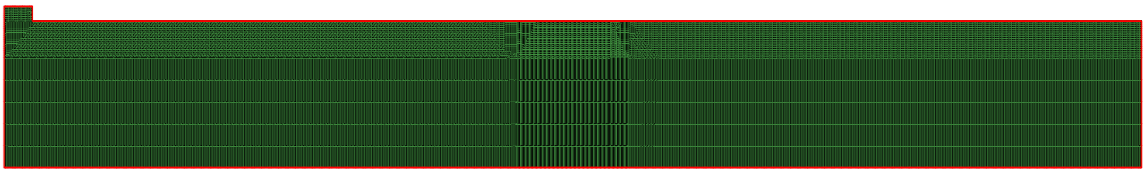

Figure 3.11: Thermal BC when the 1st cladding block is deposited on the 2D substrate during cladding simulation

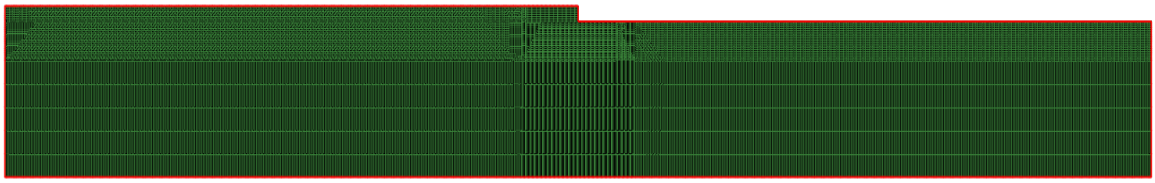

Figure 3.12: Thermal BC when the 20th cladding block is deposited *on the 2D substrate during cladding simulation*

As the model is subjected to various types of loads and pressures, it was required to have some restrictions for the movement of the model in different planes. Such mechanical BCs for the entire FE model is visible in red color in Figure 3.10. At first, the left bottom corner node was fixed in all DOF. Then, the right bottom corner node was fixed in the vertical direction so that the model does not have the vertical movement during both cladding and grinding processes.

Simulation procedure for laser cladding

In the beginning, both cladding and substrate layers were created in the same FE model which is similar to placing a plate of cladding on the plate of the substrate. This makes initial steps of both thermal and mechanical analyses to include the deactivation of all elements of the cladding layer by using a technique called 'death of elements', known as model change option in ABAQUS. Then, the thermal simulation began with preheating the substrate to 100^{o}C which contributed to reduction of temperature gradient for the upcoming blocks. Kim & Peng (2000) observed that preheating of the substrate can subsequently, increase the compatibility between the cladding and substrate layers which in turn helps in reducing the generation of residual stresses in the cladding layer and heat affected zone at the interface of cladding and substrate.

After this, each block was deposited one after another at steps which signify the cladding process along with the application of uniformly distribute heat source as prescribed node temperatures on the same block. This was carried out using a technique called 'birth of elements', known as a model change option. Once all the 40 cladding blocks were deposited, the cooling step was carried out to bring the cladding layer to room temperature as specified in Ringsberg et al., (2005). This shows one cladding and temperature cycle for an entire model. Temperature and cooling rate are the main parameters that affect the properties of the clad layer and heat affected zone. Duraiselvam et al., (2006) based on their studies concludes that heat treatment is employed to eliminate porosity and cracks effectively between the clad layers. Zhu & Chao (2002) suggest that the highly localized transient heat and high strength nonlinear temperature fields during both heating and cooling processes give rise to non-

uniform thermal expansion and contraction, which further results in plastic deformation of the weld and surrounding areas. This results in a permanent location of residual stress, strain, and distortion in the components.

The four temperature cycles were considered because the successive cladding tracks conduct heat in transverse directions. The temperature of the first cladding cycle was 1500℃ which is more than the melting point of the substrate material. The temperature of the second cladding cycle was 1500℃ and due to the conduction of heat in transverse directions on first cladding track, it was guessed to drop to 1150℃. Kim & Peng (2000) showed that the temperature near the melt pool changes at a faster rate than away from the melt pool. As the cladding speed increases, the cooling rate also increases. But, the cooling rate decreases with increase in preheating temperature. The effect of heat from the successive third and fourth cladding tracks was presumed to be 400℃. There was no need to consider next heating tracks after the fourth track because they have a very less or negligible effect on the first track. So, the temperatures for different cycles were T_1=1500℃, T_2=1150℃, T_3=T_4=400℃ respectively. The field outputs were requested at each step to get the nodal temperatures for four different temperature cycles. This was found in an object database file (.odb) after thermal simulation and this file was used in predefined fields as the thermal loads during mechanical simulation of the cladding process.

In the mechanical simulations, the mechanical boundary conditions were defined in the initial steps. Further, the thermal loads were extracted from the .odb file of thermal analysis in the form of nodal temperatures which acts as actual loads required for mechanical analysis. In the mechanical analysis, 'NLGEOM' option was selected to compensate for geometric nonlinearities as carried out by Ringsberg et al., (2005). As each block of cladding was deposited using the model change option and ADD=WITH STRAIN. In addition to this, the thermal loads were read from the .odb file and were applied to each node in that particular step. This continued for all the 40 blocks which showed the actual cladding process which is a simultaneous application of heat and cladding powder or wire. This completes the mechanical simulation and the new .odb file was generated to get the outputs of mechanical analysis which are longitudinal and shear residual stresses. These residual stresses were used for further analysis to investigate the effectiveness of cladding layer formed. The longitudinal residual stresses (S11) determines the nature (tensile or compressive) of stresses to estimate the life of substrate after laser cladding and the shear residual stresses (S12) determines the bonding of both substrate and cladding at microstructure level for better performance (Li, 2018).

Ringsberg et al., (2005) suggests that the final residual stress state in surface coated components is influenced by the post-treatment processes like annealing and grinding. Hence, the annealing temperature was added during the constitution of material models of both cladding and substrate. Along with this, the grinding process was carried out on the cladding layer which will be discussed in the next sections.

3.4 Grinding Simulation

This section explains the methodology employed in the simulation of the grinding process on the cladding layer as carried out on a 2D model with birth/death of elements technique. The flow chart of both cladding and grinding simulations can be seen in figure 3.8 to understand the sequence of grinding simulation.

Once the coating material was cladded on the substrate, the residual stresses, and the equivalent plastic strain increased because of the exposure of the cladding layer for 4 different temperature cycles as mentioned in Ringsberg et al., (2005). The various variables such as speed of laser beam power, laser scan speed, powder feed rate, material properties and others affect the quality of the cladding layer formed. Various authors including Ringsberg et al., (2005) and Mustaq et al., (2012) infers that for the components which are coated, the residual stresses after the laser cladding (either compressive or tensile near the surface) are controlled by the combination of coating and substrate materials, coating thickness, pre-heat treatment, cooling rate, welding time and the number of passes. Even though the simultaneous heating and cooling is carried out to reduce this effect, it induces the localized volumetric changes (Anca et al., 2011). This results in non-uniform cladding a surface which further requires the removal of surface material to have a better and almost uniform surface finish. The suitable manufacturing method to achieve this is 'grinding process'.

The grinding process includes the application of grinding forces on the cladding layer. This is done with the help of grinding wheel which applies the grinding forces (both normal pressure and traction load) on the cladding layer. Also, heat is generated due to the friction between the grinding wheel and the cladding layer. The entire grinding process has both mechanical and thermal effects on the cladding layer. The grinding process has various variables such as grinding wheel diameter, the material of grinding wheel, the speed of the wheel, the depth of cut, the power of the motor used for grinding wheel and others. The various research tells that it is required to model the actual grinding wheel by keeping all the parameters in mind which is possible by using ABAQUS/Explicit. But, in this thesis, the process of cladding is carried out using ABAQUS/Standard and is difficult to switch to ABAQUS/Explicit for grinding process. Even though there are possibilities to move from ABAQUS/Standard to ABAQUS/Explicit, which requires the restarting of the simulation. This results to lose all the previous conditions of cladding simulation such as the meshing, properties of the cladding layer, solver types, etc. which makes the cladding layer a new model which is not at all feasible for grinding simulation.

Hence it was necessary to find an appropriate method to simulate the grinding of the cladding layer in continuation with the previous cladding simulation. Also, the model used here is 2D which cannot use the 3D grinding wheel. Hence, the approach of combined finite element thermal and mechanical models explained by Doman et al., (2009) is used which was explained in the previous chapter. At first, the uniform rectangular heat flux distribution was applied in the form of boundary conditions which signifies the heat generated due to the friction and other grinding forces. Next was to generate the effects of grinding forces which includes the normal pressure (contact load) and tangential stress (traction load). This was achieved by applying these two stresses in the form of loads at each point of contact between the wheel and the cladding layer.

As already discussed before, it is required to grind the previously cladding layer which requires the cladding model from previous simulations. To achieve this, the output database file (.odb) which has both the thermal and mechanical simulation file of overall cladding process was used as an input for the simulation of mechanical analysis of the grinding process. Also, as mentioned above the heat generated due to the frictional effect of grinding forces have to be taken into account in the analyses. So, the separate thermal analysis was carried out on the

combined model of cladding and substrate with the predefined temperature (magnitude of the rectangular heat flux) that will be explained in upcoming sections.

Element types and meshing

The same FE model with 200 mm length which is divided into 40 blocks of cladding with 5mm each was used for grinding simulation. There are 8 vertical elements in the cladding layer of 0.25 mm each (total of 2mm of cladding layer vertically). So, we have decided to remove 0.25 mm of cladding layer which means 1 element vertically for grinding. The meshing can be seen in the Figure 3.13.

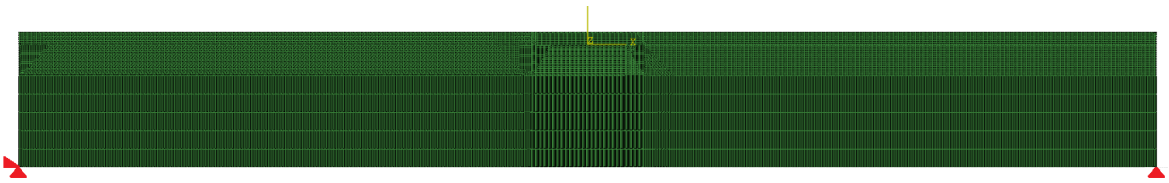

Figure 3.13: Meshing and mechanical BC for 2D model used in grinding simulation

The analysis was carried out using ABAQUS/Standard and the geometric order of elements were quadratic for efficient simulation. The calculation is of quad-reduced integration type which can be seen in the figure. In thermal simulations, element type used was DC2D8 which is an 8-node quadratic heat transfer quadrilateral that is used for heat transfer analysis. For mechanical simulations, the element type used was CPE8R which is an 8-node biquadratic plain strain quadrilateral that is used for mechanical analysis.

Thermal and Mechanical Boundary Conditions

As the cladding layer is subjected to both convection and radiation type of heat transfer, these must be considered as boundary conditions. In the convection BC, the film coefficient was 10 W/(m^2K) at sink temperature of 20^o C. In the radiation BC, emissivity was 0.8 at an ambient temperature of 20^o C. These BCs were fixed based on the mechanical BC and it was changing as the grinding process proceeded in different steps. The thermal BC (highlighted by red colour) before the grinding process can be seen in Figure 3.14.

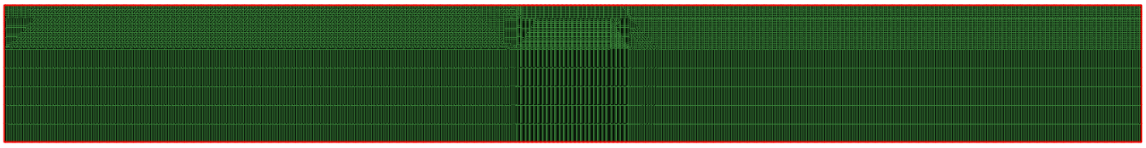

Figure 3.14: Thermal BC for 2D model used in grinding simulation

The mechanical BC is required as the model was subjected to various grinding forces which might alter the position of the model during the loading. The same mechanical BCs (as shown in Figure 3.13) were used in both cladding and grinding simulation where the left corner node is arrested in all DOF and right corner node is arrested in a vertical direction.

Simulation procedure for grinding

After overall cooling for cladding, the steps for grinding were added in the same file. The actual simulation started with the thermal analysis where the temperature of 580^{o}C was applied uniformly on the cladding surface as the nodal temperatures which are similar to the heat

generated during the actual grinding process due to various forces. As discussed in the literature study conducted by Doman et al., (2009) suggest that heat distribution can be rectangular, triangular and right-triangular. Here, we have considered the rectangular model of heat distribution which is better in getting the uniform heat flux distribution on one complete block of grinding during the simulation. The thermal analysis was concluded with uniform heat distribution of heat flux on all the 40 blocks of the cladding layer. After this, the output file (.odb) of the thermal analysis was applied as a predefined field in the mechanical simulation of the grinding process.

In the mechanical analysis, it was required to generate the grinding forces similar to that of a real grinding wheel. It was a challenging task to estimate the parameters such as the speed of the grinding wheel, the magnitude of grinding forces, the material of grinding wheel, etc. Also, finding the magnitude of these loads was difficult as these forces are dependent on other factors as discussed before. So, the necessary assumptions were made by observing the nature of grinding forces and they are mainly normal pressure and traction load. For this, the rectangular model of uniformly distributed pressure (normal to the surface) and moving traction load (along the direction of movement of grinding wheel) were considered to derive the mechanical effect of grinding wheel. A similar study has been made by Ringsberg et al., (2005) on grinding simulations on cladding which will be helpful in modeling the forces. These loads are abrasive in nature and can be modeled using the uniformly distributed load with contact load (normal) of p_0/σ_y=0.125 and traction load μ=0.30. The calculations for both the loads are discussed in Appendix A.

Once the loads were generated, it was required to simulate the material removal process which was achieved by using the model change in ABAQUS. Here, the deactivation of elements was carried out step by step to show the actual grinding process. The mechanical simulation started with the creation of the surfaces for grinding which is shown (red colour) in figure 3.18. As already discussed, this is the surface on which the grinding forces are applied which means the material is removed from the top layer of cladding till this surface.

After this, the steps were created separately by keeping each block in mind to apply loads and deactivation of elements using ‘element death’ technique. The grinding process had the movement of the wheel for 1 s for each block which means the grinding wheel takes 1s to finish the grinding process of 1 block of 5mm giving the depth of cut of 0.25 mm on the cladding layer.

The predefined fields are nodal temperatures of 580^{o}C obtained as a result of thermal analysis of the grinding process. Here, the (.odb) file of thermal analysis was imported for carrying out the mechanical analysis. The load steps were created which includes both normal pressure loads and traction loads with ramped amplitudes applied in the same step. The grinding forces calculations are shown in Appendix A. The uniform normal pressure of 61.75 MPa was applied as a pressure load and the uniform traction load of 65.45 N was applied as a shear load for each surface (block) in different steps along the direction from initial blocks to the final blocks (1st block to 40th block). The distribution of normal pressure and traction load in the same 19th step is shown in Figure 3.15.

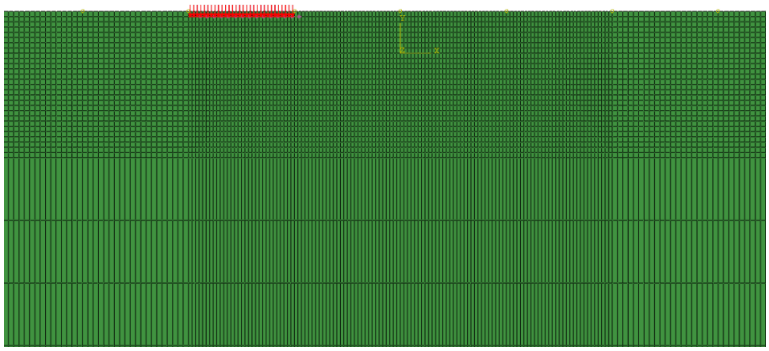

Figure 3.15: Normal pressure and traction load distribution for 19th grinding block during grinding simulation

To simulate the material removal as the grinding wheel moves from one point to another, the 'model change' interaction was employed. This is like the one that is used in the cladding process and was achieved by deactivating one block at a time (here new block was created to remove the 1 element vertically with a total of 40 blocks. This block was different from that of cladding block which has 8 elements vertically). The 'NLGEOM' was turned on due to geometric nonlinearities and the Static, General analysis type of simulation was used in the mechanical simulation. So, in each step of grinding and material removal, the heat flux was applied in the form of the predefined field, then normal pressure load and traction load were applied followed by the deactivation of elements. This shows the effect of the actual grinding process which was carried out for 40 different blocks to simulate the grinding on the entire cladding layer.

The field outputs were requested at each step to derive the outputs for mechanical analysis such as Von Mises stresses, Residual stresses (S11 and S12) and equivalent plastic strain PEEQ.

3.5 Ice impact loads Simulation

As discussed in the previous chapter, the ice loads cause severe damage to the ship components especially propellers. These repeated ice loads are impact in nature and induce fatigue and fracture over a period. The substrate material especially NAB has to be coated with suitable cladding material so that the dynamic impact loads with changing amplitude does not cause severe problems such as noise, crack initiation, etc., for a longer period of time. Stellite is the cladding material that can enhance the impact load resistance of NAB and Steels substrates effectively. So, in this section, the effect of ice impact loads having the same magnitude is studied for 2 different cases as shown in Figure 3.16. The first one is the effect of the repeated impact loads of certain magnitude on the non-cladded substrate and the second one to see the effect of the cyclic impact loads on the grounded surface. The effect of the impact loads at different load cycles are analyzed in two cases and the conclusion is made on how these cases differ from each other.

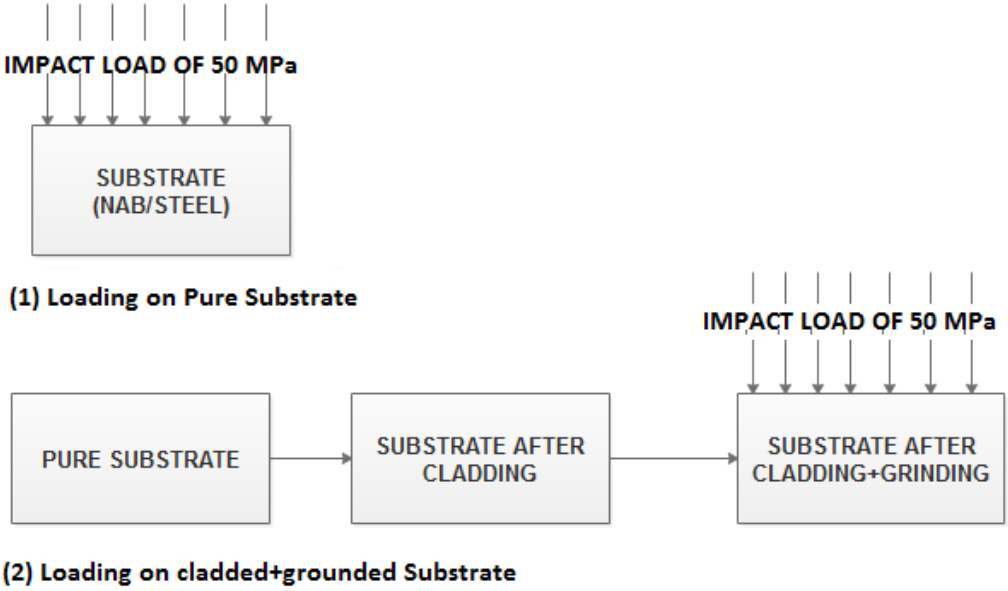

Figure 3.16: Two cases in which the impact loads are applied and analyzed, one on pure substrate and another on cladded+grounded substrate

The main challenge here is to get the magnitude of the impact loads of ice that exists during ice-propeller interaction. Though a lot of studies have been carried out, it is difficult to predict the nature of ice upon contact with propeller and this creates a dilemma in understanding what type of contact load it is. If we just consider the rotating propeller coming in contact with the ice, which makes the propeller blades to bend either forward or backward, which is resultant of centripetal forces and centrifugal forces cannot be taken as an impact load. The ice-contact loads are dynamic in nature which alters its magnitudes and directions at each point which is quite impossible to record the forces in the actual environment (Ye et al., 2017).

Various experiments are carried out to record magnitudes of ice-contact loads at different time intervals in the laboratory. Modeling of ice interaction is difficult because of high strain rates due to the sharp tip of propellers and complexity of flow of ice around the propeller blades (Jones et al., 2007). There is another method that can be used by ABAQUS/Explicit which requires the modeling of both ice and propeller (requires the material properties of ice as well). But, the problem is to apply the impact loads as in the actual conditions which is not possible in our case. Hence, we need to use a method to just extract the actual loads on the surface of a propeller and the magnitude of this load includes all the properties such as the mass of the ice, the relative velocity between ice and propeller, time period of ice-propeller interaction and so on. The strength of ice depends on various failure modes such as crushing, buckling, bending which are different from one another. Also, the friction and the angle of contact between the ice and propeller has to be considered for modeling which is difficult in our study (Broman & Nordqvist, 2013).

The shape of the ice changes when it comes in contact with the hull and upon crushing gives rise to smaller pieces of ice with irregular shapes. It is difficult to know how the interaction between these pieces of ice and propeller happens which complicates the simulation of ice-propeller interaction. This is difficult task as gathering all these data is very challenging because it is not constant, or the data are not readily available. So, based on the conclusions of

various research, we thought to proceed with a higher magnitude of the impact load to just see how the propeller behaves upon repeated loads in 2 different cases as mentioned above.

In our impact load study, we have assumed 50 MPa impact pressure load that was given as input to the ABAQUS (the full calculations can be seen in Appendix B). This impact load was applied to the central part of the FE model for 50 times which signifies the repeated cyclic loads in the actual environment. The time period for the application of one load cycle was 0.1 seconds which means the ice and propeller interact for this duration during one cycle. As already discussed, the same magnitude of impact load was applied on both non-cladded substrate layer and grounded substrate layer.

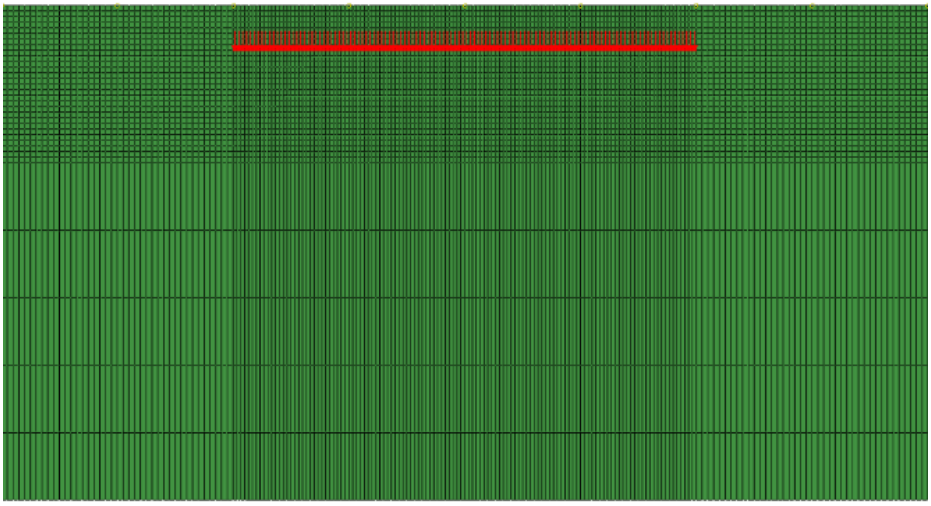

Figure 3.17: Impact load of 50 MPa applied on non-cladded substrate

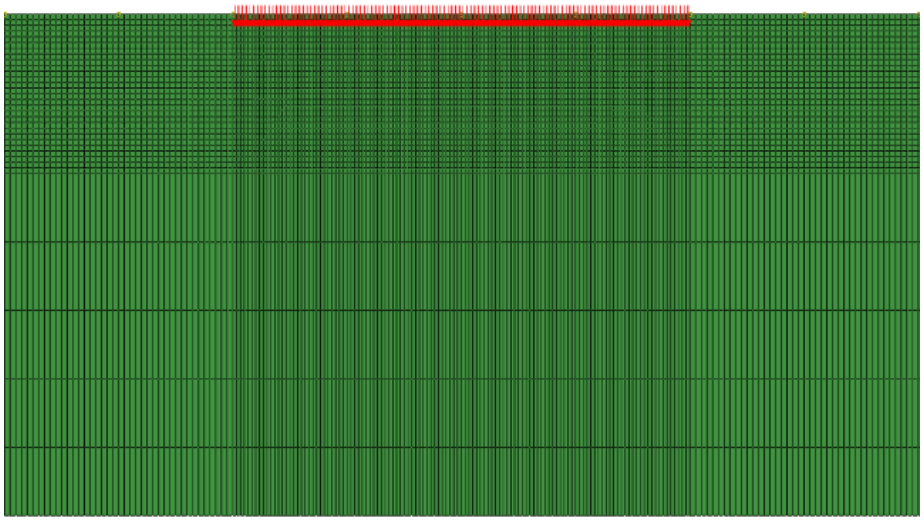

Figure 3.18: Impact load of 50MPa applied on the cladded+grounded substrate

As seen in the ***Error! Reference source not found.***, the red region indicates the middle portion of the substrate (width of 20 mm) where the impact loads were applied. The extra elements above the surface shows the cladding layer that was deactivated using model change option during impact loading which signifies that the loads were applied only on the substrate. The Figure 3.18 shows the grounded layer and the loads were applied on the surface present one

element below the top surface of the cladded area which indicates that the loads were applied on the cladded area after grinding. In each case, the results were analyzed by taking the values of residual stresses and equivalent plastic strain at both surface and 0.5 mm below the surface after applying 1st impact load cycle, 10th impact load cycle, 20th impact load cycle, 30th impact load cycle, 40th impact load cycle and 50th impact load cycle respectively. The results were plotted to compare the effect of different cycles of impact loads on the substrate and grounded surface and conclude whether the performance has improved after grinding to have resistance against ice impact loads which is the main scope of the thesis work.

4 Analyses of results and discussions

This chapter deals with the analyses of the results after the finite element simulations of laser cladding and grinding processes. Also, the effect of the ice impact load on the performance of the propeller after the grinding is analyzed and the conclusion is made regarding the efficiency of cladding and grinding processes on the propeller substrate.

Thermal analyses

As discussed in the previous sections, the entire process of cladding and grinding is a sequentially coupled thermo-mechanical simulations where the thermal simulation is followed by mechanical simulation. This gives rise to analyze the results separately although thermal simulation has an influence on the mechanical simulation as discussed in the methodology.

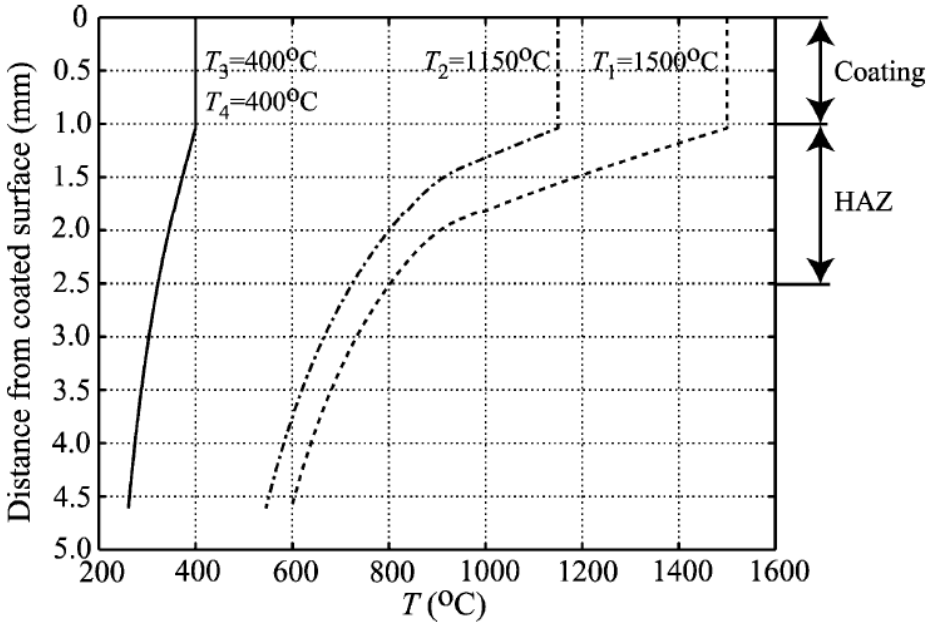

Figure 4.1:The temperature distributions of four temperature cycles through thickness as taken from Ringsberg et al., (2005)

It is required to verify the accuracy of our results with any reference of study and accordingly, we have used the results of Ringsberg et al., (2005) that has conducted a similar study on cladding and grinding process (railway application). Figure 4.1 shows the temperature

distribution for four different cycles and how the temperature declines with variation in thickness of the cladding layer and HAZ as found in the reference study material, Ringsberg et al., (2005). As already discussed in the methodology section, there are four different cycles of temperature during the cladding simulations. During the first cycle, the temperature was assumed to be 1500^{o}C, the second cycle temperature was 1150 ^{o}C and the third and fourth temperature cycle was 400 ^{o}C respectively.

Mechanical analyses

The results of the thermal simulations were analyzed and the appropriate results in form of nodal temperatures were used as the inputs for the mechanical simulations as predefined fields. After the cladding simulations, the residual stresses are analyzed for the efficiency of cladding process and these results were used as an input for the mechanical simulations of the grinding process again in the form of predefined fields. After the grinding simulations, the residual stresses are analyzed followed by the ice impact loads simulations. Finally, the residual stresses and equivalent plastic strain after impact loading on grounded substrates are compared with the impact loading on the pure substrate to analyze how the cladding and grinding processes improve the performance of the substrate. All the stress and PEEQ values are taken from the middle nodes of the model.

As already mentioned in thermal analysis, it is required to verify any results with the approved reference. So, the same reference of Ringsberg et al., (2005) as shown in Figure 4.2 where the authors have cladded the Steel substrate with Stellite as a cladding material. Then the residual hoop stress distribution against the varying thickness was plotted. In the reference study, the authors used the disc as the specimen of FE study which has the residual hoop stress in the cladding blocks (tangential direction). But, in our case, these stresses are similar to the longitudinal residuals stresses (S11) in the same direction (Li, 2018). The results were collected from the middle node position with varying thickness.

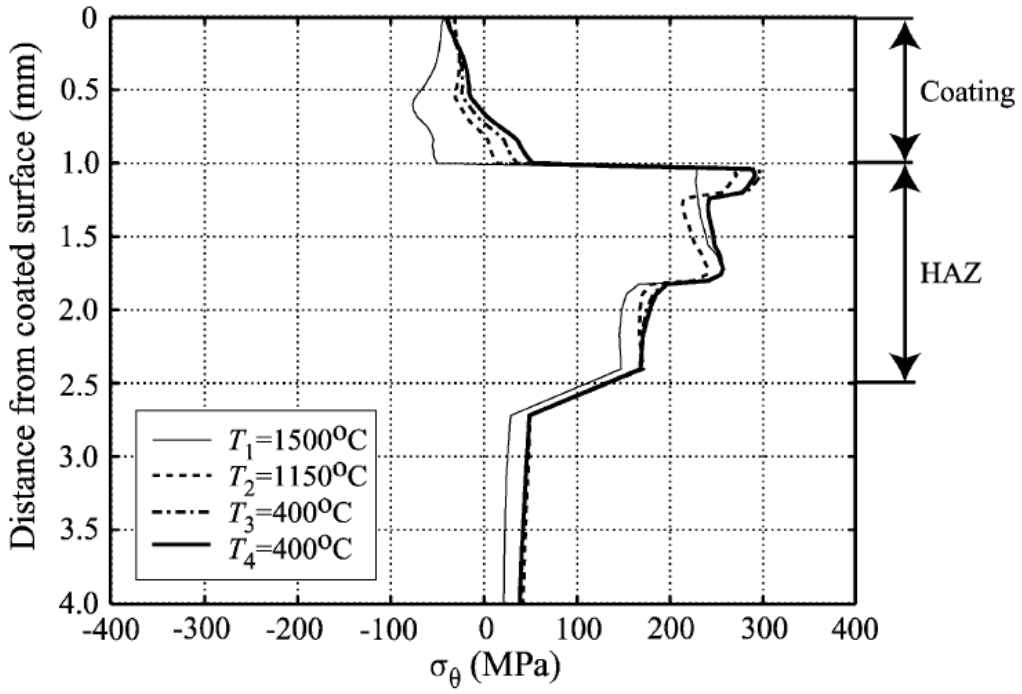

Figure 4.2: Residual hoop stress of cladding in the reference (Ringsberg et al., 2005)

4.1 Cladding simulation of NAB

This section includes the thermal and mechanical analyses of cladding on NAB as substrate material. The nodal temperatures (NT11) are the outputs of thermal analysis whereas the residual stresses (S11 and S12) and the equivalent plastic strain (PEEQ) are the outputs of mechanical analysis.

4.1.1 NT11 of cladded NAB

The results of the thermal simulations have to be verified with the results of the reference study material. For this, the nodal temperatures at different temperature cycles are recorded to analyze further. The Figures 4.3 to 4.7 show the temperature distribution contours of the thermal simulations of NAB substrate.

The temperature distribution contour after cladding the 20th block of the first track at temperature of 1500^{o}C is shown in Figure 4.3. During simulation, the thermal boundary conditions such as convection and radiation were taken into account at a specific cladding block. Due to the thermal conductivity property of material, the temperature is transferred to the surrounding nodes which signifies the heat transfer through conduction. The entire model is cooled down to room temperature of 20^{o}C once the entire cladding process of 40 blocks was completed as shown in Figure 4.7.

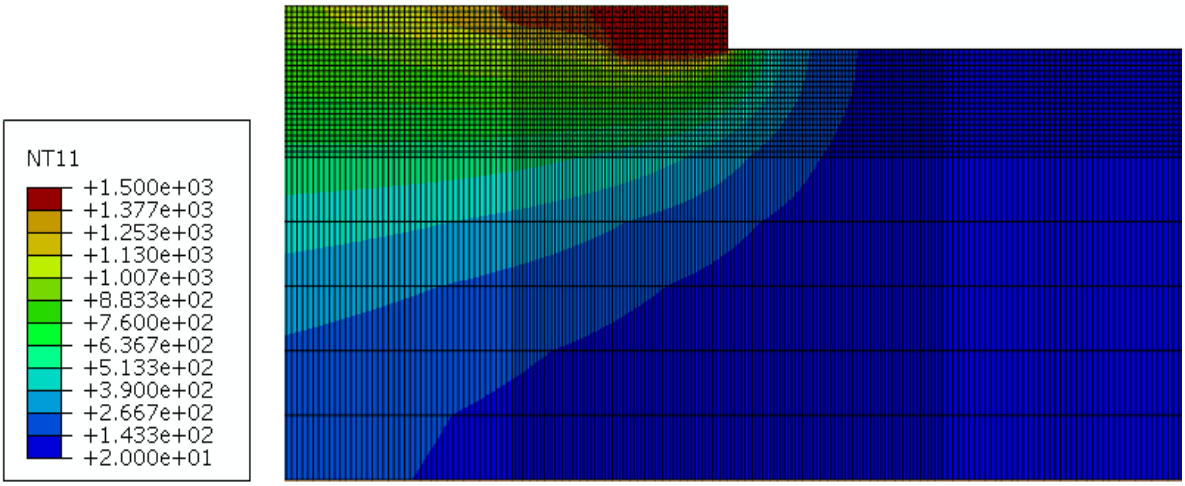

Figure 4.3: Temperature distribution for NAB for deposition of 20th block for first track

The temperature distribution contour for the first cladding track after deposition of the 20th block at second track temperature is shown in Figure 4.4. This means that the transfer of heat took place transversely to the first track which dropped down to 1150^{o}C. Once the deposition of 40th block of cladding completes, the cooling of the entire model takes place at room temperature.

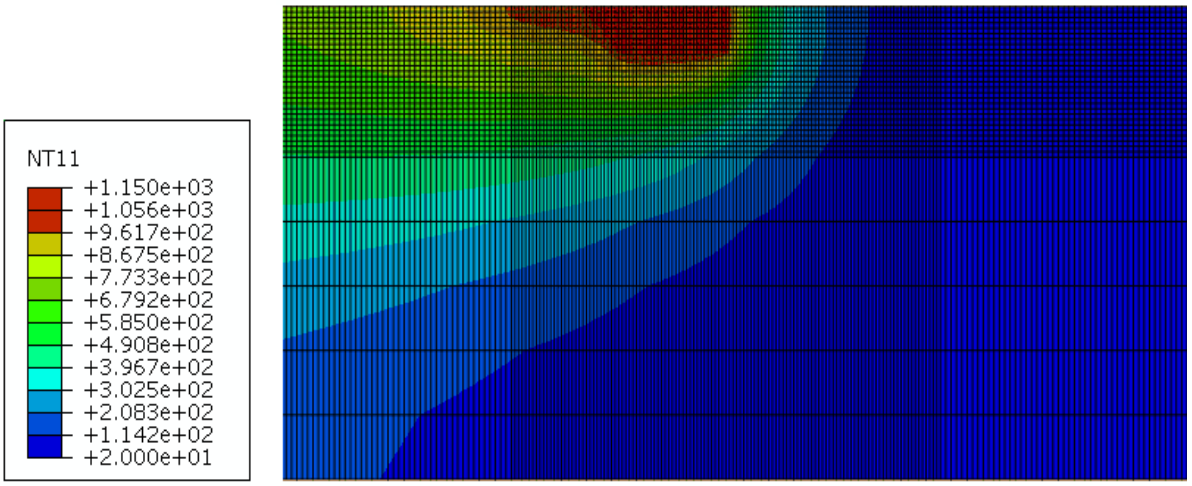

Figure 4.4:Temperature distribution for NAB for deposition of 20th block for second track

The temperature distribution contour for the first cladding track after the deposition of 20th block at third and fourth track temperatures can be seen in Figure 4.5 and Figure 4.6 respectively. The transverse temperature transfer is assumed to be 400^{o}C throughout the entire cycle till the 40th block is deposited. The entire model is cooled down to the room temperature of 20^{o}C which completes the cladding process as shown in Figure 4.7.

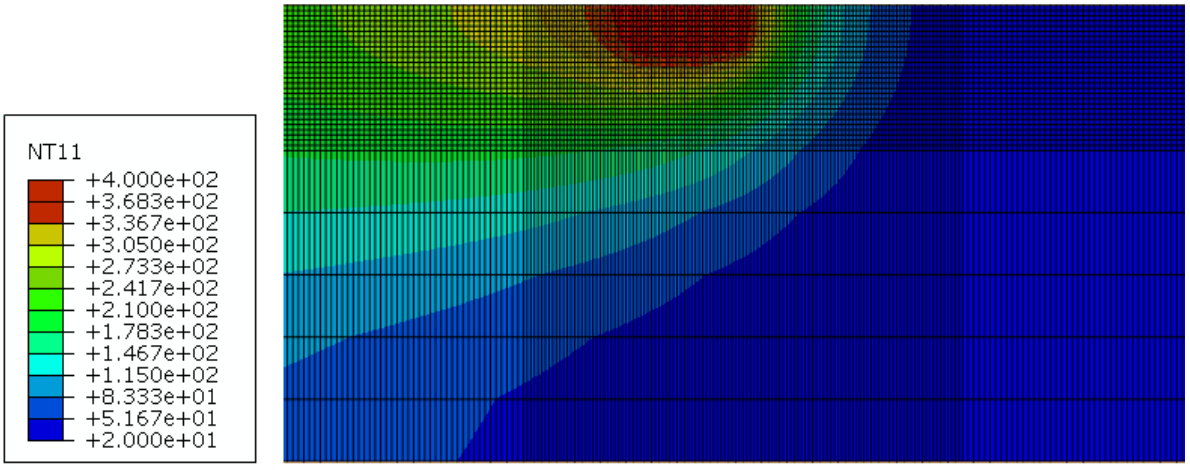

Figure 4.5: Temperature distribution for NAB for deposition of 20th block for third track

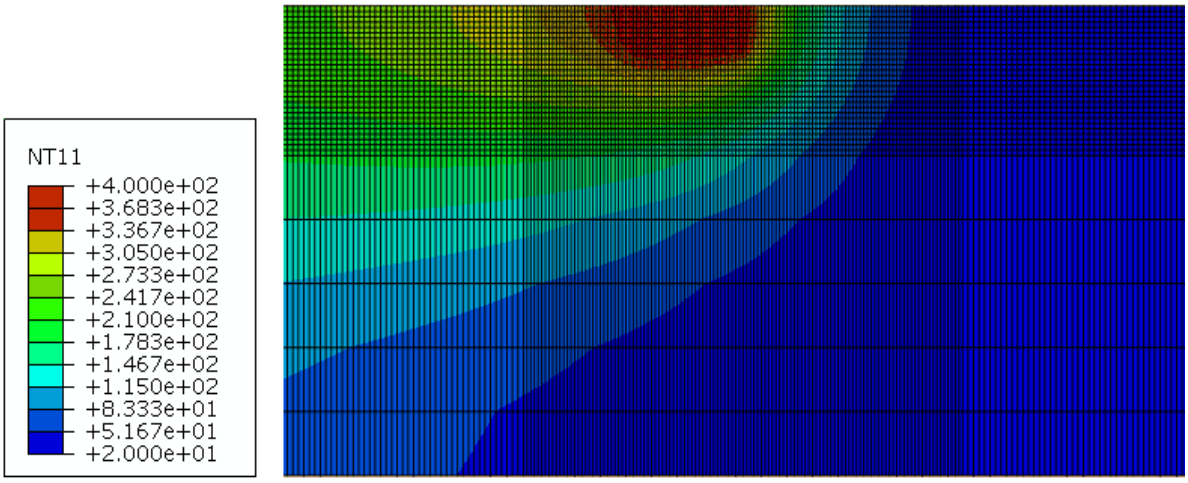

Figure 4.6: Temperature distribution for NAB for deposition of 20th block for fourth track

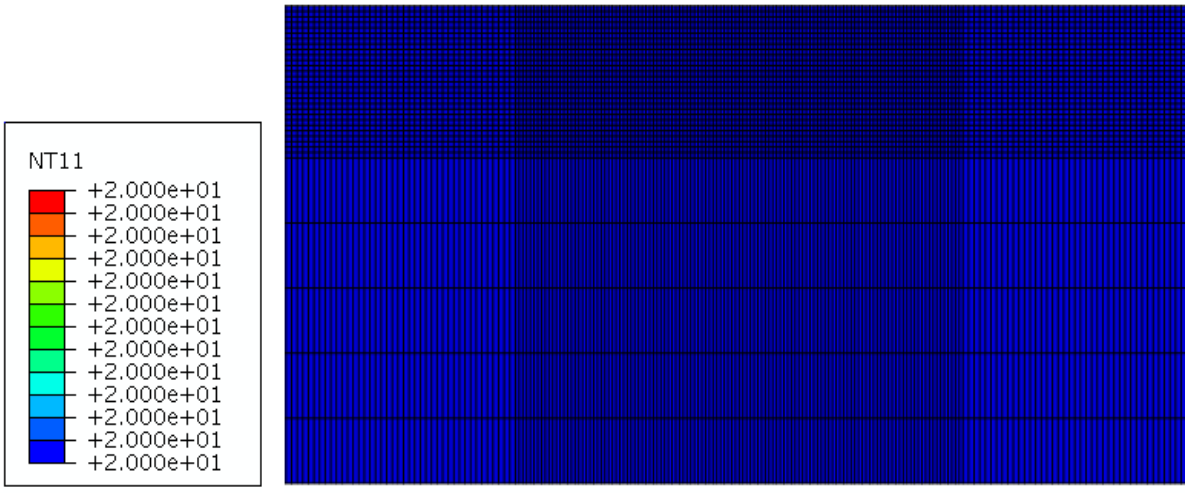

Figure 4.7:Temperature distribution for NAB after cooling step of every temperature cycle

The temperature distribution of NAB as a substrate under four different temperature cycles at the cladding layer (0 to 2 mm) and the heat affected zone (HAZ) is shown in *Figure 4.8* and these are regions where the influence of residual stresses is critical. The nodes in the middle position are chosen to collect the results of nodal temperatures. The cladding layer is influenced by four different cycles of temperatures and the due to thermal conductivity property, the temperature reduces with increase in the thickness. Also, the trend of nodal temperatures as seen in the *Figure 4.8* is similar to the results as seen in the reference (Ringsberg et al., 2005) which gives the verification of thermal analysis of cladding of Stellite on NAB as a substrate.

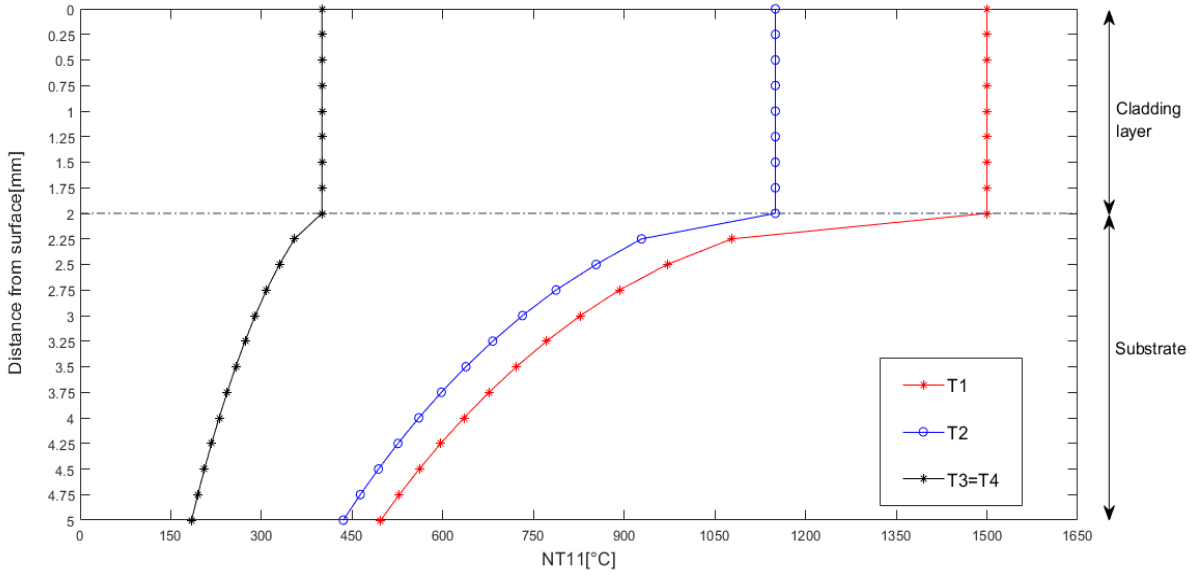

Figure 4.8: The temperature distribution for four cycles of NAB substrate after cladding

4.1.2 S11 of cladded NAB

The S11 distribution for different temperature cycles with varying thickness for NAB as a substrate is shown in Figure 4.9. The residual stresses of the consecutive temperature cycles are redistributed after the first temperature cycle. Compressive stresses are developed in the cladding layer, the largest one is 370 MPa in the first temperature cycle and then it is redistributed and reduced to 18.45 MPa in forth cycle. The compressive stresses in cladding layer are desirable and it shows less crack initiating forces in cladding layer (Alam et al., 2017). The region beneath the cladded layer and from the interface is found to have tensile stresses. The largest one is found with magnitude of 975 MPa in first temperature cycle and these tensile stresses in this region show the combination of Stellite and NAB material and this region is called HAZ as shown in Figure 4.9 having thickness of 1mm beneath the interface. Moreover, the largest magnitude of tensile stress shows the pierce of cladding material with the substrate material at the 0.25 mm beneath the interface. After that these tensile stresses are gradually reduced through the thickness and became compressive type in the lower substrate region which shows the less influence of the thermal stress due to the heat loss in this region and theses are mainly structural stresses. The pierce thickness of 0.25 mm is due the higher thermal expansion co-efficient and conductivity of NAB. As compared to the Figure 4.2, stresses are stabilized at the thickness of about 3.5 mm from the top surface of the cladding which is similar to the reference study Ringsberg et al., (2005).

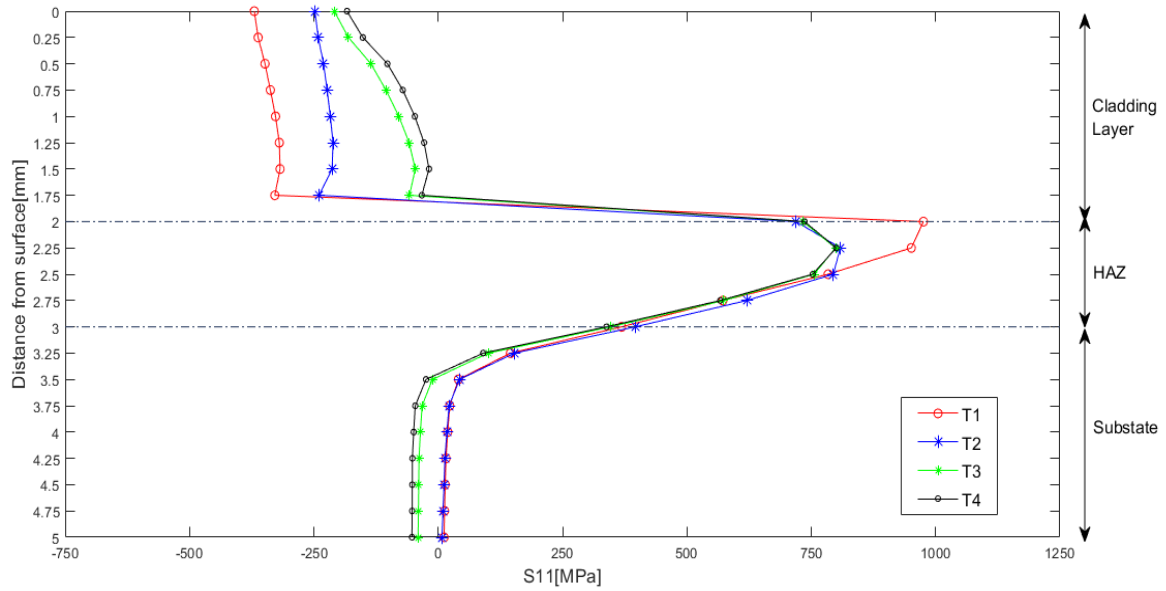

Figure 4.9: S11 distribution of cladded NAB through thickness between 0 and 5 mm

4.1.3 S12 of cladded NAB

S12 residual stress are swinging around the zero throughout the surface and Figure 4.10 shows the distribution of S12 from the top surface to the 5mm in thickness direction. It is clearly visible that magnitude of Shear residual stress S12 is quite lesser than the normal residual stress S11.

The compressive residual stresses are developed with maximum magnitude of 40 MPa in temperature cycle T2 while maximum tensile residual stress with magnitude of 31.8 MPa is recorded in same temperature cycle as compressive one. The pattern of residual stress throughout the thickness is quite similar except temperature cycle T1. Shear residual stresses are very important to consider for post processing of cladding simulation as they play an important role to analyze the bonding condition between cladded layer and substrate since the weaker bond can lead to sliding between them. Thus, cladded layer and HAZ are mostly vulnerable to dislocation. It is clearly visible from Figure 4.10 that highest magnitude of 32 MPa is found in cladded layer and 28 MPa is found in HAZ are lower than yield strength of both substrate and cladded material. Hence, cladded NAB is safe from sliding and are at acceptable level.

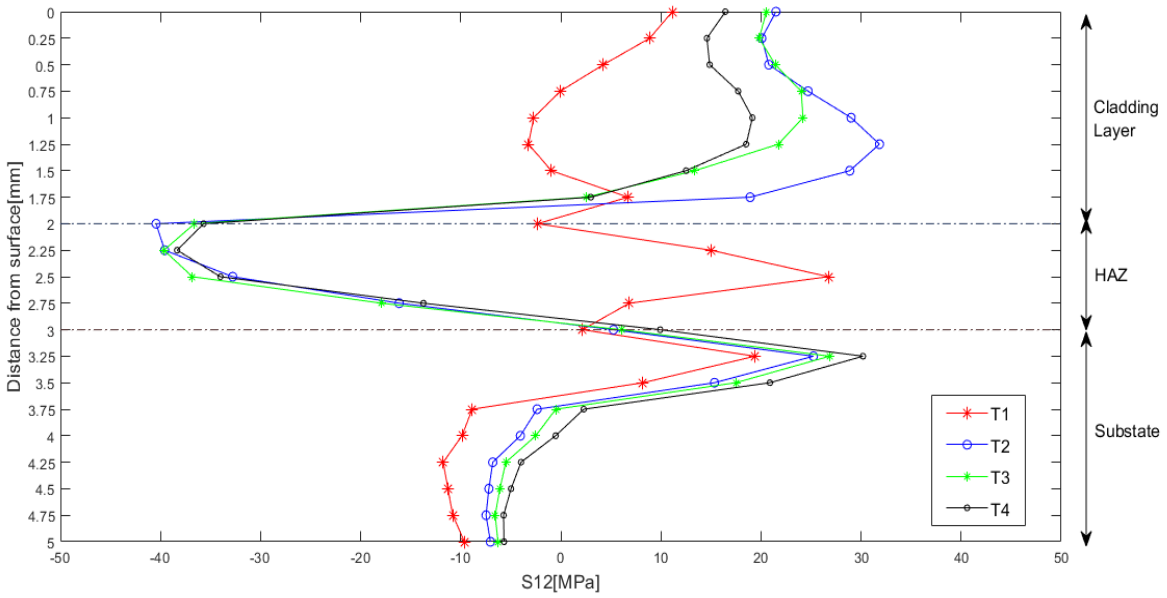

Figure 4.10: S12 distribution of cladded NAB through thickness between 0 and 5 mm

4.2 Cladding simulation of Steel

This section includes the thermal and mechanical analyses of cladding on Steel as substrate material. The nodal temperatures (NT11) are the outputs of thermal analysis whereas the residual stresses (S11 and S12) and the equivalent plastic strain (PEEQ) are the outputs of mechanical analysis.

4.2.1 NT11 of cladded Steel

The temperature distribution contours at four different temperature cycles when the 20th cladding block is deposited can be seen in figures 4.11 to 4.15. The cladding of Stellite on Steel as a substrate gives similar results as verified in NAB as a substrate and is shown in Figure 4.16 which means nodal temperature reduces as the thickness increases.

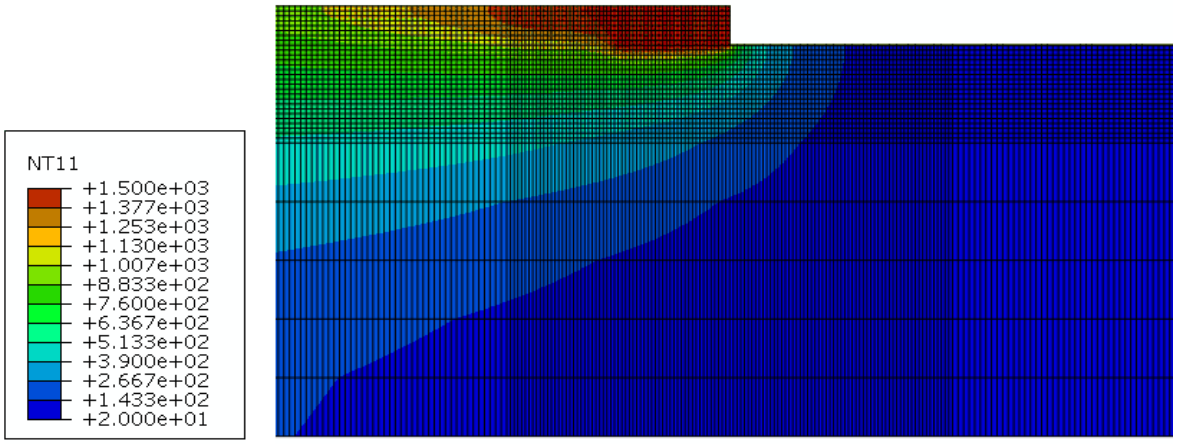

Figure 4.11:Temperature distribution for Steel for deposition of 20th block for first track

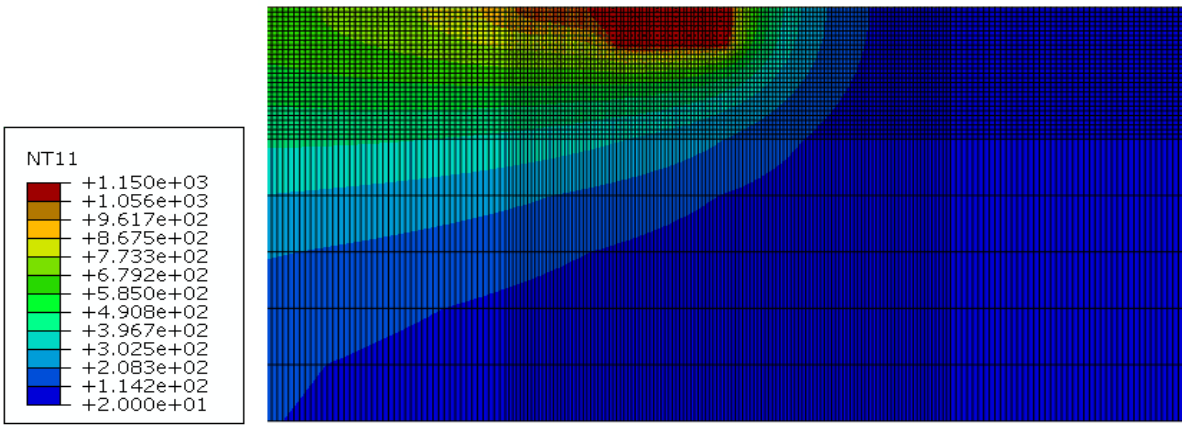

Figure 4.12:Temperature distribution for Steel for deposition of 20th block for second track

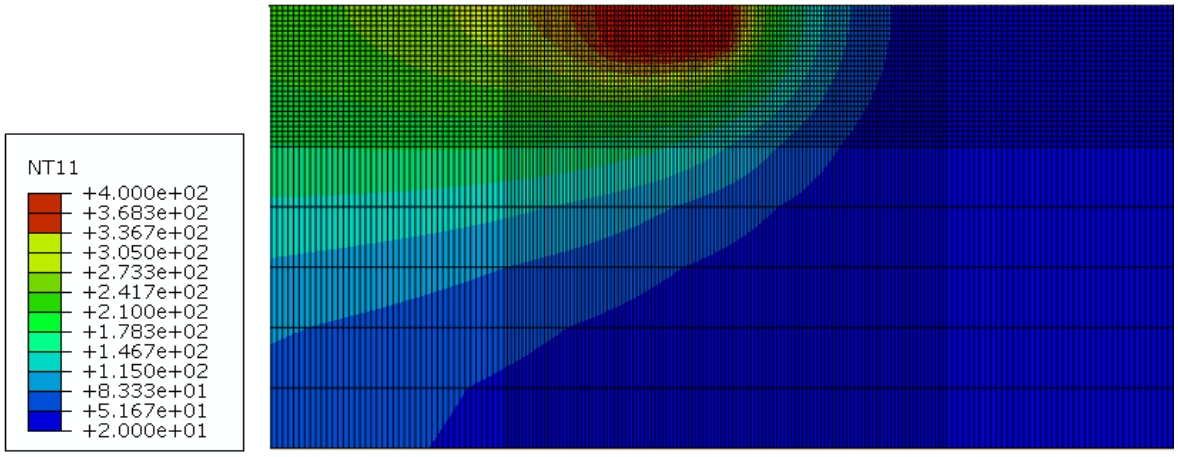

Figure 4.13:Temperature distribution for Steel for deposition of 20th block for third track

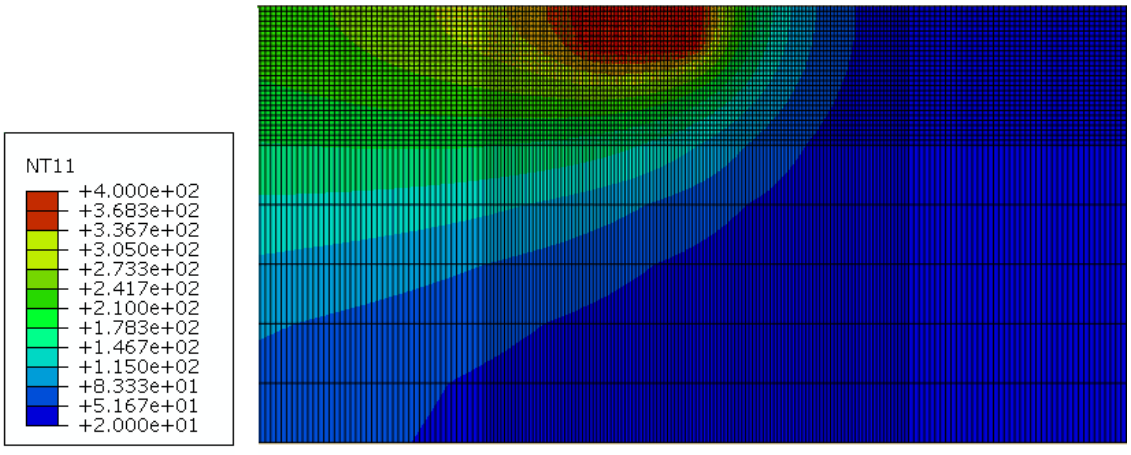

Figure 4.14:Temperature distribution for NAB for deposition of 20th block for fourth track

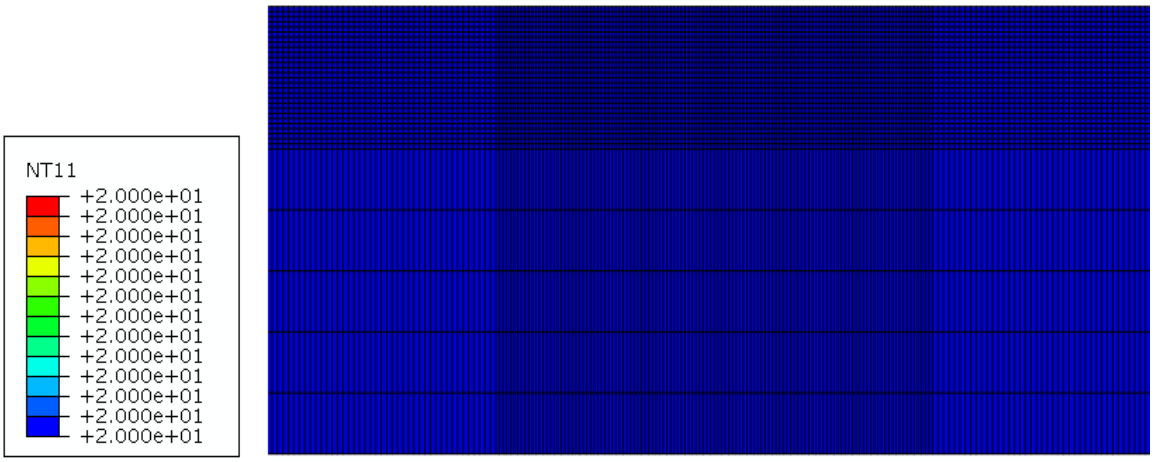

Figure 4.15:Temperature distribution for NAB after cooling step of every temperature cycle

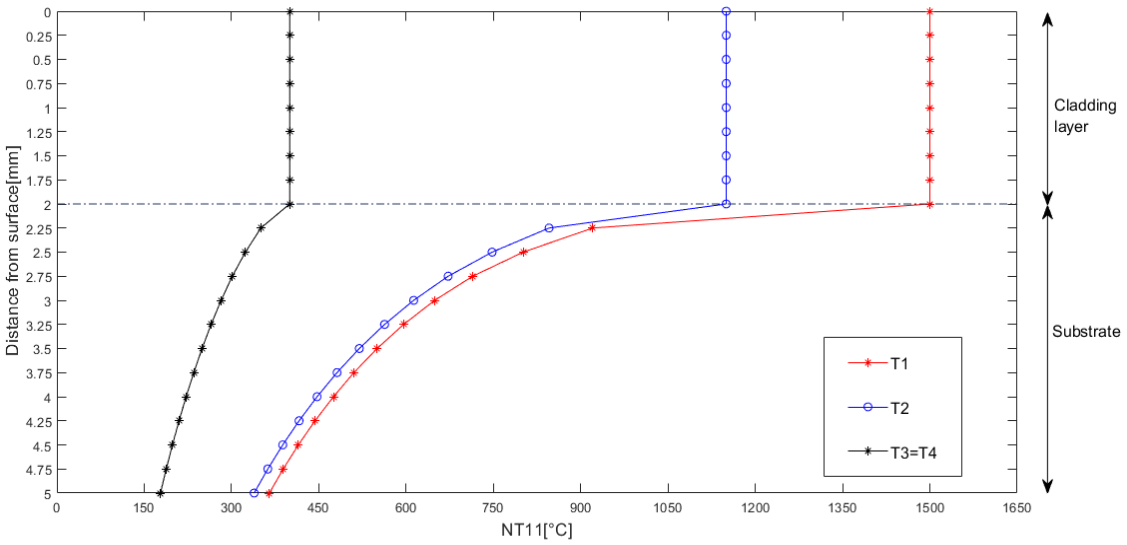

Figure 4.16: The temperature distribution for four cycles of Steel substrate after cladding

4.2.2 S11 of cladded steel

The S11 distribution for four temperature cycles for steel as a substrate is shown in Figure 4.17. The normal residual stresses of the successive temperature cycles are redistributed after the first temperature cycle. Tensile residual stresses are developed in the cladding layer, the minimum one is 12 MPa in the first temperature cycle and then it is redistributed and increased to 206 MPa in forth cycle. The region beneath the cladded layer and from the interface is found to have tensile residual stresses with larger magnitude than cladded layer. The largest one is noticed with magnitude of 420 MPa in forth temperature cycle and these tensile stresses in this region show the combination of Stellite and Steel material and this region is called HAZ as shown in Figure 4.17 having thickness of 0.75 mm beneath the interface (Ringsberg et al., 2005). In addition to this, the largest magnitude of tensile stress shows the penetration of cladding material with the substrate material at the interface and 0.25 mm beneath the interface. After that these tensile stresses are moderately diminished through the thickness and became

compressive type in the lower substrate region which shows the less influence of the thermal stress due to the heat loss in this region and theses are mainly structural stresses. As compared to the Figure 4.2, stresses are stabilized at the thickness of about 3 mm from the top surface of the cladding which is appeared as the reference study Ringsberg et al., (2005).

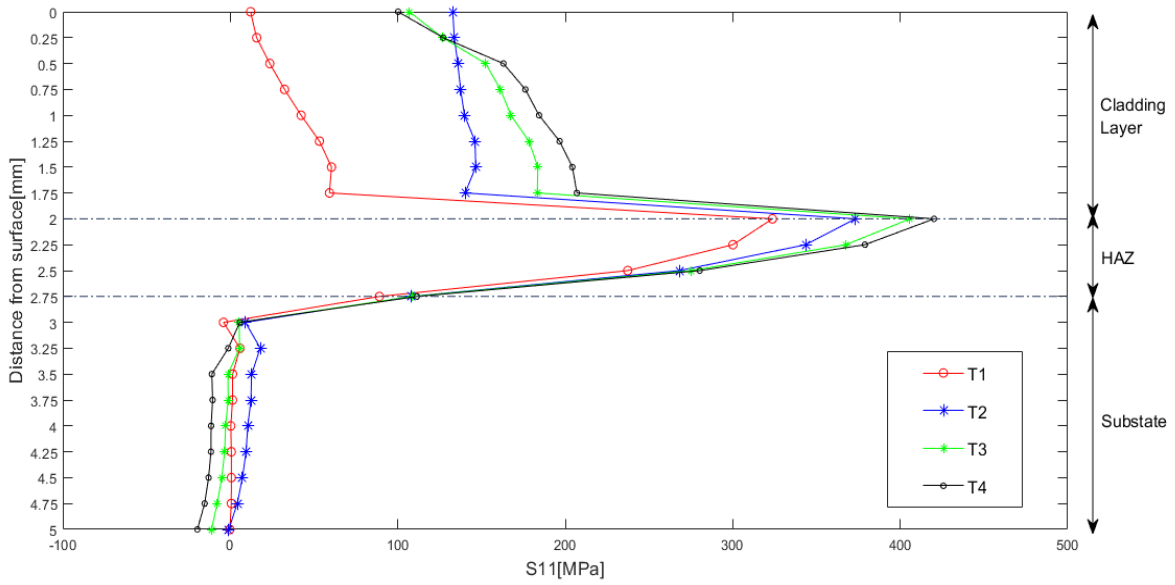

Figure 4.17: S11 distribution of cladded steel through thickness between 0 and 5 mm

4.2.3 S12 of cladded steel

S12 residual stress are swaying around the zero magnitude from top surface to substrate and the distribution of S12 from the top surface to the 5 mm in thickness direction is shown in Figure 4.18**Error! Reference source not found.**. It is clearly visible that magnitude of shear residual stress S12 is notably lesser than the normal residual stress S11.

The compressive type residual stresses are developed with maximum magnitude of 26.3 MPa in forth temperature cycle while maximum tensile residual stress with magnitude of 18.8 MPa is recorded in second temperature. The pattern of residual stress throughout the thickness is quite similar for all four temperature cycles. As explained before, shear residual stresses are very important to consider as they play a vital role to analyze the bonding condition between cladded layer. Thus, cladded layer and HAZ are mostly vulnerable to dislocation and it is clearly visible from Figure 4.18 that highest magnitude of 18.8 MPa is found in cladded layer and 15 MPa is found in HAZ are lower than yield strength of both substrate and cladded material. Hence, cladded NAB is safe from sliding and is at allowable level.

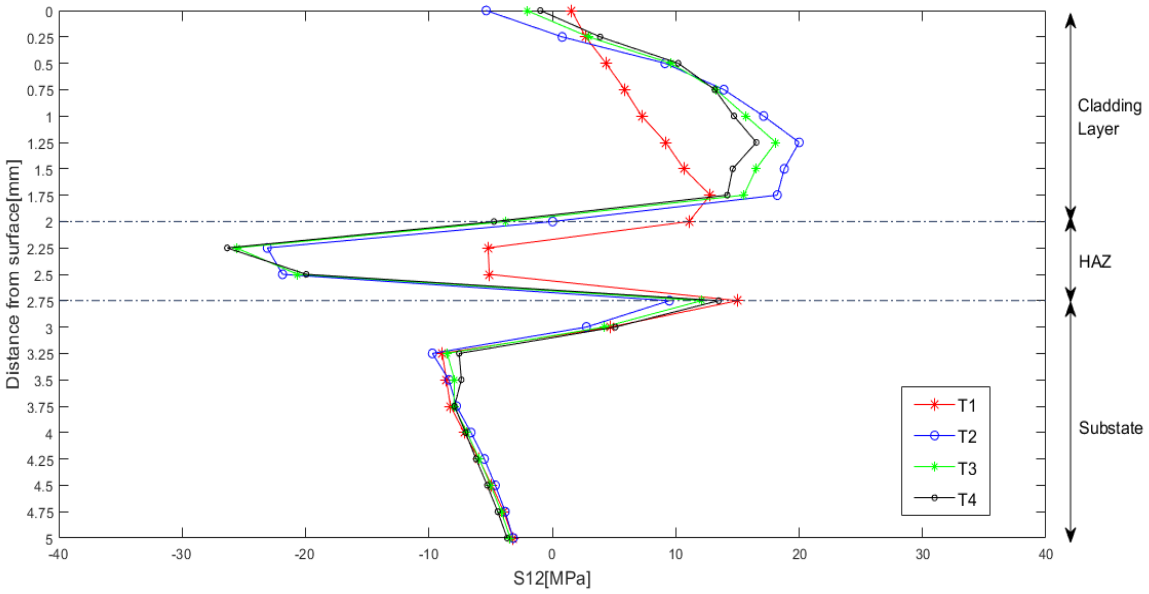

Figure 4.18: S12 distribution of cladded steel through thickness between 0 and 5 mm

4.3 Grinding simulation of NAB

This section includes the counter plots of S11 and S11 distribution with varying thickness of NAB as a substrate.

4.3.1 Contour plots of block removal during grinding on NAB

The Figure 4.19 and Figure 4.20 show the S11 after the removal of first block and 20th block which signifies the grinding process respectively.

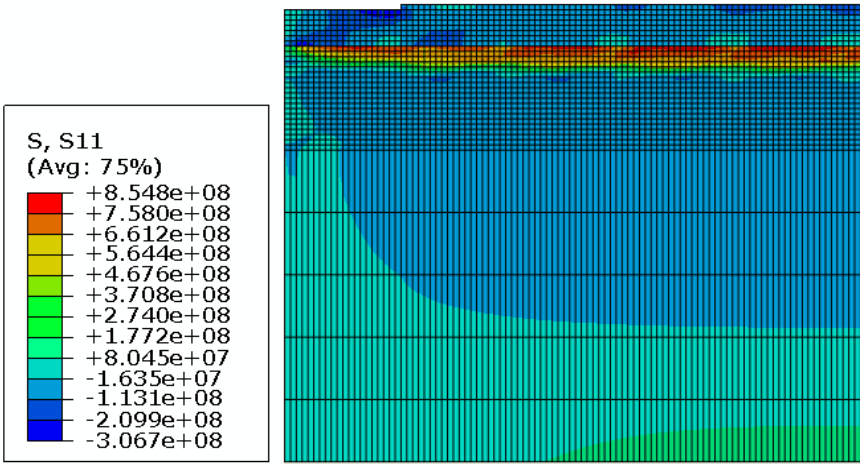

Figure 4.19: Removal of 1st block during grinding simulation on NAB as a substrate

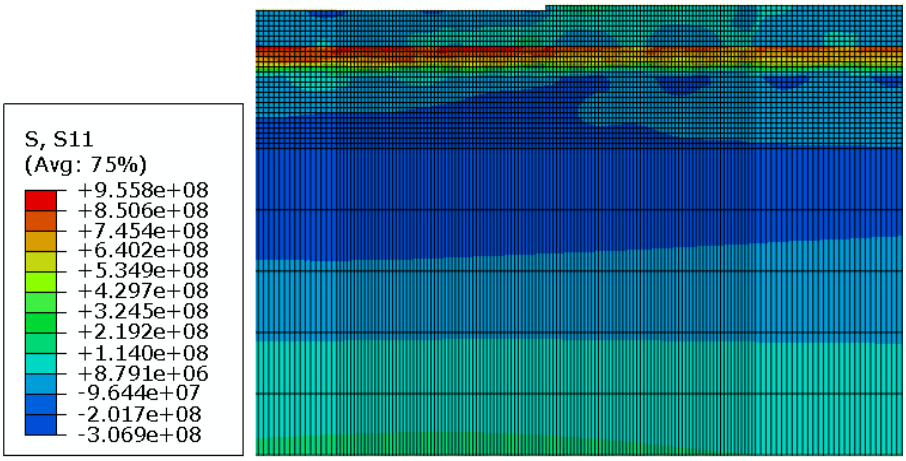

Figure 4.20: Removal of 20th block during grinding simulation on NAB as a substrate

4.3.2 S11 distribution of Grinding

The Figure 4.21 shows the S11 residual stress distribution in thickness direction from the top surface. The pattern remains quite similar after cladding and grinding process. For this material, residual stress is reduced a bit and is became more compressive at the interface at the end of grinding process compared to cladding process and grinding forces induced increment in residual tensile stresses in HAZ region. Later, residual stress magnitude is fallen gradually and is became compressive in substrate region.

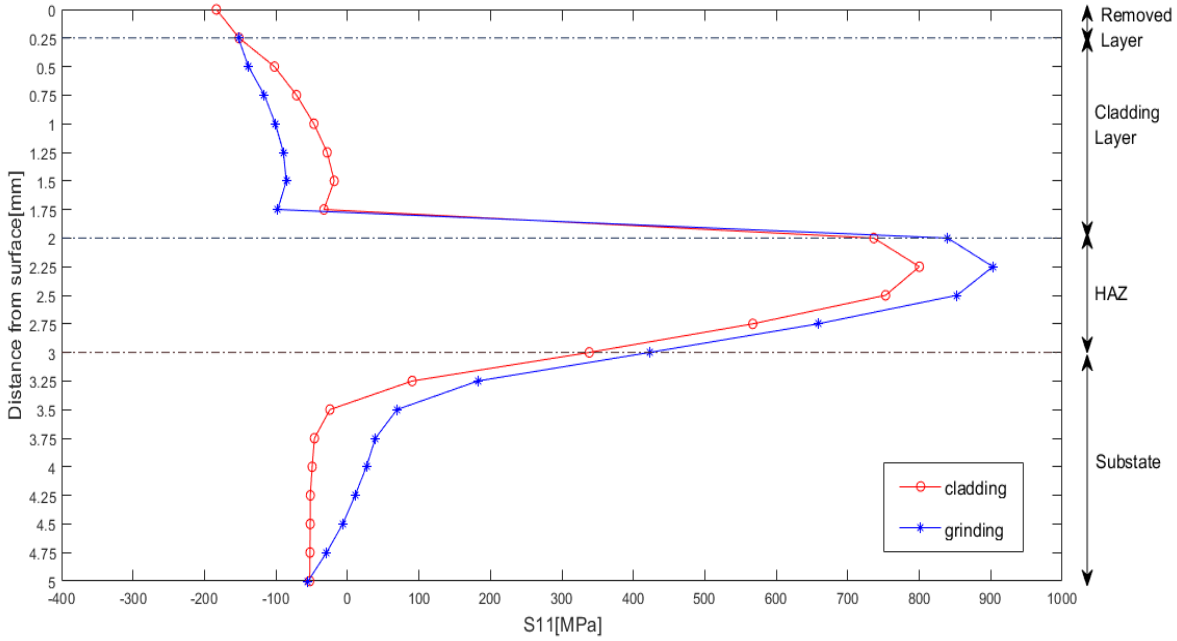

Figure 4.21: S11 distribution of grinding process on NAB as a substrate

4.4 Grinding simulation of Steel

This section includes the counter plots of S11 and S11 distribution with varying thickness of Steel as a substrate.

4.4.1 Contour plots of block removal during grinding on Steel

The Figure 4.22 and Figure 4.23 show the S11 after the removal of first block and 20th block which signifies the grinding process respectively.

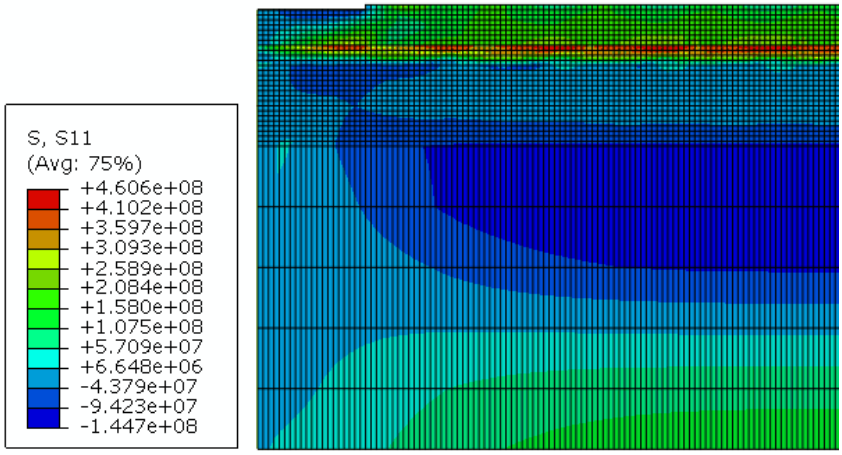

Figure 4.22:Removal of 1st block during grinding simulation on Steel as a substrate

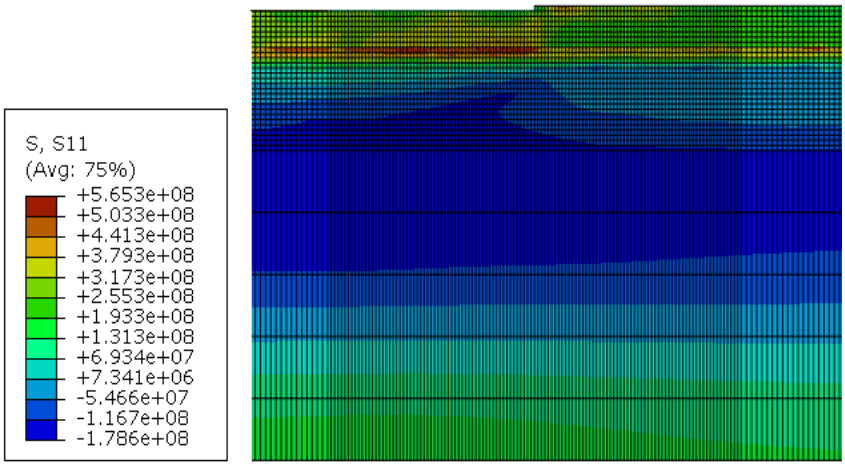

Figure 4.23: Removal of 20th block during grinding simulation on Steel as a substrate

4.4.2 S11 distribution of Grinding

The Figure 4.24 shows the S11 residual stress distribution in thickness direction from the top surface. The pattern remains very comparable in the wake of cladding and grinding process. For this material, residual stress is increased and is became more tensile at the interface at the end of grinding process compared to cladding process and the influence of grinding forces is quite negligible in the progression of tensile residual stresses in HAZ region unlike NAB substrate material. Later, residual stress magnitude is fallen gradually and is became compressive in substrate region.

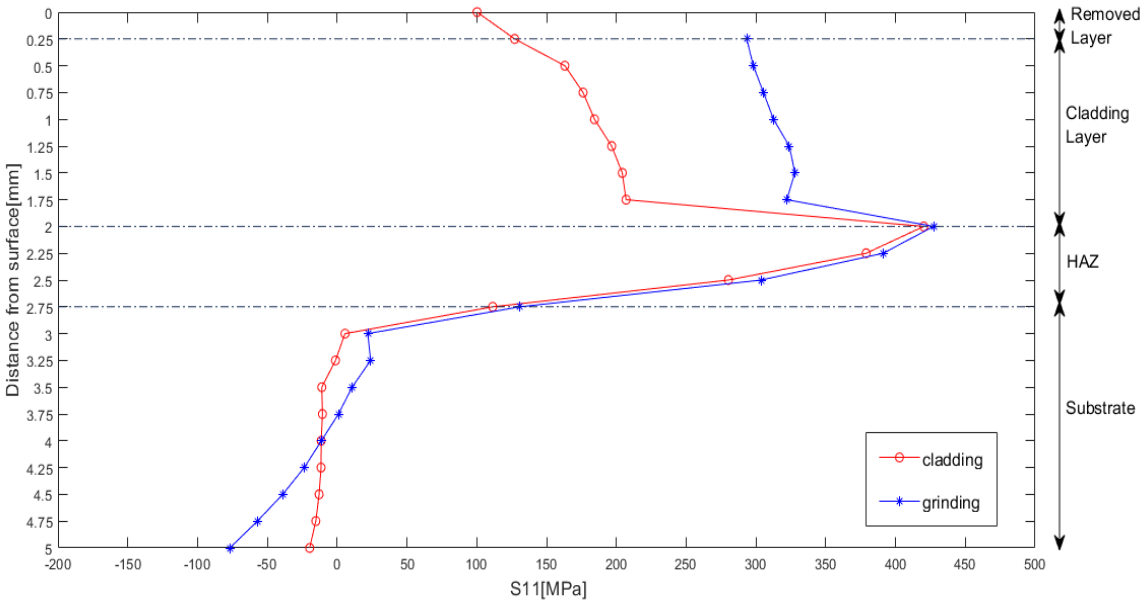

Figure 4.24:S11 distribution of grinding process on Steel as a substrate

4.5 Impact load simulation of NAB

This section includes the residual stresses and equivalent plastic strain on both non-cladded and grounded NAB after impact loading.

4.5.1 S11 distribution after repeated impact loads on grounded NAB

After the grinding process was completed, the grounded NAB was tested for repeated impact loads. The Figure 4.25 shows the S11 distribution of Cladded + Grounded NAB through surface thickness. It can be found that first impact load is increased S11 at top of the surface from 152 MPa compressive residual stress to tensile residual stress of 197 MPa. After that stress pattern remained same for 10^{th} and 50^{th} impact load. Grinding process can cause residual stresses and cracks in the cladded layer due to the effect of generated heat, applied normal and tangential forces (Bulletin, 2019) & (Zhou, 2016) . Therefore, it is indeed important to analyze such a condition in the cladded layer after grinding and each repeated impact loads. It is found that cladded layer after grinding process is contained compressive stresses and maximum of 197 MPa after first impact load are well below yield strength of cladding material. Hence it is at acceptable level.

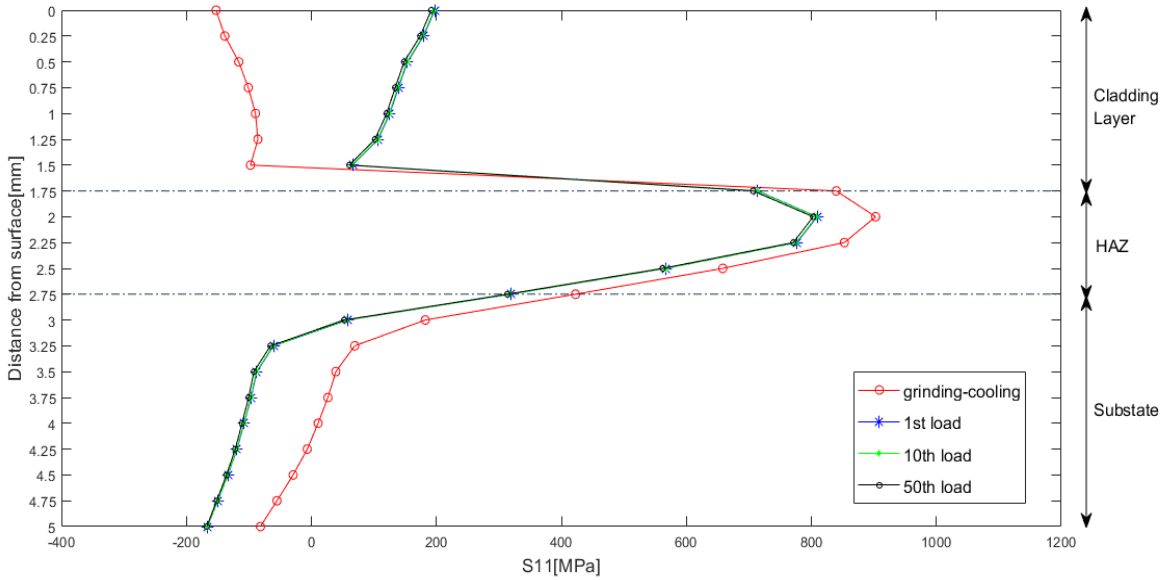

Figure 4.25: S11 distribution of grounded NAB through thickness after repeated impact loads

4.5.2 S12 distribution after repeated impact loads on grounded NAB

Shear residual S12 distribution of Cladded + Grounded NAB through surface thickness is shown in Figure 4.26. It is good to see the bonding between cladding layer and substrate after grinding process and repeated impact loads. It is shown in the Figure 4.26 that largest tensile residual stress is occurred after first impact load with 34 MPa of magnitude and mainly compressive stresses are contained in HAZ. This signifies that cladded + grounded NAB has good bond between cladded and substrate layers even after grinding process and repeated impact loads.

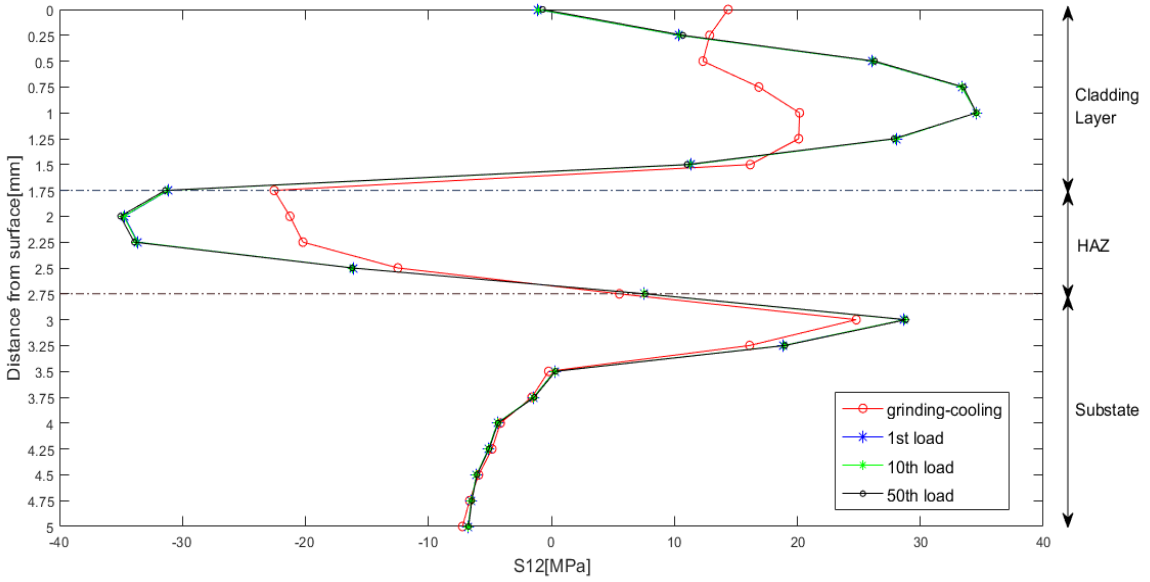

Figure 4.26: S12 distribution of grounded NAB through thickness after repeated impact loads

4.5.3 S11 distribution at top surface after repeated impact loads on grounded NAB

The Figure 4.27 shows S11 at top surface after repeated ice impact loads of grounded NAB. The first impact caused 197.3 MPa of tensile stress on top surface and then it is reduced gradually to 191.7 MPa after the 50th impact load. This shows that S11 will be reduced further with a greater number of cyclic impact loads. Thus, the top surface is improved against the ice impacts.

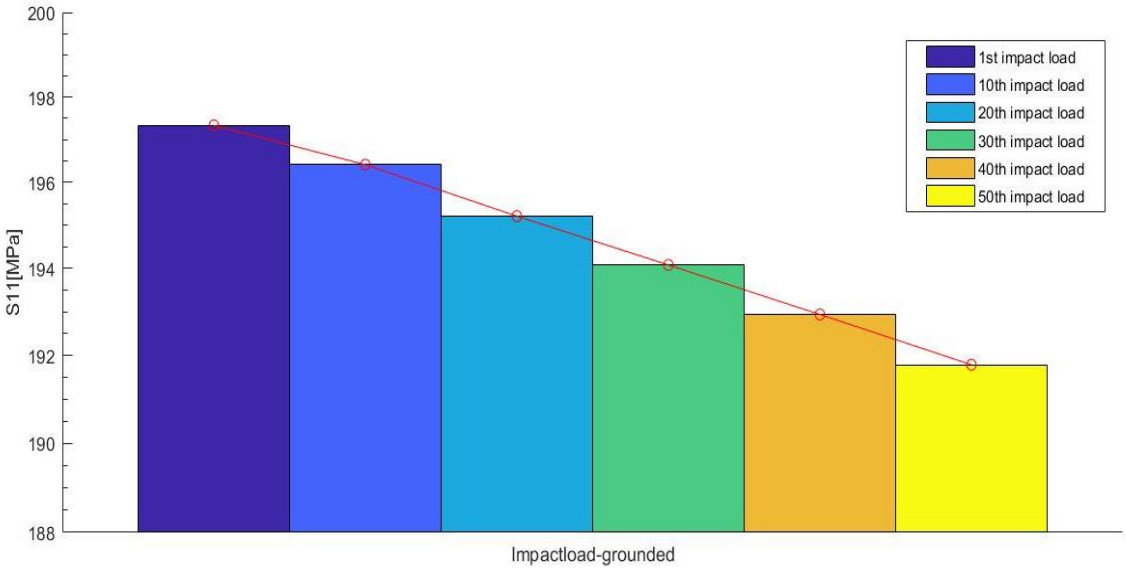

Figure 4.27: S11 distribution of grounded NAB at top surface for repeated impact loads

4.5.4 S12 distribution at interface after repeated impact loads on grounded NAB

The Figure 4.28 shows S12 distribution after each impact loads at the interface of grounded NAB. Shear residual stresses at interface are quite low and compressive one with the smallest magnitude of 31.15 MPa and increasing marginally to 31.41 MPa after 50th impact load which ensures that bonding quality remains good after repeated ice induced impact loads.

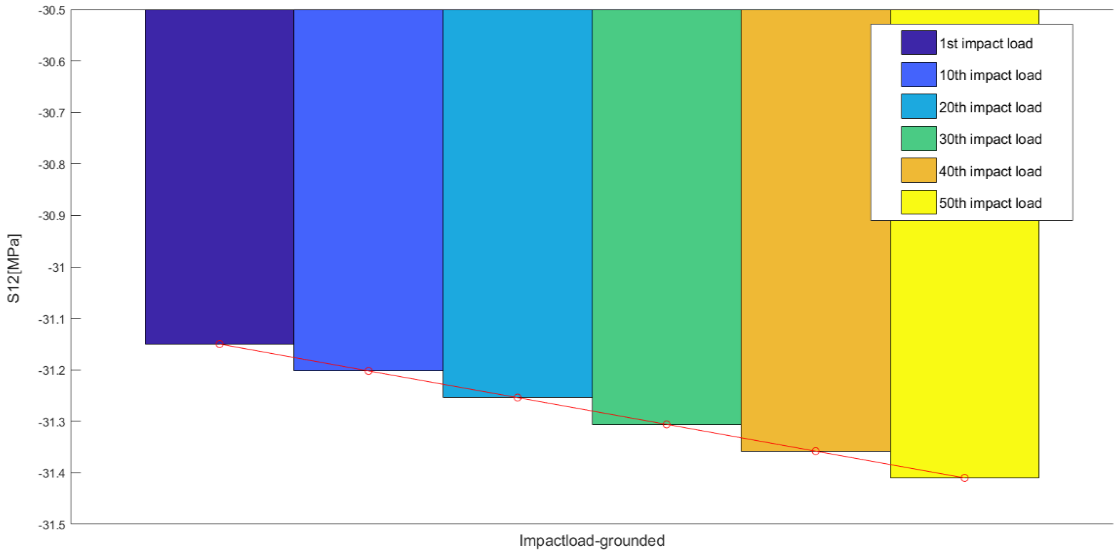

Figure 4.28: S12 distribution of grounded NAB at interface for repeated impact loads

4.5.5 PEEQ at top surface of grounded NAB & Substrate after impact loads

Plastic equivalent strain comparison is done between non-cladded NAB and cladded + grounded NAB after each repeated impact loads. Because ice impact load can cause local plastic deformation after cyclic loads. Figure 4.29 and Figure 4.30 show how repeated impact loads affect the non-cladded and cladded + grounded NAB with respect to plastic strain.

From the Figure 4.29, the first impact load is generated $2.26*10^{-3}$ of PEEQ at the top surface which is relatively small magnitude. Then the PEEQ is increased after 10^{th} impact load with 1.84% to $2.30*10^{-3}$. After that $2.34*10^{-3}$ of PEEQ is accumulated subsequent to 20^{th} impact load with change of 2.02%. In the following impact loads, PEEQ is increased more with almost constant change of 1.95% to the $2.49*10^{-3}$ after 50^{th} impact load.

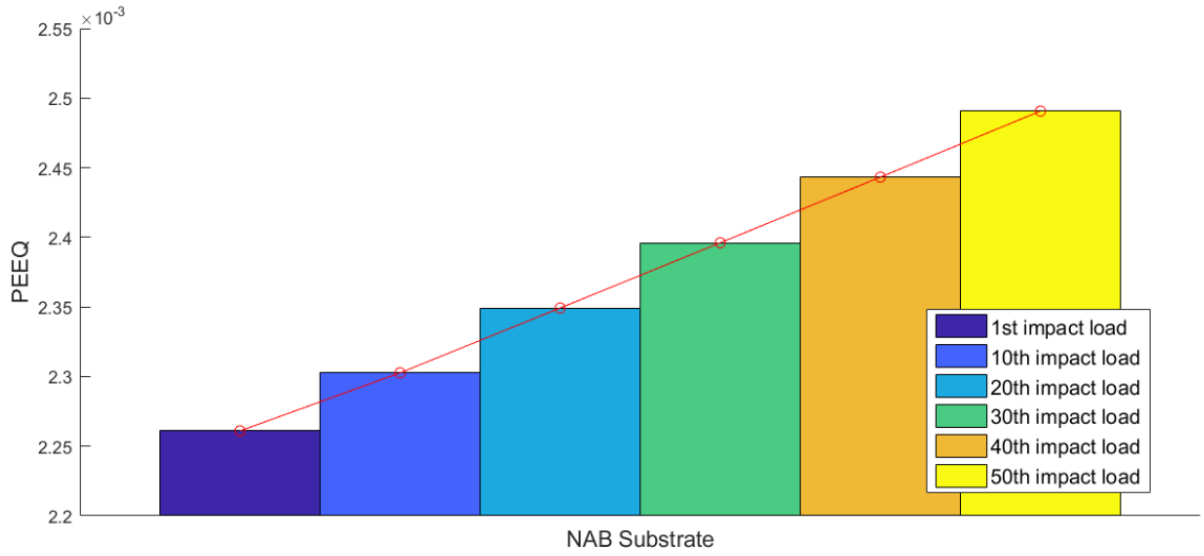

Figure 4.29: PEEQ at the top surface of the substrate for repeated impact loads

The Figure 4.30 with detailed scale shows the impact loads influence on PEEQ on cladded + grounded NAB. The initial PEEQ magnitude is more compared to non-cladded NAB due to cladding and grinding process. The first impact load induced $18902*10^{-5}$ of PEEQ at the top surface. Then the PEEQ is increased after 10^{th}, 20^{th}, 30^{th}, 40^{th} and 50^{th} impact load with almost constant change of 0.015% to $18905*10^{-5}$, $18908*10^{-5}$, $18911*10^{-5}$, $18913*10^{-5}$, $18917*10^{-5}$ respectively.

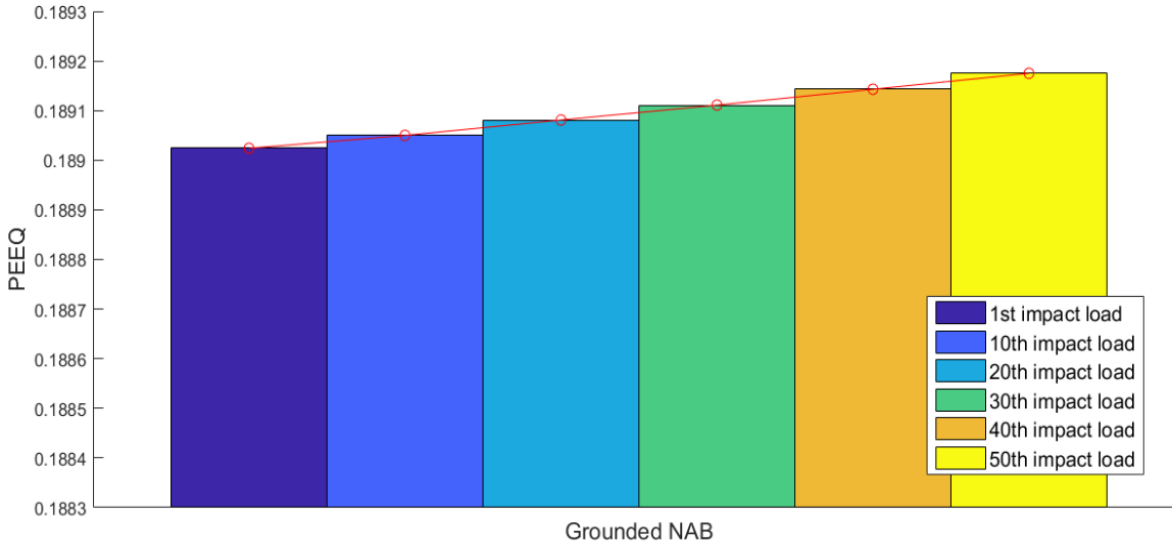

Figure 4.30: PEEQ at the top surface of the Grounded NAB for repeated impact loads

4.5.6 PEEQ at 0.5 mm below surface of grounded NAB & substrate after impact loads

Impact load influence is also analyzed 0.5mm beneath top surface as it is carried out for top surface explained earlier. From the Figure 4.31, the first impact load gathered $2.03*10^{-3}$ of PEEQ at the top surface which is relatively small magnitude, then the PEEQ is hiked after 10^{th} impact load with 1.87% to $2.07*10^{-3}$. After that $2.11*10^{-3}$ of PEEQ is accumulated and increased with 2.06% after 20^{th} impact load and in the following impact loads, PEEQ is increased with almost constant change of 2.03% to the $2.24*10^{-3}$ after 50^{th} impact load.

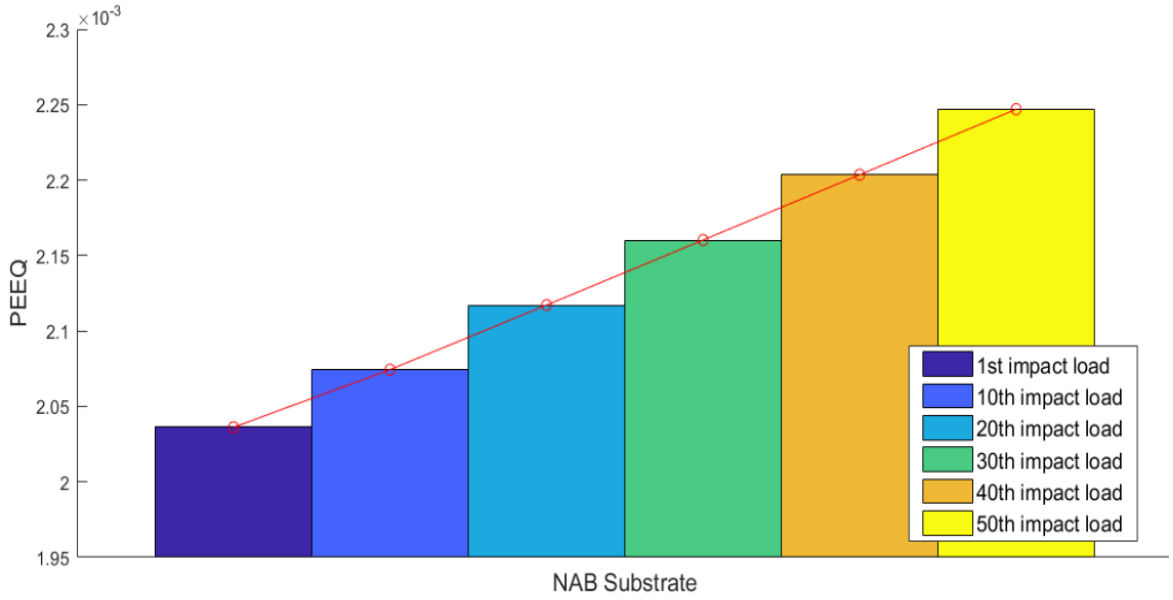

Figure 4.31: PEEQ at the 0.5 mm below the surface of substrate for repeated impact loads

The Figure 4.32 with featured scale shows the impact loads effect on PEEQ on cladded + grounded NAB. The first impact load induced $18136*10^{-5}$ of PEEQ at the top surface. Following to this, 10^{th} impact load is caused $18138*10^{-5}$ of PEEQ with change of 0.011%, then the PEEQ is further increased after 20^{th} impact load with of 0.016% to $18141*10^{-5}$. The 30^{th}, 40^{th} and 50^{th} impact load resulted in PEEQ of $18143*10^{-5}$, $18145*10^{-5}$, $18147*10^{-5}$ respectively with change of 0.11%.

This is how ice induced impact load cause the damage to propeller for longer period and affects the overall life of the propeller. From above comparisons and analysis, it is noted that percentage change in PEEQ is marginal in cladded + grounded NAB compared to non-cladded NAB. Thus, it may increase the overall life of propeller and slowed down the effect of ice impacted loads on propeller.

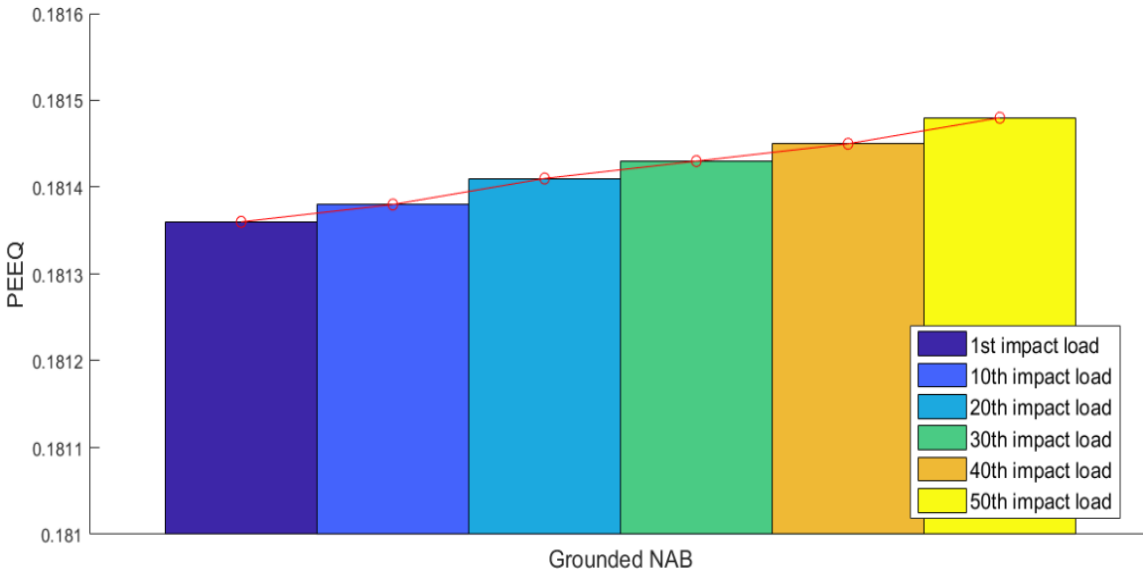

Figure 4.32: PEEQ at the 0.5 mm below the surface of grounded NAB for repeated impact loads

4.6 Impact load simulation of Steel

This section includes the residual stresses and equivalent plastic strain on both non-cladded and grounded Steel as a substrate.

4.6.1 S11 distribution after repeated impact loads on grounded steel

Once the grinding process was completed, the grounded steel was investigated for cyclic impact loads. The Figure 4.33 shows the S11 distribution of Cladded + Grounded steel in thickness direction from top surface. It can be found that first impact load is increased S11 at top of the surface from 293.4 MPa tensile residual stress to 324.3 MPa. After that stress pattern remains same for 10^{th} and 50^{th} impact load. Grinding process can cause residual stresses and cracks in the cladded layer because of generated heat, applied normal and tangential forces. Therefore, it is certainly important to analyze such a condition in the cladded layer after grinding and each repeated impact loads. It is found that cladded layer after grinding process is held tensile residual stresses well below yield strength of cladding material with maximum magnitude of 322 MPa. Hence it is at allowable level.

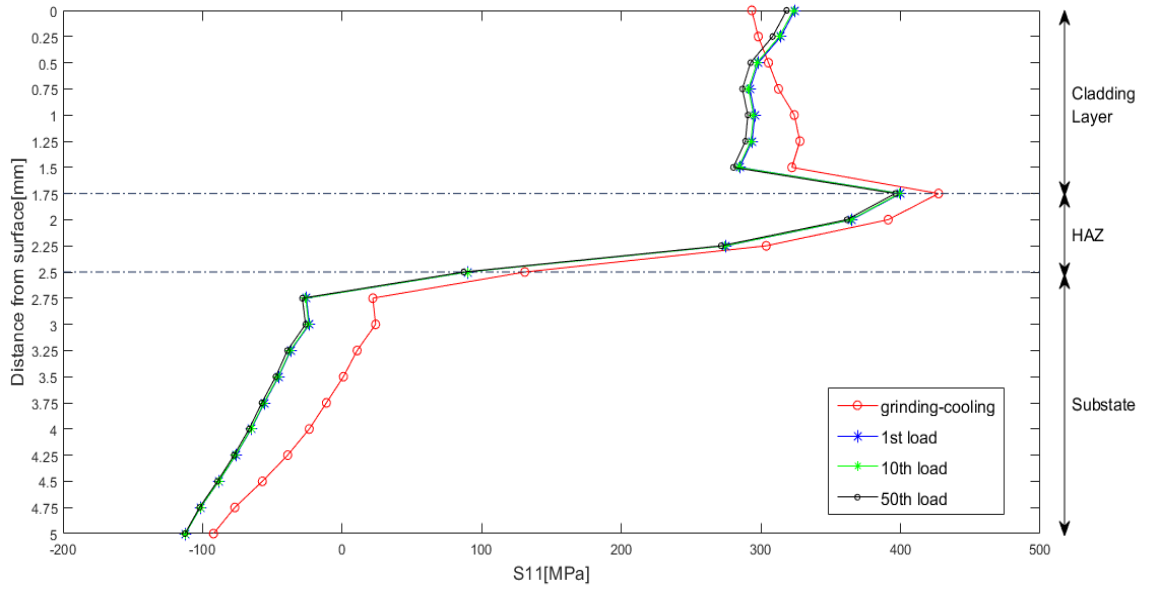

Figure 4.33; S11 distribution of grounded steel through thickness after repeated impact loads

4.6.2 S12 distribution after repeated impact loads on grounded steel

Shear residual S12 distribution of Cladded + Grounded steel through surface thickness is shown in Figure 4.34. It is important to analyze the possible chances of sliding between cladded layer and substrate after grinding process and repeated impact loads. It is displayed from Figure 4.34 that the tensile residual stresses are reduced after grinding with magnitude of 22MPa to around 21MPa in 1st, 10th, 50th impact loads. HAZ is mainly contained compressive stresses with largest magnitude of around 24MPa. This signifies that cladded + grounded steel has good bond between cladded and substrate layers even after grinding process and repeated impact loads.

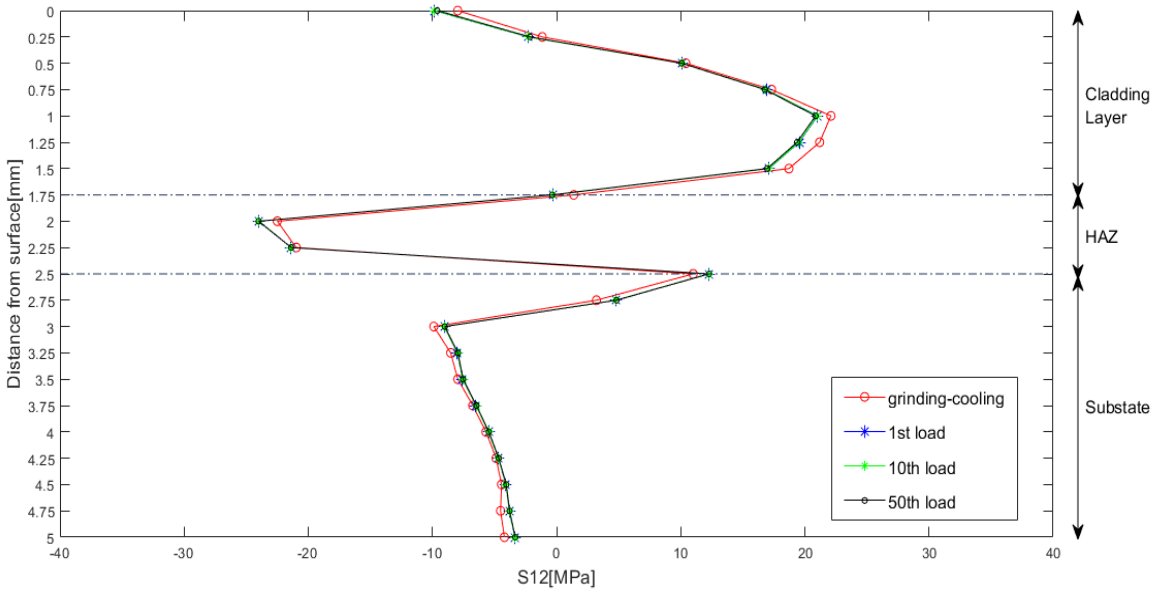

Figure 4.34: S12 distribution of grounded steel through thickness after repeated impact loads

4.6.3 S11 distribution at top surface after repeated impact loads on grounded Steel

The Figure 4.35 shows S11 at top surface after repeated ice impact loads on grounded steel. The first impact induced 324.3 MPa of tensile residual stress on top surface and then it is reduced gradually to 318.3 MPa after the 50th impact load. This shows that S11 will be reduced further with a greater number of repeated impact loads. Thus, the top surface is improved against the ice impacts.

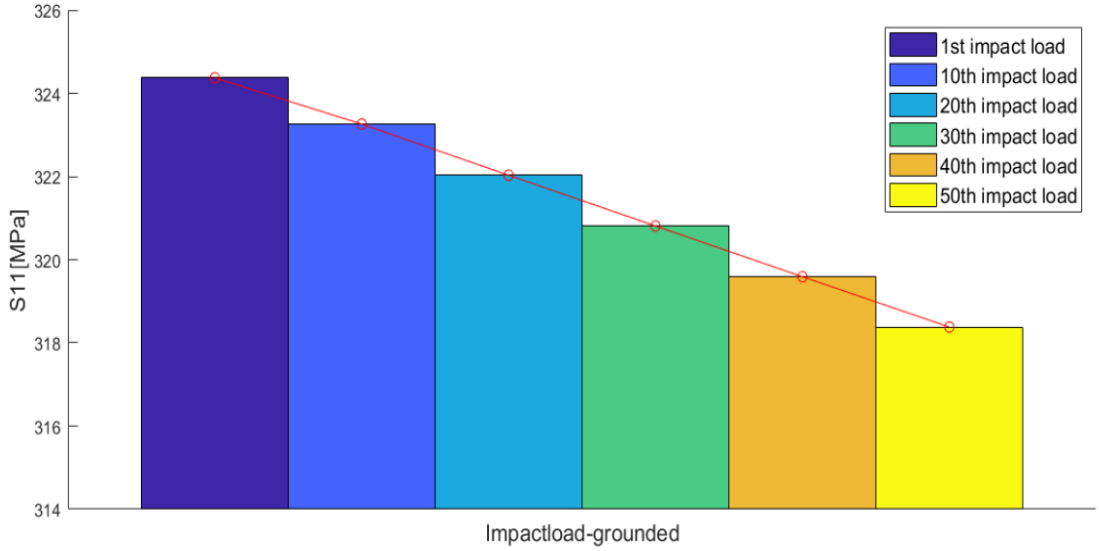

Figure 4.35: S11 distribution of grounded steel at top surface for repeated impact loads

4.6.4 S12 distribution at interface after repeated impact loads on grounded Steel

The Figure 4.36 shows S12 distribution after each impact loads at the interface of grounded NAB. Shear residual stresses at interface are compressive one with the least magnitude of 0.28 MPa and increased slightly to 0.35 MPa after 50th impact load which ensures that bonding quality remains in good condition after repeated ice induced impact loads.

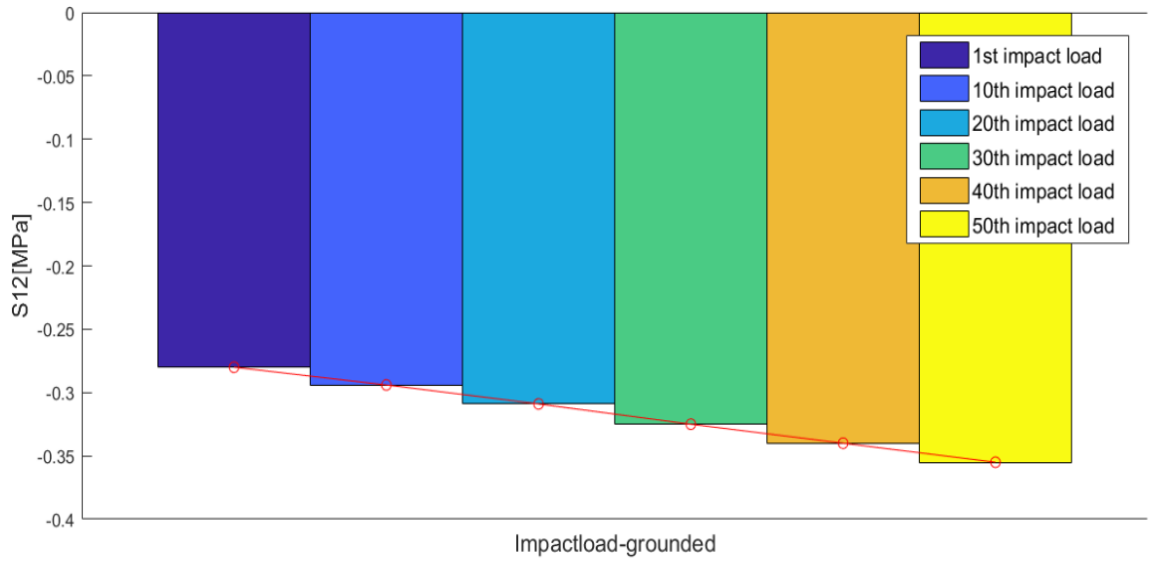

Figure 4.36: S12 distribution of grounded steel at interface for repeated impact loads

4.6.5 PEEQ at top surface of grounded Steel & Substrate after impact loads

Plastic equivalent strain comparison is carried out same as NAB between non-cladded steel and cladded + grounded steel after each repeated impact loads. Because repeated ice impact load can cause propeller to deform plastically. Figure 4.37 and Figure 4.38 show how repeated impact loads affect the non-cladded and cladded + grounded NAB with respect to plastic strain.

From the Figure 4.37, the first impact load is generated $1.76*10^{-3}$ of PEEQ at the top surface which is relatively small magnitude, then the PEEQ is increased after 10^{th} impact load with 1.057% to $1.78*10^{-3}$. Later $1.80*10^{-3}$ of PEEQ is accumulated after 20^{th} impact load with change of 1.18. PEEQ is increased further with almost constant change of 1.14% to the $1.86*10^{-3}$ after 50^{th} impact load.

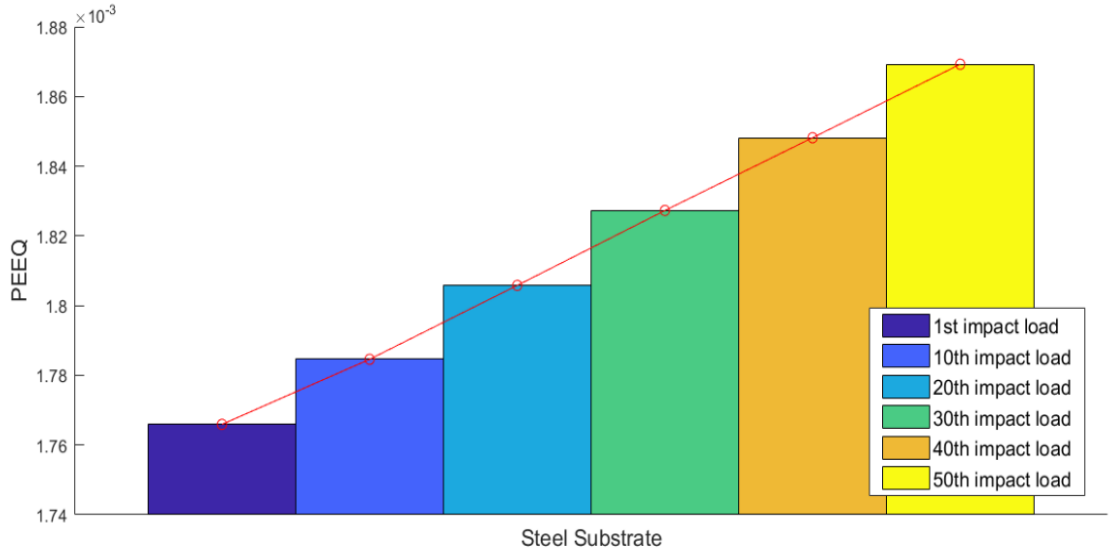

Figure 4.37: PEEQ at the top surface of the substrate for repeated impact loads

The Figure 4.38 demonstrates the effect of impact loads on PEEQ on cladded + grounded steel. The initial PEEQ magnitude is more compared to non-cladded NAB due to cladding and grinding process. The first impact load is prompted $11816*10^{-5}$ of PEEQ at the top surface. Then the PEEQ is increased after 10^{th}, 20^{th}, 30^{th}, 40^{th} and 50^{th} impact load with almost constant change of 0.0084% to $11817*10^{-5}$, $11818*10^{-5}$, $11819*10^{-5}$, $11820*10^{-5}$, $11821*10^{-5}$ respectively.

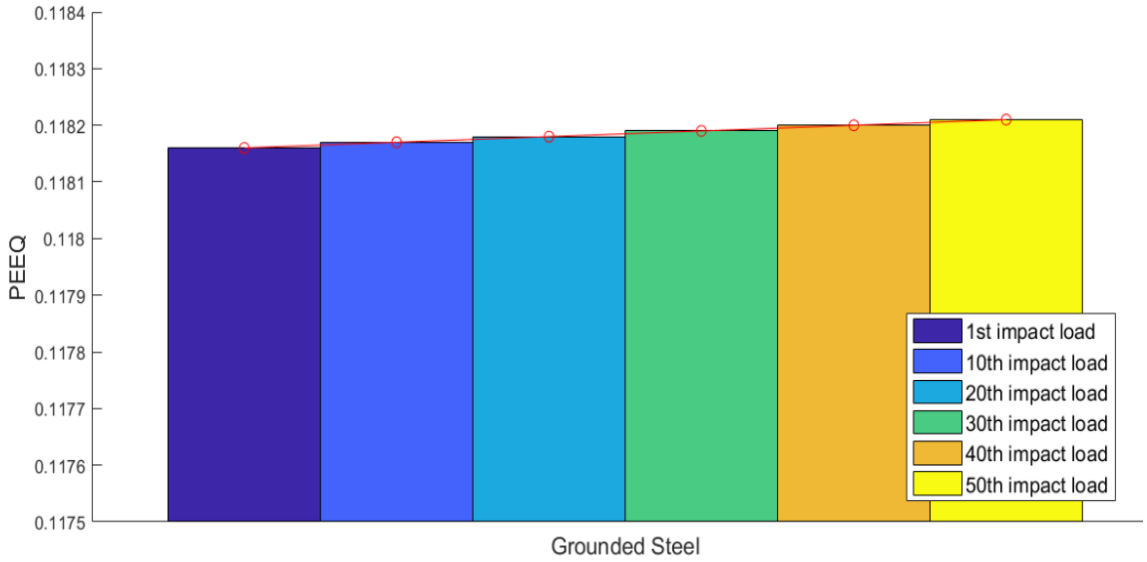

Figure 4.38: PEEQ at the top surface of the Grounded steel for repeated impact loads

4.6.6 PEEQ at 0.5 mm below surface of grounded Steel & substrate after impact loads

Effect of impact loads is also analyzed 0.5mm beneath top surface as it is performed for top surface explained before. From the Figure 4.39, the first impact load is gathered $1.6 * 10^{-3}$ of PEEQ at the top surface which is relatively small magnitude. Then the PEEQ is hiked after 10^{th} impact load with 1.19% to $1.62*10^{-3}$. After that $1.64*10^{-3}$ of PEEQ is accumulated with 1.19% of change after 20^{th} impact load and in the consecutive impact loads, PEEQ is increased with almost constant change of 1.15% to the $1.70*10^{-3}$ after 50^{th} impact load.

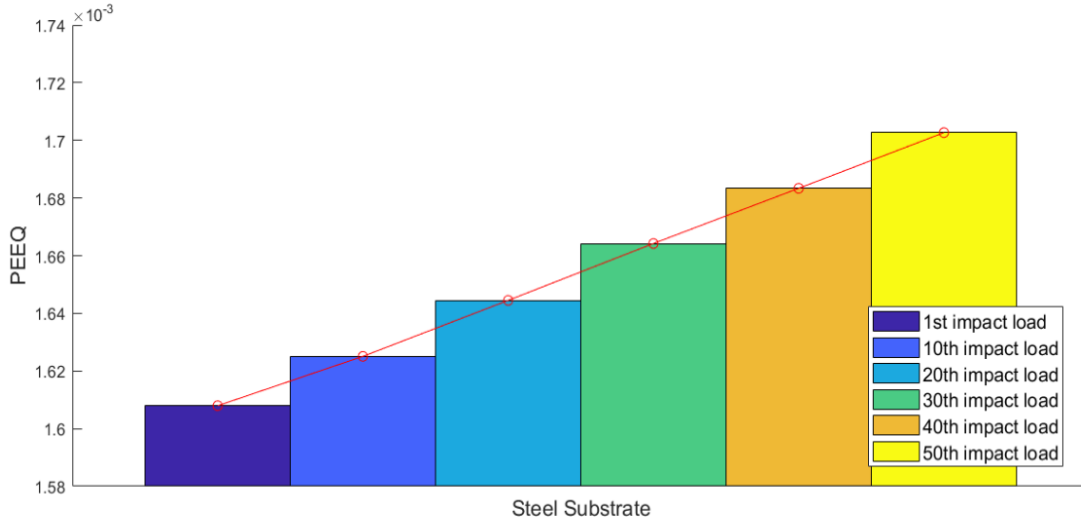

Figure 4.39: PEEQ at the 0.5 mm below the surface of substrate for repeated impact loads

The Figure 4.40 demonstrates the impact loads effect on PEEQ on cladded + grounded steel. The first impact load induced $11145*10^{-5}$ of PEEQ at the top surface. Following to this, 10^{th} impact load caused $11146*10^{-5}$ of PEEQ with change of 0.0089%. Then the PEEQ is further increased after 20^{th} impact load with of 0.0044% to $11146.5*10^{-5}$. The PEEQ is increased with same rate of change with magnitude of $11147*10^{-5}$ after 30^{th} impact load. The 40^{th} and 50^{th} impact loads resulted in PEEQ of $11148*10^{-5}$, $11149*10^{-5}$ respectively with change of 0.0089%.

The ice induced impact loads are dangerous to propeller's life and can induce severe damage to the blades while coming in contact. From above comparison, the percentage change in PEEQ of cladded + grounded steel after each repeated ice impact loads are quite lower and minimal compared to non-cladded one. Hence, cladded + grounded propeller is proved to perform better and safer than non-cladded steel propeller.

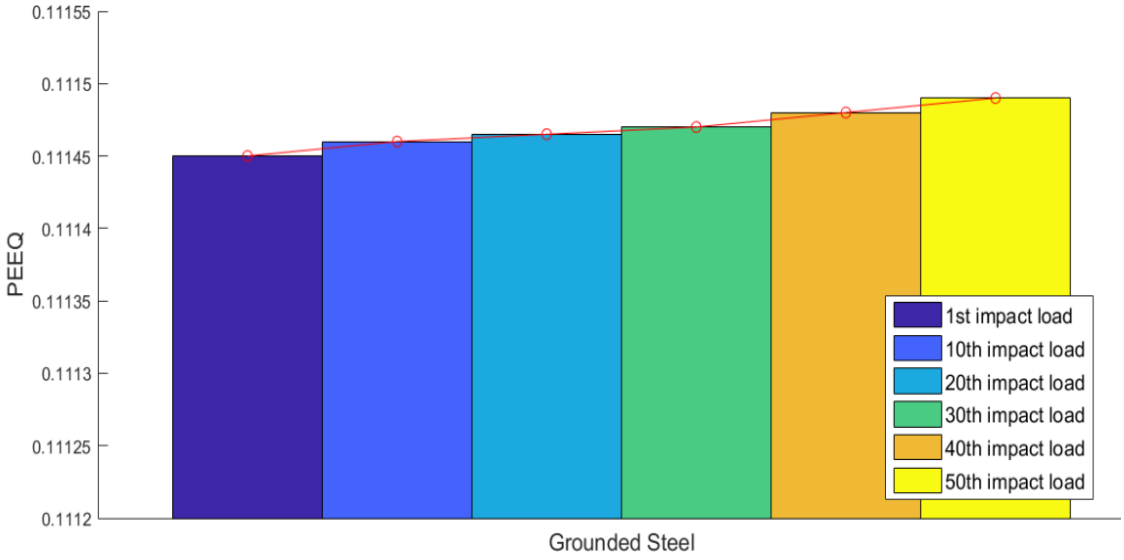

Figure 4.40: PEEQ at the 0.5 mm below the surface of grounded steel for repeated impact loads

5 Conclusions

The main scope of the thesis is to improve the performance of the marine propellers against the ice impact loads. To achieve this the laser cladding process and grinding process were used. These processes were simulated using ABAQUS. The Stellite was cladded on the substrate (both NAB and Steel, separately) with the help of moving laser beam using two approaches. In the first approach, the 3D model was created, and the moving laser beam was modelled using DFLUX subroutine and the coupled thermo-mechanical analysis was carried out. In the second approach, the 2D model (2 mm cladding and 20 mm substrate) was created that was divided into 40 cladding blocks. Each cladding block was irradiated with the nodal temperature with four different temperature cycles for cladding. The model change option was used in activation/deactivation of elements which shows the effect of deposition of cladding layers in 2D model. Once, the cladding layer was formed, the sequentially coupled thermo-mechanical analysis was carried out.

Combination of Stellite as cladding layer and NAB as a substrate material resulted in compressive residual hoop stress in the cladding layer due to the martensitic transformation in HAZ during the cladding process. Region at and beneath the interface witnessed tensile residual stress shows a combination of both (cladding+substrate) materials due to thermal and structural stress contribution. Then, the material was ground polished to achieve a cladding layer thickness of 1.75 mm. Grounded NAB is showing a little bit of increment in compressive residual stress at the interface while grounded steel increased tensile residual stress slightly at the interface.

Cladding and grinding contributed to increment in overall PEEQ but later grounded propeller is proved to be more resistant to encountered ice impact loads and forces. Thus, it lowers the formation of residual stresses and plastic strain that progress in the surface of the material. Bonding quality resists the sliding between two layers. Therefore, it is thoroughly investigated for such a case and shear residual stress S12 is well below the yield strength of the material which denies the occurrence of such a condition in grounded material. Furthermore, investigation of impact load analysis confirms that bonding quality remains better after repeated impact loads. Based on the results obtained after thermo-mechanical analysis, it is understood that the non-cladded substrate material contributes more to PEEQ for the longer operational period of the propeller. So, cladding and grinding processes are convincing and are beneficial for propeller's life that are operating in the polar and arctic region.

6 Recommendations for future work

The main limitation of this thesis was to get the exact material data for both NAB and Steel. For NAB as a substrate, we collected the physical and thermal material properties until 1200^{o}C of nearly the same chemical composition as that of NAB from the Demo version of JMatPro software. The properties after 1200^{o}C were assumed using linear extrapolation. Also, the demo version of JMatPro did not provide the plasticity properties like yield stress and plastic strain of NAB, hence based on the suggestions of our supervisor, we used plasticity properties of Steel and combined with other necessary properties of NAB. Also, the conductivity properties were assumed based on linear interpolation of data obtained by CES software which are not accurate. Furthermore, the Steel used in railways was used as a substrate along with Stellite as a substrate which is not used for marine applications. Hence, the main recommendation for future work is to find the temperature dependent properties of both NAB and Steel substrates that are used in the production of marine propellers. Along with that, the other cladding materials such as Hastelloy and NiTiNOL can be cladded on the substrates to see how the performance of propellers increase.

By considering the tip region of the propeller, the FE models created are similar to plates which makes the surface of the cladding and substrate nearly flat during simulations. But, in reality, the propeller has an irregular shape similar to hydrofoil which complicates the laser cladding and grinding processes. So, it is suggested to use the actual propeller model for the next phase of simulations. This helps to visualize actual stresses and temperature distributions throughout the profile of the propeller clearly.

In the simulation of laser cladding using DFLUX subroutine, it was difficult to control or record the nodal temperatures. So, it is suggested to find the appropriate method to achieve control over the stresses and nodal temperatures. Also, we went with 5 paths of moving heat source simulation just at the center of the model. In the next phases, one can try to work on the entire model of a propeller. Along with this, one can try to use the subroutines such as DLOAD to simulate the grinding process on the 3D model.

The 2D model of 200 mm length which was divided into 40 cladding blocks was used for both cladding and grinding. Here, the model change option was employed to achieve the activation/deactivation of elements. Also, the grinding forces were generated using the combination of normal pressure and traction load instead of the actual grinding wheel. So, in the future, one can try to simulate both laser cladding and grinding processes using 3D models along with the modelling of the actual grinding wheel. This could eliminate the limitations of assuming various parameters of grinding wheel that helps to get the desired effect of grinding.

During ice-impact load simulation, it was challenging for finding the actual magnitudes of the ice impact loads that hit the propellers in a real-time environment. Due to the nature of the ice impact loads, we were forced to use some equations of physics to estimate this magnitude based on various assumptions. Also, it was difficult to find the frequency and time period with which the ice impact loads meet the propellers. So, we just went with 50 cycles of impact loads as these were sufficient to see the effect on the performance of the propeller before and after cladding. In the future, one can try to find the real nature of the ice impact loads which helps to find the information regarding the magnitude, frequency and time period.

Laser cladding depends mainly on the laser beam parameters such as the power, scanning speed, intensity, voltage, current and other parameters such as dilution, powder feeding rate, quality of melt pool and so on. But, in this thesis, we used only limited parameters that do not give the actual results as we get in the laboratory experiments on real propellers. So, in the

future one can use any suitable method to make use of all the necessary parameters of a laser beam and cladding which can give better results.

7 References

Alam, M. et al. (2017). Microhardness and Stress Analysis of Laser-Cladded AISI 420 Martensitic Stainless Steel. Material Engineering and Performance, Vol. 26, No. 3, pp. 1076-1084.

Anca, A. et al. (2011) 'Finite element modeling of welding processes', Applied Mathematical Modelling, 35(2), pp. 688–707. doi: 10.1016/j.apm.2010.07.026.

Arias-González, F., Del Val, J., Comesaña, R., Penide, J., Lusquiños, F., Quintero, F., . . . Pou, J. (2017). Laser cladding of phosphor bronze. Surface and Coatings Technology, 313, 248-254.

Barsoum, Z. and Lundbäck, A. (2009) 'Simplified FE welding simulation of fillet welds - 3D effects on the formation residual stresses', Engineering Failure Analysis. Elsevier Ltd, 16(7), pp. 2281–2289. doi: 10.1016/j.engfailanal.2009.03.018.

Bhatti, A. A., & Barsoum, Z. (2012). Development of efficient three-dimensional welding simulation approach for residual stress estimation in different welded joints. The Journal of Strain Analysis for Engineering Design, 47(8), 539-552.

Broman, M., & Nordqvist, P. (2013). Global response of ship hull during ramming of heavy ice features. Citeseer.

Brückner, F., & Lepski, D. (2017). Laser Cladding: The Theory of Laser Materials Processing (pp. 263-306): Springer.

Bulletin, S. (2019) 'Grinding Residual Stresses'. [online] Available at : https://www.stresstech.com/download_file/view_inline/415/ [Accessed 27 May 2019]

Cambridge Engineering Selector (CES): A Material Selection software by Granta Design Available at: https://grantadesign.com/industry/products/ces-selector/ [Accessed 15th February 2019]

Cottam, R., & Brandt, M. (2015). Laser surface treatment to improve the surface corrosion properties of nickel-aluminum bronze Laser Surface Engineering (pp. 469-481): Elsevier.

Dassault Systemes. (2013) ABAQUS Online Documentation v6.13. [online] Available at: http://dsk.ippt.pan.pl/docs/abaqus/v6.13/index.html [Accessed 20 April 2019]

Dassault Systemes. (2013a). Abaqus Analysis User's Guide, 6.5.2 Uncoupled heat transfer analysis. Abaqus 6.13.

Dassault Systemes. (2013b). Abaqus Analysis User's Guide, 6.5.3 Fully coupled thermal-stress analysis. Abaqus 6.13.

Dassault Systemes. (2013c). Abaqus Analysis User's Guide, 16.1.2 Sequentially coupled thermal-stress analysis. Abaqus 6.13.

Dassault Systemes. (2013d). Abaqus Analysis User's Guide, 23.2.5 Annealing or melting. Abaqus 6.13

Dassault Systemes. (2013e). Abaqus Theory Guide, 2.11.1 Uncoupled heat transfer analysis. Abaqus 6.13.

Dassault Systemes. (2013f). Abaqus Theory Guide, 4.3.5 Models for metals subjected to cyclic loading. Abaqus 6.13.

De Freitas Teixeira, P. R., De Araújo, D. B. and Da Cunha, L. A. B. (2014) 'Study of the Gaussian distribution heat source model applied to numerical thermal simulations of tig welding processes', Ciencia y Engenharia/ Science and Engineering Journal, 23(1), pp. 115–122. doi: 10.14393/19834071.2014.26140.

Doman, D. A. Ã., Warkentin, A. and Bauer, R. (2009) 'Finite element modeling approaches in grinding International Journal of Machine Tools & Manufacture Finite element modeling approaches in grinding', (February 2009). doi: 10.1016/j.ijmachtools.2008.10.002.

Duraiselvam, M. et al. (2005) Laser clad WC reinforced Ni-based intermetallic-matrix composites to improve cavitation erosion resistance', 297(2006).

Duraiselvam, M., Galun, R., Wesling, V., Mordike, B. L., Reiter, R., & Oligmüller, J. (2006). Cavitation erosion resistance of AISI 420 martensitic stainless steel laser-clad with nickel aluminide intermetallic composites and matrix composites with TiC reinforcement. Surface and Coatings Technology, 201(3-4), 1289-1295.

Eagar, T. W. and Tsai, N.-S. (1983) 'Use of a Gaussian heat distribution in dimensionless form indicates final weld pool shape can be predicted accurately for many welds and materials', (December). Available at: http://eagar.mit.edu/Publications/Eagar036.pdf.

Earthobservatory.nasa.gov. (2019). World of Change: Global Temperatures. [online] Available at: https://earthobservatory.nasa.gov/world-of-change/DecadalTemp [Accessed 15 Mar. 2019].

Esfahani, M. M. (2016) 'Welding simulation of steels welded with low transformation temperature (LTT) filler materials', p. 91.

Flint, T. F. et al. (2017) 'Journal of Materials Processing Technology Extension of the double-ellipsoidal heat source model to narrow-groove and keyhole weld configurations', Journal of Materials Processing Tech. Elsevier B.V., 246, pp. 123–135. doi: 10.1016/j.jmatprotec.2017.02.002.

Fu, G. et al. (2015) 'Parameter determination of double-ellipsoidal heat source model and its application in the multi-pass welding process', Ships and Offshore Structures, 10(2), pp. 204–217. doi: 10.1080/17445302.2014.937059.

Gan, Z., Liu, H., Li, S., He, X., & Yu, G. (2017). Modeling of thermal behavior and mass transport in multi-layer laser additive manufacturing of Ni-based alloy on cast iron. *International Journal of Heat and Mass Transfer*, *111*, 709-722.

Ganesh, P. et al. (2010). Fatigue behavior of laser-clad joint of Stellite 21 on AISI 316L stainless steel. Materials Science and Engineering:A. Vol. 527, No. 16-17, pp.3748-3756.

Gedda, H. (2004). Laser cladding: an experimental and theoretical investigation. Luleå tekniska universitet.

Gery, D., Long, H. and Maropoulos, P. (2005) ‘Effects of welding speed, energy input and heat source distribution on temperature variations in butt joint welding’, 167, pp. 393–401. doi: 10.1016/j.jmatprotec.2005.06.018.

Goldak J, Chakravarti A, Bibby M. (1984). A new finite element model for welding heat source. Metall Mater Trans B. 15B:299–305.

Hongyuan, F. et al. (2005) ‘New general double ellipsoid heat source model’, Science and Technology of Welding and Joining, 10(3), pp. 361–368. doi: 10.1179/174329305x40705.

Hyatt, C. V., Magee, K. H. and Betancourt, T. (1998) ‘The effect of heat input on the microstructure and properties of nickel aluminum bronze laser clad with a consumable of composition Cu-9.0Al-4.6Ni-3.9Fe-1.2Mn’, Metallurgical and Materials Transactions A: Physical Metallurgy and Materials Science, 29(6), pp. 1677–1690. doi: 10.1007/s11661-998-0090-5.

Jeyakodi, G. K. (2016) ‘Finite Element Simulation of the In - Situ AFP process for Thermoplastic Composites using Abaqus’.

JMatPro Software by SenteSoftware Available at: https://www.sentesoftware.co.uk/ [Accessed 20th March 2019]Jones, S. J. et al. (2007) ‘Ice Loads Acting on a Model Podded Propeller Blade (OMAE2005-67416)’, Journal of Offshore Mechanics and Arctic Engineering, 129(3), p. 236. doi: 10.1115/1.2426993.

Karlsson, S. (2016). Arctic sea ice drift-A comparison of modeled and remote sensing data.

Kim, J.-D., & Peng, Y. (2000). Temperature field and cooling rate of laser cladding with wire feeding. KSME international journal, 14(8), 851-860.

Kim et al., (2004) ‘Nd : YAG laser cladding of marine propeller with hastelloy C-22’, 1585, pp. 1583–1585. doi: 10.1007/s00339-004-2854-0.

Koskinen, P., & Jussila, M. (1991). Long term measurements of ice loads on propeller blade of M/S Gudingen. VTT Technical Research Centre of Finland. VTT Research Notes, 1260.

Kukreja, L. M. et al. (2014) ‘Cobalt-Free Laser Cladding on AISI Type 316L Stainless Steel for Improved Cavitation and Slurry Erosion Wear Behavior’, Journal of Materials Engineering and Performance, 23(12), pp. 4463–4471. doi: 10.1007/s11665-014-1244-9.

Kwok, C. T. et al. (2016) ‘Developments in laser-based surface engineering processes: With particular reference to protection against cavitation erosion’, Surface and Coatings Technology, 291, pp. 189–204.

Laser technology: Voestalpine HPM International, (2019) "Laser technology" Available at: https://www.voestalpine.com/highperformancemetals/international/en/service/beschichtung/laser-technology/ [Accessed 18th June 2019]

Li. (2018) 'Finite element simulation of the laser surface treatment process of a two-material propeller'. Master thesis 2018/47, Chalmers University of Technology, Gothenburg, Sweden

Man, H. et al. (2000). Cavitation erosion and corrosion behaviour of laser surface alloyed MMC of SiC and Si3N4 on AI alloy AA6061. Surface and Coating Technology, Vol. 132, No. 1, pp. 11-20.

Maya-Johnson, S. et al. (2015). Fatigue crack growth rate of two pearlitic rail steels. Engineering Fracture Mechanics. Vol. 138, pp.63-72.

Moulik, P., Yang, H., & Chandrasekar, S. (2001). Simulation of thermal stresses due to grinding. International Journal of Mechanical Sciences, 43(3), 831-851.

Mushtaq, S. and Shah, A. (2012) 'Prediction of residual stresses due to grinding with'.

Muthukumaran, S. et al. (2014) 'Simulation of laser butt welding of AISI 316L stainless steel sheet using various heat sources and experimental validation', Journal of Materials Processing Technology. Elsevier B.V., 219, pp. 48–59. doi: 10.1016/j.jmatprotec.2014.12.008.

Norhamo, L., Bakken, G. M., Deinboll, O., & Iseskär, J. J. (2009). Challenges related to propulsor–ice interaction in arctic waters. Paper presented at the Proc., First Intl. Symp. on Marine Propulsors (SMP'09), Trondheim.

Pilipenko, A. (1992) 'Computer simulation of residual stress and distortion of thick plates in multi-electrode submerged are welding. Their mitigation techniques', Trondheim, (1289).

Ringsberg, J. W., Skyttebol, A. and Josefson, B. L. (2005) 'Investigation of the rolling contact fatigue resistance of laser cladded twin-disc specimens: FE simulation of laser cladding, grinding and a twin-disc test', International Journal of Fatigue, 27(6), pp. 702–714. doi: 10.1016/j.ijfatigue.2004.10.006.

Ringsberg, J. W. et al. (2000) 'Rolling contact fatigue of railsÐfinite element modelling of residual stresses , strains and crack initiation', (October 1999), pp. 7–19.

Rosenthal D. (1941). Mathematical theory of heat distribution during welding and cutting. Weld J 20(5):220s–234s.Arias-González, F., Del Val, J., Comesaña, R., Penide, J., Lusquiños, F., Quintero, F., . . . Pou, J. (2017). Laser cladding of phosphor bronze. *Surface and Coatings Technology, 313*, 248-254.

Sarwar, M. G. M. (2014) 'Impacts of climate change on maritime industries'. Available at: http://dlib.wmu.se/jspui/handle/123456789/682%5Cnhttp://dlib.wmu.se/jspui/bitstream/123456789/682/1/19308.pdf.

Shukla, M., & Verma, V. (2014). *Finite Element Simulation and Analysis of Laser Metal Deposition.* Paper presented at the 6th International Conference on Mechanical, Production and Automobile Engineering (ICMPAE'2014) Cape Town, South Africa.

Smurov, I. (2008). Laser cladding and laser assisted direct manufacturing. *Surface and Coatings Technology, 202*(18), 4496-4502.

Shepeleva, L. et al. (2000) 'Laser cladding of turbine blades', Surface and Coatings Technology, 125(1–3), pp. 45–48. doi: 10.1016/S0257-8972(99)00603-9.

Sudhakar Indurthi (2014) 'What is the main difference between implicit and explicit analysis', discussion at online researchgate forum, Available at:

https://www.researchgate.net/post/What_is_the_main_difference_between_implicit_and_explicit_analysis/amp [Accessed 18th June 2019]

Techniques, D. (2017) 'Writing User Subroutines in ABAQUS', Writing User Subroutines with ABAQUS, p. 8. Available at: http://imechanica.org/files/Writing User Subroutines with ABAQUS_0.pdf. [Accessed 20th May 2019]

Trivedi, A. et al. (2011) 'Modeling of Welding Heat Source for Laser Spot Welding Process', National Conference on Recent Trends in Engineering and Technology, (May).

United Nations (2015). Transforming our world: the 2030 agenda for sustainable development. Available at: http://www.un.org/ga/search/view_doc.asp?symbol=A/RES/70/1&Lang=E [Accessed 26 March 2019]

United Nations (2019). 'About the Sustainable Development Goals'. Available at: https://www.un.org/sustainabledevelopment/sustainable-development-goals/ [Accessed 29th June 2019]

Vilar, R. M. (2003). *Laser cladding.* Paper presented at the ALT'02 International Conference on Advanced Laser Technologies.

Wesling, V. et al. (2006) 'Cavitation erosion resistance of AISI 420 martensitic stainless steel laser-clad with nickel aluminide intermetallic composites and matrix composites with TiC reinforcement', Surface and Coatings Technology, 201(3–4), pp. 1289–1295. doi: 10.1016/j.surfcoat.2006.01.054.

Winczek, J. (2016) 'The influence of the heat source model selection on mapping of heat affected zones during surfacing by welding', 15(3), pp. 167–178. doi: 10.17512/jamcm.2016.3.16.

Ye, L. Y., Wang, C., Chang, X., & Zhang, H. Y. (2017). Propeller-ice contact modeling with peridynamics. *Ocean Engineering*, *139*, 54-64.

Zhang, Z., Yu, T., & Kovacevic, R. (2017). Erosion and corrosion resistance of laser cladded AISI 420 stainless steel reinforced with VC. Applied Surface Science, 410, 225-240.

Zhao, H. Y., Zhang, H. T., Xu, C. H., & Yang, X. Q. (2009). Temperature and stress fields of multi-track laser cladding. Transactions of Nonferrous Metals Society of China, 19, s495-s501.

Zhou, N. (2016). Influence of grinding operations on surface integrity and chloride induced stress corrosion cracking of stainless steels (Doctoral dissertation, KTH Royal Institute of Technology).

Zhu, X. K., & Chao, Y. J. (2002). Effects of temperature-dependent material properties on welding simulation. Computers & Structures, 80(11), 967-976.

Zou, B. (1996). Ships in ice: the interaction process and principles of design (Doctoral dissertation, Memorial University of Newfoundland).

Appendix A: Grinding forces calculations

According to Ringsberg et al., (2005), the abrasive contact loads in the mechanical analysis are identified with the uniformly distributed load with normal contact pressure load of $p_0/\ \sigma_y = 0.125$,

$\sigma_{y\ at}\ 20^o\ c = 494$ MPa (for Stellite),

Normal Pressure (p_0) = 61.75 MPa

According to Ringsberg et al., (2000),

$P_0 = 3P_z/(2\pi a^1 c^1)$

where a^1 - longitudinal semi-axes of Hertzian contact ellipse (m)

c^1- longitudinal semi-axes of Hertzian contact ellipse (m)

By taking $a^1 = 1.5$ mm and $c^1 = 1.125$ mm (Assuming based on the profile of Hertzian contact ellipse)

Magnitude of the vertical force (P_z)= 218.13 N (f_n)

By taking $\mu = 0.30$ = traction load/ normal load = $f_t/f_n = 0.3*218.13$

Traction load (f_t)= 65.43 N

Appendix B: Impact load calculations

According to Newton's laws of motion,

$f * t = mv - mu = m_{prop}\, v_{prop} - m_{ice}\, v_{ice}$

To find velocity of a Propeller (v_{prop})

Taking rotational speed N=60 rpm (1rps), so angular velocity $\omega = 2\pi N = 6.28$ rad/s

So, velocity $r\,\omega = 12.56$ m/s (by taking radius of propeller=2m)

(v_{prop})=12.56 m/s

To find Mass of the propeller (m_{prop})

For controllable pitch diameter of 4 m,

Weight of the propeller $W_{prop} = 0.008\,[A_E/A_o]\,D^3_{Prop}$

$W_{prop} = 0.008\,(0.5)\,(13.12)^3$ As 1ft=0.3048m (so, D=1.8288ft)

W_{prop} =9039 kg and we know that W=mg (g = acceleration due to gravity=9.81 m/s^2)

So, Mass of the propeller (M_{prop}) = 921.4 kg

By taking mass of ice = 5400 kg and velocity of ice= 2.5 m/s

The ice-propeller interaction time period = 0.1 s

$f * t = m_{prop}\, v_{prop} - m_{ice}\, v_{ice}$

$f * 0.1 = [\,(921*12.56) - (5400*2.5)]$

Impact load f = 19.32 kN

Impact Pressure exerted by ice on the propeller = force/ area

Area of the Propeller FE model = 20mm * 20 mm = 0.0004 m2

So, Impact pressure = $19.32 * 10^3 / 0.0004$

Ice impact pressure = 48.306 MPa

Appendix C: DFLUX Subroutine for moving heat source

```
SUBROUTINE DFLUX (FLUX,SOL,JSTEP,JINC,TIME,NOEL,NPT,COORDS,JLTYP,1
TEMP,PRESS,SNAME)

INCLUDE 'ABA_PARAM.INC'

DIMENSION COORDS(3),FLUX(2),TIME(2)
CHARACTER*80 SNAME


vx = 0.003   ! speed of welding in x direction is 3mm/sec
vy = 0.00
vz = 0.00


!  effective welding arc *for surface heatflux a,b  *Body heatflux
a,b,c[m]
a = 0.0022
b = 0.0018
c = 0.0030

!  Path 1 Linear moving heat source
x0=0.00
y0=0.0036
z0=0.011

xarc=vx*time(1)+x0
yarc=vy*time(1)+y0
zarc=vz*time(1)+z0


Xf=coords(1)-xarc! coordinate of position x
Yf=coords(2)-yarc! coordinate of position y
Zf=coords(3)-zarc! coordinate of position z

!  Path 2 Linear moving heat source
x2=0.00
y2=0.0018
z2=0.011

xarc2=vx*time(1)+x2
yarc2=vy*time(1)+y2
zarc2=vz*time(1)+z2


Xf2=coords(1)-xarc2    ! coordinate of position x
Yf2=coords(2)-yarc2    ! coordinate of position y
Zf2=coords(3)-zarc2    ! coordinate of position z


!  Path 3 Linear moving heat source
x3=0.00
y3=0.00
```

```
z3=0.011

xarc3=vx*time(1)+x3
yarc3=vy*time(1)+y3
zarc3=vz*time(1)+z3


Xf3=coords(1)-xarc3    ! coordinate of position x
Yf3=coords(2)-yarc3    ! coordinate of position y
Zf3=coords(3)-zarc3    ! coordinate of position z


!  Path 4 Linear moving heat source
x4=0.00
y4=-0.0018
z4=0.011

xarc4=vx*time(1)+x4
yarc4=vy*time(1)+y4
zarc4=vz*time(1)+z4

Xf4=coords(1)-xarc4    ! coordinate of position x
Yf4=coords(2)-yarc4    ! coordinate of position y
Zf4=coords(3)-zarc4    ! coordinate of position z

!  Path 5 Linear moving heat source
x5=0.00
y5=-0.0036
z5=0.011

xarc5=vx*time(1)+x5
yarc5=vy*time(1)+y5
zarc5=vz*time(1)+z5


Xf5=coords(1)-xarc5    ! coordinate of position x
Yf5=coords(2)-yarc5    ! coordinate of position y
Zf5=coords(3)-zarc5    ! coordinate of position z


Q=190  ! heat flux core : current135*voltage14*efficiency0.4

! Gaussian Heat Source Distribution
heatf=(1.86632*Q)/(a*b*c)   ! 1.86632=6*sqrt(3)/(pi^3/2)


shapef=EXP(-3*(Xf)**2./a**2.-3*(Yf)**2./b**2.-3*(Zf)**2./c**2.)

shapef2=EXP(-3*(Xf2)**2./a**2.-3*(Yf2)**2./b**2.-3*(Zf2)**2./c**2.)

shapef3=EXP(-3*(Xf3)**2./a**2.-3*(Yf3)**2./b**2.-3*(Zf3)**2./c**2.)

shapef4=EXP(-3*(Xf4)**2./a**2.-3*(Yf4)**2./b**2.-3*(Zf4)**2./c**2.)

shapef5=EXP(-3*(Xf5)**2./a**2.-3*(Yf5)**2./b**2.-3*(Zf5)**2./c**2.)
```

```
if(jstep.eq. 3) then
      if(shape.gt.1.0) then
        flux(1)=0
      else
        flux(1)=heatf*shapef
      endif
endif

if(jstep.eq. 5) then
      if(shape.gt.1.0) then
        flux(1)=0
      else
        flux(1)=heatf*shapef2
      endif
endif

if(jstep.eq. 7) then
      if(shape.gt.1.0) then
        flux(1)=0
      else
        flux(1)=heatf*shapef3
      endif
endif

if(jstep.eq. 9) then
      if(shape.gt.1.0) then
        flux(1)=0
      else
        flux(1)=heatf*shapef4
      endif
endif

if(jstep.eq. 11) then
      if(shape.gt.1.0) then
        flux(1)=0
      else
        flux(1)=heatf*shapef5
      endif
endif


RETURN
END
```